Title
Nonlinear Spectroscopic Studies of Interfacial Molecular Ordering

Author
Superfine, R.

Publication Date
1991-07-01

LBL-31130

Lawrence Berkeley Laboratory
UNIVERSITY OF CALIFORNIA

Materials & Chemical Sciences Division

Nonlinear Spectroscopic Studies of Interfacial Molecular Ordering

R. Superfine
(Ph.D. Thesis)

July 1991

Prepared for the U.S. Department of Energy under Contract Number DE-AC03-76SF00098

DISCLAIMER

LBL-31130

NONLINEAR SPECTROSCOPIC STUDIES OF INTERFACIAL MOLECULAR ORDERING

RICHARD SUPERFINE
Ph.D. Thesis

DEPARTMENT OF PHYSICS
University of California

and

MATERIALS SCIENCES DIVISION
Lawrence Berkeley Laboratory
University of California
Berkeley, CA 94720

JULY 1991

This work was supported by the Director, Office of Energy Research, Office of Basic Energy Sciences, Materials Sciences Division, of the U.S. Department of Energy under Contract No. DE-AC03-76SF00098.

Nonlinear Spectroscopic Studies of Interfacial Molecular Ordering

by

Richard Superfine

Abstract

The second order nonlinear optical processes of second harmonic generation and sum frequency generation are powerful new probes of surfaces. They possess unusual surface sensitivity due to the symmetry properties of the nonlinear susceptibility. In particular, infrared-visible sum frequency generation (SFG) can obtain the vibrational spectrum of sub-monolayer coverages of molecules. In this thesis, we explore the unique information that can be obtained from SFG. We take advantage of the sensitivity of SFG to the conformation of alkane chains to study the interaction between adsorbed liquid crystal molecules and surfactant treated surfaces. The sign of the SFG susceptibility depends on the sign of the molecular polarizability and the orientation, up or down, of the molecule. We experimentally determine the sign of the susceptibility and use it to determine the absolute orientation of a surface molecule. Then we use the sign of the susceptibility of an adsorbate with a previously known orientation to obtain the sign of the molecular polarizability and show that this quantity contains important information about the dynamics of molecular charge distributions. Finally, we study the vibrational spectra and the molecular orientation at the pure liquid/vapor interface of methanol and water and present the most detailed evidence yet obtained for the structure of the pure water surface.

Acknowledgement

And now, in one or two pages, as if it could be possible with fifty or a hundred, to express my gratitude for the life that brought me to graduate school, the kindness and support that saw me through, and the life that arrived just as I was finishing.

To Mom and Dad, for somehow both encouraging my curiosity and bearing the accompanying irreverance with love and understanding.

I had the remarkable good fortune to work for Joe Orenstein before arriving at Berkeley. His combination of humanity and intellect allowed me to see that research could be both fulfilling and fun. His encouragement was a major influence in my pursuing my own research interests.

My advisor, Y. Ron Shen, has been a tremendous source of knowledge, insight and professionalism. He has always been unselfish with his time and generous in providing his students with exposure in the scientific community. I will be answering to his search for the simple, essential physical issues for many years to come.

Rita Jones has been a wellspring of how-to's and has been unselfish with Ron's compliments. I'm not sure that Ron speaks as well of us as often as you relate. But when research is bogged with difficulties, there is no time to question these matters and your encouragement in the group cannot be overestimated.

Marla has been there from day one. From classes through research, her unabashed search for right, in physics and in life, with commitment, bravery and humor, has

challenged me to be a better person and scientist. Molly will learn to throw a baseball, unless her train set takes up all of her time.

Jim Bartlett has shared weekly lunches which have always been stimulating, about physics and more, and have served as an outlet for the frustrations of the week past and nourishment for the week to come.

To Shen group members past: To Jeff, thank you for the laser, really. Phillipe got me started on research with a great model of unrelenting focus that I drew upon, sometimes rather desperately, to get me through these experiments. Wei was, and is, a great source of calm deliberation on physics, our future research and families.

I had the opportunity to work with two very talented postdocs. Jung Huang's quiet determination well complimented my memories of Phillipe's lessons as the hours of the night gave way to morning spectra. Viola Vogel had a great sense of the experimental drama and her enthusiasm and insight were inspiring.

To the Shen group members present: You are a talented group of physicists who have taught me a great deal, both in hallway conversations and in group meetings that ran overtime. You have made graduate school a shared, dynamic learning and emotional experience that I know I will miss dearly. To the members that arrived shortly after my joining the group, Xu Dong, Chris, and Tom, a special thank you for the many years of support and insight. I hand the laser system over to the latest talented member to join the group, Du Quan. You have made the last months very

exciting, minus the experimental frustrations, and I only hope that you will forgive me as you renovate the system.

Dear Ellen, you are the grace, beauty and love of my life. Your love of scholarship has been truly inspiring during these years, more than I can know or ever tell you. You gave me the courage and unfailing support to pursue my goals, and then gave us a wonderful child that watched me graduate. Molly is simply, joyously overwhelming and has taught me to smile with my whole face and heart. Thank you.

Table of Contents

I. Introduction

The study of surfaces and interfaces has enjoyed enormous growth in recent years. The fields of science that involve surface science include biology, chemistry, physics and electrical engineering, to name a few. The interfaces that are studied cover the full range of material interfaces. While chemistry is interested in the solid/liquid and solid/gas interfaces,[1] biology is interested in membrane phenomena, which occur at the liquid/liquid interface.[2] Physics and electrical engineering have particular interests in solid/solid interfaces.[3] The questions to be answered include the interfacial composition and structure, as well as the dynamics of surface processes which can take place on ultrafast time scales. What is common among this wide range of interests is the demand for versatile techniques that can provide detailed information.

We can list the desired properties that a valuable surface probe should possess:

1. submonolayer sensitivity
2. versatility - the ability to be applied at a wide variety of interfaces
3. surface specificity - to discriminate between surface and bulk contributions
4. time resolution - to probe down to the subpicosecond time scale
5. energy resolution - < 1 cm^{-1} for vibrational spectroscopy, for example

Many of the techniques that have been assembled for UHV studies of solid surfaces,[1,3] including photoemission, electron and helium diffraction, and electron energy loss spectroscopy,[4] involve the injection or emission of particles such as electrons or atoms. This prohibits their application outside of the vacuum chamber.

Optical spectroscopy has the potential to fulfill the requirements listed above. In general, optical spectroscopy offers unsurpassed energy resolution and the use of ultrafast laser sources makes possible the study of processes on the femtosecond time scale. Access to the interface is assured as long as the intervening medium is not strongly absorbing at the probing frequencies, a condition that is most often met. For vibrational spectroscopy,[5] reflection absorption infrared spectroscopy (RAIRS) has been used extensively over the last two decades with sensitivity to coverages on the order of a thousandth of a monolayer.[6] Most recently, this technique has been brought into the ultrafast time regime with the use of picosecond infrared sources.[7] Raman spectroscopy, the traditional counterpart of absorption spectroscopy, has also been applied with success to surface studies.[8] However, due to symmetry considerations which will be discussed later, both RAIRS and Raman spectroscopy lack surface specificity. While this is usually not a problem for vibrational spectroscopy of adsorbates on metal or semiconductor surfaces in UHV, it is a serious drawback in gaseous or liquid environments.

The second order nonlinear optical techniques of second harmonic generation (SHG) and sum frequency generation (SFG) satisfy all of the requirements of a versatile surface probe.[9,10-14] Using laser sources, they share all of the advantages of optical techniques. Most importantly, symmetry requirements strongly suppress the generation of a signal from the bulk of a centrosymmetric sample , making SHG and SFG uniquely surface specific among optical probes. Their sensitivity to submonolayer coverages of adsorbates has been demonstrated in many experiments.[15] Widespread applications of SHG include the equilibrium[16] and dynamic properties of molecular adsorption, surface symmetry[17] and bonding with most of the studies being done off resonance, where neither the fundamental nor the second harmonic is tuned to a sample excitation frequency. By tuning the frequency

of the incident laser beam, SHG can be used for surface spectroscopy.[18] However, for performing surface vibrational spectroscopy, one encounters the problem that the second harmonic frequency to be detected falls in the infrared, outside the range of photomultiplier tubes. This is remedied by infrared-visible sum frequency generation where a fixed visible beam is mixed at the surface with an infrared beam which is tunable about the vibrational resonance.[9] The sum frequency is then in the visible, allowing photon counting sensitivity. It is interesting that the application of SFG to vibrational spectroscopy and a comparison of its abilities with surface Raman spectroscopy brings us back to the emergence of SHG as a surface probe over a decade ago.

While attempting to apply Raman spectroscopy to adsorbed species at an electrode surface, Fleischman reported unusually large signals.[19] It was later appreciated that the signal enhancement was explained by an increase of the molecular scattering cross section by $\sim 10^6$! Surface enhanced Raman spectroscopy (SERS) subsequently developed into a field of intense activity.[20] The effect is now understood to be limited to the roughened surface of a few specific metals with the increased signal being due to either an enhancement of the local electromagnetic field or due to chemical effects such as adsorption induced resonances. Raman scattering is in general described as a third order nonlinear optical effect and SERS was first studied with spontaneous scattering, an incoherent scattering process. It became of interest to look for similar effects in SHG, a second order, coherent nonlinear optical process. Indeed, the SHG signals also showed enhancements.[21] More importantly, however, it was realized that the adsorbates could be detected without enhancement effects. Further development over the last decade has led to the application of SHG and SFG to smooth metal, semiconductor and dielectric interfaces. The first demonstration of SFG to obtain the vibrational spectrum of

surface adsorbates was accomplished by Zhu et al in 1987.[22] Most recently, the technique has been used to obtain unique information about the structure and dynamics of interfaces.

In this article we will discuss the theory and practice of SFG. In chapter two we will discuss the theory of SFG from an interface including the simple case of a single monolayer of molecules, and the more complicated situation where the higher order multipole contributions from the interface and bulk are present.[12] We will present the symmetry properties of SFG that make it a surface sensitive probe and, through an analysis of the multipole contributions, explore the strategies available for deducing the interesting surface dipole contributions to the detected signal. Chapter two ends with a discussion of our experimental setup to produce the intense laser pulses necessary to obtain SFG spectra.[13]

This thesis has sought to develop certain aspects the technique that are unique to SFG. First, based on the symmetry considerations for a second order susceptibility, it is sensitive to the lack of inversion symmetry of an adsorbate and of the interface. We will take advantage of these properties in chapter three and in the final section. In chapter three the sensitivity of SFG to the conformation of an alkane chain, which alters the molecular symmetry, is exploited to study the interactions between a liquid crystal monolayer and a surfactant coated surface.[23] In the last section, we study the liquid/vapor interface of the pure liquids methanol and water.[24] Here the major difference between the surface and the bulk is the breaking of inversion symmetry at the surface where the molecules assume preferential orientations. The study of liquid interfaces is certaintly one of the most promising areas where SFG will be applied in the future.

A second unique feature of SFG is its sensitivity to the polar orientation of an adsorbate. The sign of the SFG susceptibility on resonance depends on the

orientation, up or down, of a molecule. In chapter four we present two experimental techniques for the determination of this sign and apply them to the problem of the absolute orientation of a surface molecule.[25] If the orientation of an adsorbate is already known by some other means, then the sign of the susceptibility, the macroscopic quantity, gives the sign of the molecular quantity, the polarizability. This is a third unique property of SFG which we will explore in chapter five where we show that the sign of the molecular polarizability contains important information about the dynamics of the molecular charge distribution.[26] This information is not obtainable by other experimental means.

References

[1] G. A. Somorjai, *Chemistry in Two Dimensions: Surfaces* (Cornell University Press, Ithaca, 1981); A. W. Adamson, *Physical Chemistry of Surfaces* (Wiley, New York, 1990).

[2] H. Tien, *Bilayer Lipid Membranes: Theory and Practice* (Marcel Dekker, New York, 1974);

[3] Zangwill, *Physics at Surfaces* (,,1989)

[4] H. Ibach and D. L. Mills, *Electron Energy Loss Spectroscopy and Surface Vibrations*, (Academic, New York, 1982).

[5] R. F. Willis, ed., *Vibrational Spectroscopy of Adsorbates*, Springer Series in Chemical Physics, Vol. 15 (Springer, Berlin, 1980).

[6] Y. Chabal, Surf. Sci. Reports,

[7] E. J. Heilweil, M. P. Casassa, R. R. Cavanagh, and J. C. Stephenson, Annu. Rev. Phys. Chem. **40**, 143 (1989);

[8] A. Campion in *Vibrational Spectroscopy of Molecules on Surfaces*, J. T. Yates and T. E. Madey, eds. (Plenum, New York, 1987).

[9] Y. R. Shen, Ann. Rev. Mat. Sci. **16**, 69 (1986); Y. R. Shen, Nature, **337**, 519 (1989)

[10] T. F. Heinz, Ph. D. Thesis, University of California, Berkeley, 1982, unpublished.

[11] H. W. K. Tom, Ph. D. Thesis, University of California, Berkeley, 1984, unpublished.

[12] P. Guyot-Sionnest, Ph. D. Thesis,University of California,Berkeley,1987,unpublished.

[13] J. H. Hunt, Ph. D. Thesis, University of California, Berkeley, 1988, unpublished.

[14] X. Zhu, Ph. D. Thesis, University of California, Berkeley, 1989, unpublished.

[15] H. W. K. Tom, C. M. Mate, X. D. Zhu, J. E. Crowell, T. F. Heinz, G. A. Somorjai, and Y. R. Shen, Phys. Rev. Lett. **52**, 348 (1984); S. G. Grubb, A. M. DeSantolo, and R. B. Hall, J. Phys. Chem. **92**, 1419 (1988).

[16] X. D. Zhu, Th. Rasing, and Y. R. Shen, Chem. Phys. Lett. **155**, 459 (1989).

[17] T. F. Heinz, M. M. T. Loy, and W. A. Thompson, Phys. Rev. Lett. **54**, 63 (1985).

[18] T. F. Heinz, C. K. Chen, D. Ricard, and Y. R. Shen, Phys. Rev. Lett. **48**, 478 (1983); T. F. Heinz, F. J. Himpsel, E. Palange and E. Burstein, Phys. Rev. Lett. **63**, 644 (1989).

[19] M. Fleischman, P. J. Hendra, and A. J. McQuillan, Chem. Phys. Lett. **26**, 163 (1974).

[20] R. K. Chang, and T. E. Furtak, eds., *Surface Enhanced Raman Scattering*, (Plenum, New York, 1982). M. Moskovits, Rev. Mod. Phys. **57**, 783 (1985).

[21] C. K. Chen, A. R. B. Castro, and Y. R. Shen, Phys. Rev. Lett. **46**, 145 (1981); G. T. Boyd, Th. Rasing, J. R. R. Leite, and Y. R. Shen, Phys. Rev. B **30**, 519 (1984).

[22] X. D. Zhu, H. Suhr, and Y. R. Shen, Phys. Rev. B **35**, 3047 (1987).

[23] J. Y. Huang, R. Superfine and Y. R. Shen, Phys. Rev. B, **42**, 3660 (1990).

[24] R. Superfine, J. Y. Huang and Y. R. Shen, Phys. Rev. Lett. **66**, 1066 (1991).

[25] R. Superfine, J. Y. Huang and Y. R. Shen, Opt. Lett. **15**, 1276 (1990).

[26] R. Superfine, J. Y. Huang and Y. R. Shen, Chem. Phys. Lett. **172**,303 (1990).

II. Infrared -Visible Sum Frequency Generation: Theory and Practice

A. Theory

In this section we will describe the second order nonlinear optical process of sum frequency generation (SFG), its importance for surface vibrational spectroscopy and the details of its application to the interfaces between centrosymmetric bulk media.[1-3] First we will present the simple case where the only contribution to the nonlinear signal from an interface is from the electric dipole response of a monolayer of molecules. This will allow us to immediately discuss the information obtainable from SFG and the expected signal from an interface. Then we will present a more complete discussion that includes the multipole contributions from the interface and the bulk.[4]

I. Monolayer Susceptibility

When two light fields are incident on an interface, Fig. 1, they drive a polarization at the interface and in the bulk material which may subsequently radiate.[3,5,6] The surface dipole polarization **P** is written as

$$\mathbf{P}(\omega_s) = \boldsymbol{\chi}_D^{(2)} (\omega_s = \omega_1 + \omega_2) : \mathbf{E}_1(\omega_1)\, \mathbf{E}(\omega_2) \qquad (1)$$

where $\mathbf{E}_1$ and $\mathbf{E}_2$ are the local fields in the monolayer and $\boldsymbol{\chi}_D^{(2)}$ is the second order susceptibility (hereafter we will drop the (2) in the superscript). The microscopic expression for $\boldsymbol{\chi}^D$ can be obtained from second order perturbation theory.[7,8] For the case of only one frequency, ω_1, on resonance, $\boldsymbol{\chi}^D$ can be written as $\boldsymbol{\chi}^D = \boldsymbol{\chi}^D{}_{NR} +$

χ^D_R where χ^D_{NR} is the non-resonant part and χ^D_R, the resonant contribution, is given by[9]

$$\chi^D_R = \sum_n \frac{\langle g|\mu_k|n\rangle}{\hbar(\omega_1 - \omega_{ng} + i\Gamma_{ng})} M_{ij} \qquad (2)$$

$$M_{ij} = \sum_m \left(\frac{\langle n|\mu_i|m\rangle\langle m|\mu_j|g\rangle}{\hbar(\omega_s - \omega_{mg})} + \frac{\langle g|\mu_i|m\rangle\langle m|\mu_j|n\rangle}{\hbar(\omega_s + \omega_{mn})} \right)$$

where μ_i is the component of the electric dipole moment operator and ω_{ng} ($\hbar\omega_{ng} = E_n - E_g$) and Γ_{ng} are the resonance frequency and phenomenological damping constant of the transition. The spectrum of the surface excitations is detected by the enhancement of the signal due to the dispersion of χ^D_R at the sum frequency when ω_1 is tuned through the resonances. The sum frequency process and its selection rules are described by the terms $\langle g|\mu_i|m\rangle$ and M_{ij}. The field at ω_1 excites a polarization by coupling to the transition dipole moment between states g and n while the field at ω_2 upconverts the polarization in a Raman process as described by M_{ij}.[10] Thus, a transition must be both optically active and Raman active in order to be detected by SFG. This is consistent with the requirement from macroscopic symmetry considerations that there must be a lack of inversion symmetry in the medium for χ^D to be non-zero. An excitation of a centrosymmetric medium cannot both have a nonzero dipole matrix element and be Raman active. However, at a surface, the inversion symmetry is necessarily broken, and χ^D will be non-zero.

This thesis is concerned with the application of SFG to surface molecular vibrational spectroscopy.[11-27] The experiments we will discuss all involve this application. In the following, we write the general expression that describes SFG when χ^D is due to the vibrational excitations of surface adsorbates, and describe the

variety of information that can be obtained. The susceptibility is described by Eq.(2) with ω_1 replaced by ω_{ir}, and the state n replaced with the vibrational mode q. The surface dipole susceptibility in the absence of local field effects can then be written as

$$\chi^{D}_{ijk} = N < G^{lmn}_{ijk} > \alpha_{lmn} \tag{3}$$

where N is the surface density and **G** is the transformation matrix connecting the molecular polarizability $\boldsymbol{\alpha}$ written in the molecular coordinate system with the lab coordinate system. The brackets denote an average taken over the molecular orientational distribution. For the case where ω_2 and ω_s are away from electronic resonances, the molecular polarizability can be written as $\alpha = \alpha_{NR} + \alpha_R$ with [19]

$$\boldsymbol{\alpha}_R = \sum_q \frac{\mathbf{A}_q}{\hbar(\omega_q - \omega_{ir} - i\Gamma_q)} \Delta\rho_{gq} \tag{4a}$$

$$A_{q,lmn} = \frac{1}{2\omega_q} \frac{\partial \mu_n}{\partial Q} \frac{\partial \alpha^{(1)}_{lm}}{\partial Q} \tag{4b}$$

$$\frac{\partial \mu_n}{\partial Q} = \left(\frac{2\omega_q}{\hbar}\right)^{1/2} < g \mid \mu_n \mid q > \tag{4c}$$

$$\frac{\partial \alpha^{(1)}_{lm}}{\partial Q} = \left(\frac{2\omega_q}{\hbar}\right)^{1/2} M_{lm} \tag{4d}$$

where the amplitude $\mathbf{A}_q$ is proportional to the product of the infrared dipole moment derivative, $\partial\boldsymbol{\mu}/\partial Q$, and the Raman polarizability $\partial\boldsymbol{\alpha}^{(1)}/\partial Q$ for the normal mode Q and $\Delta\rho_{gq}$ is the difference in the population between the ground and excited states. This explicitly provides us with the selection rule for SFG vibrational

spectroscopy. The normal mode must be both Raman and infrared active in order to be detected by SFG.

We can use Eq. (4) to obtain the susceptibility of a monolayer of molecules with the values of the infrared dipole transition moment, $\mu_q = < g | \mu | q >$ and the differential Raman scattering cross section, $d\sigma/d\Omega$, available from the literature.[28] The polarizability of Eq. (4) on resonance ($\omega_{ir} = \omega_q$) can be written approximately as

$$\alpha_R = \frac{c^2}{\hbar \omega_s^2} \frac{\mu_q}{\Gamma_q} \left(\frac{d\sigma}{d\Omega} \right)^{1/2}. \qquad (5)$$

As an example, we consider the symmetric stretch vibration of the CH_3 group. We have measured for a compact monolayer of CH_3 groups $\chi^D_{yyz} = 1\times10^{-15}$ esu.[14] From the literature we obtain the transition dipole moment $\mu_q \sim .05$D (1 Debye = 10^{-18} esu),[29] the differential Raman scattering cross section $d\sigma/d\Omega \sim 5.3\times10^{-30}$ $cm^2 sr^{-1}$,[28] and for the resonance width and peak position, $\Gamma_q \sim 10$ cm^{-1} and $\omega_q \sim 2875$ cm^{-1}, respectively. For our laser system, $\omega_v = 3.5\times10^{15}$ ($\lambda_v = .532\,\mu m$), therefore $\omega_s = 4.04\times10^{15}$ on resonance. Inserting these values into Eq. (5) we obtain $\alpha_R \sim 3.6\times10^{-30}$ esu. With $N = 5\times10^{14}$ cm^2, we obtain $\chi^D = 1.8\times10^{-15}$ esu, in reasonable agreement with the measured value. The difference might be explained by the explicit inclusion of the surface orientation distribution.

II. Information That Can Be Deduced From χ^D

The information obtainable from infrared-visible SFG is clear from an inspection of eqs.(3) and (4).

1) The surface vibrational spectrum is obtained from the resonance enhancement of the signal as ω_{ir} is tuned. The peak positions and widths can be used to identify

surface species and determine their interaction with the substrate and other molecules.[10,12-14,16]

2) Through the dependence of χ^D on N, the surface concentration of different adsorbate species can be monitored.[15,21]

3) The SFG signal contains a great deal of information about the adsorbate orientation distribution.[14,17,20,27] The non-zero components of $\chi^D{}_{ijk}$ are determined by α and the orientational distribution of the molecules. By using different polarization combinations of ω_1, ω_2 and ω_s, these susceptibility components can be measured. Then , with a model for α, important features of the orientation distribution can be deduced. SHG has been applied to obtain detailed information about the in-plane rotational symmetry of the distribution and the same capabilities are certainly present in SFG.[30] Since SFG detects vibrational modes, which are rather localized to specific groups of atoms within the molecule, one can obtain the relative orientation of different groups within the same molecule and hence deduce the molecular conformation.

4) In many cases, it is important to know the absolute orientation of the molecule with respect to the surface. Is the molecule pointing up or down? Since the polar orientation of the molecule determines the sign of the quantity $\langle G \rangle$, it is clear that in order to deduce this sign we need to measure the complex phase of χ^D. Since the experiment to obtain the SFG spectrum measures the intensity of the radiated field,and hence the absolute magnitude of χ^D, we need a separate experiment to determine its phase.[19,24] This will be the subject of chapter IV.

5) One of the most attractive features of SFG is the ability to probe dynamics on the picosecond time scale. All of the above quantities can be time dependent and many problems can be listed which would benefit from time resolved studies. Of particular interest is the time dependence of $\Delta\rho_{gq}$. After energy from the resonant infrared

beam is deposited in a normal mode, the vibrational energy will decay through various pathways, including surface phonons and other normal modes of the molecule. The lifetime of the excited state, which often can be deduced from the time dependence of the difference in the population of the ground and excited states, $\Delta\rho_{gq,}$ is the first step in understanding the dynamics of this energy transfer.[22,23,25,26]

6) The ability to fix the orientation of a molecule at the surface provides an opportunity to study properties of molecules that are usually unavailable in bulk studies either due to the isotropic averaging of the molecular quantity or due to the inherent limitations of standard techniques. For example, if the orientation of the molecule is known, then the sign of $\boldsymbol{\chi}^D$ can determine the sign of $\boldsymbol{\alpha}$, therefore providing the relative sign of $\partial\boldsymbol{\mu}/\partial Q$ and the Raman polarizability $\partial\boldsymbol{\alpha}^{(1)}/\partial Q$. If the sign of one is known by other means, then the sign of the other is determined. This is unique information since infrared absorption and Raman scattering measure the absolute magnitude of these quantities. This sign information can provide valuable insight into the charge distribution and dynamics in molecular bonds.[18]

III. Radiation from Surface Polarization

The polarization of a monolayer can be idealized as a sheet with dielectric constant $\varepsilon'(\omega)$ at the interface between media 1 and 2. The field radiated from this polarization sheet into medium 1 can be written as[3,31]

$$\mathbf{E}(r,t) = i\,2\pi\,\frac{\omega_s}{c}\,\frac{\sec\theta_s}{\sqrt{\varepsilon_1^{\,s}}}\,(\mathbf{L}_s\cdot\mathbf{e}_s\,\boldsymbol{\chi}^S:\mathbf{L}_1\cdot\mathbf{e}_1\;\mathbf{L}_2\cdot\mathbf{e}_2)\;E_1\,E_2\exp(i\mathbf{k}_{1s}\cdot\mathbf{r} - i\omega_s t) \qquad (6)$$

where $\varepsilon_1^{\,s}$ is the dielectric constant of medium 1 at ω_s, $\mathbf{e}_i$ and E_i are the unit vector and amplitude, respectively, for the field at ω_i, and θ_s and $\mathbf{k}_{1s}$ are respectively, the

angle with respect to the surface normal and the wavevector for the reflected sum frequency beam in medium 1. The wavevector $\mathbf{k}_{1s}$, and hence the collimated direction of the sum frequency signal, is given by the momentum conservation condition, $k_{s,x} = k_{1,x} + k_{2,x}$ where $k_{i,x}$ is the component of the wavevector of the field at ω_i that is parallel to the interface. The local field factors, $\mathbf{L}_i$, relate the incident field at ω_i in medium 1 to the field inside the polarization sheet. They are given by[3]

$$\mathbf{L}_{xx}(\omega) = \frac{2\,\varepsilon_1\,k_{2z}}{\varepsilon_2\,k_{1z} + \varepsilon_1\,k_{2z}} \tag{7a}$$

$$\mathbf{L}_{zz}(\omega) = \frac{2\,\varepsilon_1\,k_{1z}}{\varepsilon_2\,k_{1z} + \varepsilon_1\,k_{2z}} \left(\frac{\varepsilon_2}{\varepsilon'}\right) \tag{7b}$$

$$\mathbf{L}_{yy}(\omega) = \frac{2\,k_{1z}}{k_{1z} + k_{2z}} \tag{7c}$$

where the dielectric constants and wavevectors are evaluated at the frequency ω. With the convention that the physical quantities are given by adding the complex quantities to their complex conjugates, we have the sum frequency intensity I given by $I(\omega_s) = (c\,\sqrt{\varepsilon_1^s}/2\pi)\ |E(\omega_s)|^2$ and the signal, in photons per pulse is given by

$$S(\omega_s) = 8\pi^3 \frac{\omega_s\ \sec^2\theta_s}{\hbar\, c^3\, (\varepsilon_1^s \varepsilon_1^1 \varepsilon_1^2)^{1/2}} |\mathbf{e'}_s \cdot \boldsymbol{\chi}^S : \mathbf{e'}_1\, \mathbf{e'}_2|^2 \frac{U_1\,U_2}{AT} \tag{8}$$

where $\mathbf{e'}_i = \mathbf{L}_i \cdot \mathbf{e}_i$, U is the energy per pulse for the beam at frequency ω_i, and A and T are the beam overlap area and temporal pulse width, respectively. As an example of the signal for a typical experiment, we use the parameters of our laser system. Typical energies of the laser pulses at the surface are .5 mj in the visible at .532μm

and 100μj in the infrared. The pulses are about 20ps. in duration and are focused at the surface to a beam spot 400μm in diameter. For a dielectric interface, with the laser beams incident at ~45°, the local field factors are of order unity. The susceptibility on resonance for a compact monolayer of CH_3 groups is ~10^{-15} esu. From Eq. (8) we then have signal of about 500 photons per pulse from the sample. With a detection efficiency of ~2% and a photomultiplier tube dark count rate of ~.1 photon /pulse, we have a signal to noise ratio of approximately 10^4. This implies that we should be able to detect 1% of a monolayer without difficulty. The experimental setup and practical issues will be discussed in the following section.

IV. Interface and Bulk Multipole Contributions

The above discussion has focused on the case of an adsorbed monolayer at the surface, ignoring the nonlinearity of the substrate. The actual physical situation can be considerably more complicated. First of all, the surface molecules might have polar ordering over several layers. Secondly, the discontinuities of the fields and the susceptibilities at the interface oblige us to consider higher order multipole contributions to the interface susceptibility.[32-34] Lastly, we must consider the nonlinearity of the bulk, especially in the cases where the bulk has resonances at frequencies similar to the surface molecules.[35,36] Such will be the case in our experiments studying the surface of pure liquids where the interface and bulk are distinguished only by the possible ordering present at the surface. In the following we will discuss each of these contributions to the measured nonlinearity, paying particular attention to strategies for separating the interesting surface dipole contribution from those due to multipole susceptibilities.

In general, we can define an effective polarization which contains the dipole and multipole polarizations[35]

$$\mathbf{P}_{eff}^{(2)} = \mathbf{P}^{(2)}(\omega_s) - \nabla \cdot \mathbf{Q}^{(2)}(\omega_s) - \frac{c}{i\omega_s} \nabla \times \mathbf{M}^{(2)}(\omega_s) \tag{9}$$

which in turn can be expanded in a series of higher order derivatives of the applied fields

$$\mathbf{P}^{(2)} = \boldsymbol{\chi}^{D} : \mathbf{E}_1 \mathbf{E}_2 + \boldsymbol{\chi}^{P} : \nabla \{\mathbf{E}_1(\omega_1) \mathbf{E}(\omega_2)\} \tag{10a}$$

$$\mathbf{Q}^{(2)}(\omega_s) = \boldsymbol{\chi}^{Q} : \mathbf{E}_1 \mathbf{E}_2 \tag{10b}$$

$$\mathbf{M}^{(2)}(\omega_s) = \boldsymbol{\chi}^{M} : \mathbf{E}_1 \mathbf{E}_2 \tag{10c}$$

We have kept terms that contribute to the effective polarization up to the first order derivative in the fields. The microscopic expressions for the multipolar susceptibilities have been discussed in the literature.[8,37,38] Each susceptibility corresponds to the replacement of one of the electric dipole operators in Eq. (2) with an electric quadrupole or magnetic dipole operator. The nonzero elements of these susceptibilities are then determined by the requirement that they be consistent with the symmetries of the medium with respect to spatial symmetry operations and time reversal.[39] The term $\boldsymbol{\chi}^{D}$, which is of greatest interest for surface studies, is a polar third rank tensor and is therefore necessarily zero in the bulk of media with inversion symmetry. This is the fundamental reason for the unique surface specificity of the second order non-linear optical processes. The remaining terms, including the polar fourth rank tensors $\boldsymbol{\chi}^{P}$ and $\boldsymbol{\chi}^{Q}$, and the axial third rank tensor $\boldsymbol{\chi}^{M}$ are not forbidden by any crystal symmetry. These higher order terms are responsible for the interface and bulk multipole contribution to the total signal radiated from the interface between two media with inversion symmetry. The effective polarization can then be written as

$$\mathbf{P}_{eff}^{(2)} = \boldsymbol{\chi}^{D} : \mathbf{E}_1 \mathbf{E}_2 + \boldsymbol{\chi}^{P} : \nabla \{\mathbf{E}_1(\omega_1)\, \mathbf{E}(\omega_2)\} - \nabla \cdot \{\boldsymbol{\chi}^{Q} : \mathbf{E}_1 \mathbf{E}_2\} \qquad (11)$$

where, for simplicity, we have left out the magnetization term since it always appears in the following discussion along with the electric quadrupole terms. Therefore, it neither simplifies nor significantly complicates the problem of separating the surface dipole and quadrupole contributions.

We now break the sample into two regions, the interface and the bulk. The interfacial region can be simply defined as the distance over which the susceptibilities and the fields are different from their bulk values. Since the interfacial region is usually on the order of a few molecular diameters, much smaller than the wavelength of the fields, the nonlinearity of the interface radiates as a polarization sheet with a polarization given by[3,33]

$$P_{eff,i}^{s} = \eta_i(\omega_s) \int_I s_i(z)\, P_{i,eff}(z)\, dz \qquad (12)$$

where $\eta_i = 1$ for i = x,y and $\eta_z = \varepsilon'$. From the solution of the boundary value problem for three wave mixing , it can be shown that the bulk contribution will also radiate as a surface sheet with an effective polarization given by[40]

$$P_{eff,i}^{b} = i\, L_c\, P^{B}_{i}\, f_i^{-1}(\omega_s) \qquad (13)$$

where $f_i = 1$ for i = x,y and $f_z(\omega) = \varepsilon_2(\omega)/\varepsilon'(\omega)$. The coherence length L_c, the distance of coherent interaction between the polarization and radiating electromagnetic wave in the bulk, is given by $L_c = (k_{z,1} + k_{z,2} \pm k_{z,s})^{-1}$, with the plus sign for the reflected signal and the minus sign for transmission.

It is convenient to describe the fields by $E_i(z) = s_i(z,\omega_i)\eta_i F_i \exp(i\mathbf{k}\cdot\mathbf{r}-i\omega t)$ where $s_i = 1$ for i = x,y and $s_z = E_z(z) / D_z$, D_z is the z-component of the displacement field at the interface and $F_i = E_i$ for i = x,y and $F_z = D_z/\varepsilon'$. We see that F_i and η_i are continuous through the interface and that the rapid variation of the fields at the interface due to the change of the linear dielectric constants is contained in the z-dependence of s_z which becomes constant ($s_z = \varepsilon^{-1}$) in the bulk. In the interfacial region, the spatial derivatives in Eq. (11) act on the fields through $s(z,\omega)$ as well $\boldsymbol{\chi}^Q$, whereas in the bulk, the only nonzero derivative is on the fields through the exponential factor. Using Eqs. (12) and (13) we can directly compare the interface and bulk contributions to the radiated signal. This can be taken one step further by expressing these contributions in terms of interface and bulk susceptibilities through the relation $\chi^{s,b}_{ijk} \equiv P_{eff,i}^{s,b} / F_j(\omega_1) F_k(\omega_2)$. Though the route to this expression may appear unnecessarily tortuous, it is useful in that we now have a susceptibility that describes the nonlinear response integrated through the interface.[32] The original definition of the nonlinear susceptibility, Eq. (1), would have in detail a z-dependence. In addition, the use of $\chi^{s,b}_{ijk}$ permits all of the contributions, interface and bulk, to be compared to each other without the field amplitudes, which is proper since all terms are quadratic in the fields.

We can obtain the effective surface susceptibility, $\boldsymbol{\chi}^s$, by inserting the definition for $\mathbf{P}_{eff}$, Eq. (11), into Eq. (12),

$$\chi^{s}_{ijk} = \eta_i \int_I \Big(\chi^{D}_{ijk}\, s_i(\omega_s)\, s_j(\omega_1)\, s_k(\omega_2) + \chi^{P}_{iizz}\, s_i(\omega_s) \frac{d}{dz}\big(s_j(\omega_1)\, s_k(\omega_2)\big) + \\ + s_i(\omega_s) \frac{d}{dz} \big(\chi^{Q}_{izjk}\, s_j(\omega_1)\, s_k(\omega_2)\big) \Big) dz \qquad (14)$$

The last term can be evaluated as

$$\int_I s_i(\omega_s)\frac{d}{dz}(\chi^{Q}_{izjk}\, s_j(\omega_1)\, s_k(\omega_2))\, dz = \int_I \chi^{Q}_{izjk}\frac{d}{dz}(s_i(\omega_s))\, s_j(\omega_1)\, s_k(\omega_2)\, dz + \left(\{\chi^{Q}_{izjk}\, s_i(\omega_s)\, s_j(\omega_1)\, s_k(\omega_2)\}_{z=0^-} - \{\chi^{Q}_{izjk}\, s_i(\omega_s)\, s_j(\omega_1)\, s_k(\omega_2)\}_{z=0^+} \right) \quad (15)$$

So, finally, we have for the effective surface susceptibility

$$\chi^{s}_{ijk} = \eta_i \int_I \left(\chi^{D}_{ijk}\, s_i(\omega_s)\, s_j(\omega_1)\, s_k(\omega_2) + \chi^{Q}_{izjk}\frac{d}{dz}(s_i(\omega_s))\, s_j(\omega_1)\, s_k(\omega_2) + \right.$$
$$\left. + \chi^{P}_{iizz}\, s_i(\omega_s)\frac{d}{dz}(\, s_j(\omega_1)\, s_k(\omega_2)) \right) dz +$$
$$+\eta_i \left(\{\chi^{Q}_{izjk}\, s_i(\omega_s)\, s_j(\omega_1)\, s_k(\omega_2)\}_{z=0^-} - \{\chi^{Q}_{izjk}\, s_i(\omega_s)\, s_j(\omega_1)\, s_k(\omega_2)\}_{z=0^+} \right). \quad (16)$$

where the z-dependence of the function s is implicit. The first term is a generalization from the earlier expression of the dipole susceptibility from a single monolayer. Here we see that it is the total integrated susceptibility that is measured so, for example, two layers with $\chi^{D}(z)$ of opposite sign, as might occur in two oppositely oriented molecular monolayers, will cancel each other. Secondly, since $s_z(z,\omega) \cong \varepsilon^{-1}(z,\omega)$ where ε is the linear dielectric constant, layers of χ^{D} with large dielectric constants will have a reduced contribution due to the screening of the fields.

The second and third terms of Eq. (16) are due to the rapid change in the fields through the interface as described by the function $s(z,\omega_i)$. These terms are surface terms because any modification of the surface will in principle change both the susceptibilities and the functions $s(z,\omega)$. In addition , it is clear that the integrand is nonzero only over the short distance at the interface where the linear dielectric function is changing.

In contrast, the last two terms represent a bulk contribution.[34] These terms arise from the divergence acting on the quadrupole susceptibility χ^Q (Eq. (11)), which produces a radiating polarization from the interfacial region where the quadrupole susceptibility is changing. However, since the effective surface polarization is an integral of the effective polarization through the interface (Eq. (12)), the net result is the difference in the bulk quadrupole susceptibilities for the two media. This contribution should then be considered a bulk term in that it is insensitive to the modification of the surface.

Lastly, we treat the contribution arising from the bulk polarization. This has been discussed in the literature since the earliest papers on non-linear optics.[35,41] Here our concern is with isolating or eliminating this contribution to the SFG signal. The bulk polarization for an isotropic medium, to be inserted in eq.(7) is written as

$$\mathbf{P}^B_i = A_1 (\mathbf{E}_2 \cdot \nabla) E_{1i} + A_2 (\mathbf{E}_1 \cdot \nabla) E_{2i} + B_1 (\nabla \cdot \mathbf{E}_1) E_{2i} + B_2 (\nabla \cdot \mathbf{E}_2) E_{1i} + \\ + C_1 E_{2j} \nabla_i E_{1j} + C_2 E_{1j} \nabla_i E_{2j} \qquad (17)$$

where A, B and C are scalars which are simple linear combinations of components of the susceptibilities χ^P, χ^Q, and χ^M. Immediately we can see that, with the plane wave approximation in an isotropic medium, the third and fourth terms will not contribute since $\nabla \cdot \mathbf{E}=0$. For the four remaining terms to vanish simultaneously, we require $\mathbf{E}^1 \perp \mathbf{E}^2$, $\mathbf{E}^1 \perp \mathbf{k}^2$ and $\mathbf{E}^2 \perp \mathbf{k}^1$, all of which can be accomplished with orthogonally polarized collinear beams. In general, for non-collinear beams, one of the terms will always be nonzero.[35] For example, in the case of two non-collinear beams with the same plane of incidence, if the input beam polarizations are $\mathbf{E}^1$ - s polarized and $\mathbf{E}^2$ - p polarized, then the A_1 term is non-zero and the output sum

frequency is s polarized. The effective susceptibility to be directly compared with the effective surface susceptibilities of Eq.(16) can be written as

$$\chi^{b}_{yyz} = L_c\, k_v\, (\varepsilon_2(\omega_{ir}) \sin\theta_{ir})^{-1}\, (\chi^{P}_{yzzy} - \chi^{Q}_{zyyz})\, \sin(\theta_v - \theta_{ir}) \qquad (18)$$

We note, however, that the multipole susceptibilities that appear in the constants in the expression for the bulk polarization, Eq. (17), do not have the same values as the susceptibilities that appear in the interface terms of Eqs. (14 - 16). For example, the interface susceptibilities have the symmetry of the interface, while the bulk susceptibilities assume the symmetry of the interior of the medium. For a molecular system, an expression similar to Eq. (3) holds relating the multipole susceptibilities to the multipolar polarizabilities and the difference between the surface and bulk values in the simplest case is due to the difference in the orientational distributions of the bulk and interface. In addition, the resonant frequencies of the interface and bulk multipole susceptibilities can be different.

We will now discuss strategies for separating the various contributions to the nonlinear signal radiated from an interface. We write these contributions as

$$\boldsymbol{\chi}^{(2)} = \boldsymbol{\chi}^{D} + \boldsymbol{\chi}^{I} + \boldsymbol{\chi}^{SB1} + \boldsymbol{\chi}^{SB2} \qquad (18)$$

where $\boldsymbol{\chi}^{D}$ is the surface dipole term, $\boldsymbol{\chi}^{I}$ is the interface quadrupole term due to the field gradients at the surface, $\boldsymbol{\chi}^{SB1}$ is the bulk quadrupole term due to the discontinuity of the quadrupole susceptibility at the interface and $\boldsymbol{\chi}^{SB2}$ is responsible for the bulk multipole polarization. In the following, we list the various experimental approaches for separating these terms along with the susceptibilities that they potentially isolate.

1) Comparing SFG and traditional bulk spectra; χ^{SB1} and χ^{SB2} : The resonances of the bulk and surface in many cases will be different. The bulk resonances are easily measured using standard transmission techniques such as infrared absorption or Raman scattering. If an SFG resonance does not coincide with a bulk resonance, then it is clearly a surface feature. This is the most definitive way of assigning a spectral feature to surface species.

2) Modifying the surface; χ^{D}, χ^{I} : The first two terms, χ^{D} and χ^{I} are surface terms and will possibly change upon modification of the surface. The change of the SFG signal accompanying this modification can then be positively identified with a change in these susceptibilities. However, a model for the interface susceptibility is then needed to determine the full value for the surface and bulk susceptibilities.

3) Varying the dielectric discontinuity; χ^{I} : This term depends on the field gradient at the interface, which, in the simplest model of a linear dielectric function connecting the bulk dielectric constants across the interface, can be written as

$$\chi^{I}_{yyz} = \int_{I} \chi^{P}_{yyzz} \frac{d}{dz}\left(s_k(\omega_2)\right) dz = \left(\chi^{P}_{yyzz}\right)_{ave} \left(\frac{1}{\varepsilon_1(\omega_2)} - \frac{1}{\varepsilon_2(\omega_2)}\right) \qquad (18)$$

where the first term is the average of the quadrupole susceptibility through the interface and ε_1 and ε_2 are the dielectric constants of medium 1 and 2, respectively. In some instances, such as in the case of strongly adsorbed molecules on a substrate, the dielectric constant on one side of the interface can be changed without altering the molecules at the surface. Then, a linear dependence of χ^{S} on ε_1^{-1} can be attributed to the interface susceptibility, χ^{I}.[20,33]

4) Comparing SFG in transmission and reflection geometries; χ^{SB2} : The bulk susceptibility χ^{SB2} depends linearly on the coherence length, L_c (Eq. (13)), which can differ by over two orders of magnitude between the two geometries. Meanwhile, the

surface susceptibilities, χ^D and χ^I, as well as the bulk term χ^{SB1} do not change appreciably. The difference in the signal in the two geometries can then be directly related to χ^{SB2}.[20]

5) Polarization dependence of signal; ? : By varying the input and output beam polarizations, different components of χ^S can be accessed. Unfortunately, for an isotropic interface, this does not help us separate the susceptibility contributions. There is no polarization combination that measures a component of χ^D without a contribution from each of the susceptibilities χ^I, χ^{SB1} and χ^{SB2}. In this case, symmetry considerations demand that for a nonzero component $\chi_{D,ijk}$, at least one of the indices be equal to z. However, from Eq. (16), this is also the condition for a nonzero χ^I and χ^{SB1} because of the gradient of the fields and the quadrupole susceptibility with respect to the surface normal. It can also be shown that χ^{SB2} will appear in all of the polarization geometries that measure a component of χ^D. Conversely, there is no polarization combination for which only χ^I, χ^{SB1} or χ^{SB2} are nonzero.

We can further ask whether the symmetries of the quadrupole and dipole susceptibilities will be different. The spatial symmetries of the susceptibilities depend on the symmetries of the media and on the permutation symmetries that might be applicable. To understand the permutation symmetries of the quadrupole susceptibilities, we can write the microscopic expressions

$$\chi^{P1}_{ijlk} = \frac{N}{\hbar^2} \frac{\langle q|\mu_j|g\rangle}{(\omega_{ir} - \omega_q + i\Gamma_q)} \sum_n \left(\frac{\langle g|\mu_i|n\rangle\langle n|Q_{lk}|q\rangle}{(\omega_s - \omega_{ng})} - \frac{\langle g|Q_{lk}|n\rangle\langle n|\mu_i|q\rangle}{(\omega_s + \omega_{nq})} \right)$$

$$\chi^{P2}_{ijlk} = \frac{N}{\hbar^2} \frac{\langle q|Q_{lk}|g\rangle}{(\omega_{ir} - \omega_q + i\Gamma_q)} \sum_n \left(\frac{\langle g|\mu_i|n\rangle\langle n|\mu_j|q\rangle}{(\omega_s - \omega_{ng})} - \frac{\langle g|\mu_j|n\rangle\langle n|\mu_i|q\rangle}{(\omega_s + \omega_{nq})} \right)$$

$$\chi^{Q}_{ijkl} = \frac{N}{\hbar^2} \frac{\langle q|\mu_l|g\rangle}{(\omega_{ir} - \omega_q + i\Gamma_q)} \sum_n \left(\frac{\langle g|Q_{ij}|n\rangle\langle n|\mu_j|q\rangle}{(\omega_s - \omega_{ng})} - \frac{\langle g|\mu_j|n\rangle\langle n|Q_{ij}|q\rangle}{(\omega_s + \omega_{nq})} \right)$$

where **Q** is the electric quadrupole operator, $\boldsymbol{\chi}^{P1}$ and $\boldsymbol{\chi}^{P2}$ are the quadrupole susceptibilities applicable when the gradient in Eq. (10a) is taken sequentially on the fields $\mathbf{E}_1$ and $\mathbf{E}_2$, respectively. In addition, the prime on the functions $s(\omega)$ indicates a derivative with respect to z, the surface normal. It can be seen that if ω_s is much less than the lowest electronic excitation and $\omega_{ng} \sim \omega_{nq}$, then $\boldsymbol{\chi}^{P1}_{ijlk} = \boldsymbol{\chi}^{Q}_{lkij}$. If we then define the interface quadrupole susceptibility as

$$\chi^{I}_{ijk} = \int_{I} \Big(\delta_{zj}\, \chi^{P1}_{ikzz}\, s_i(\omega_s) s'_z(\omega_v) s_k(\omega_{ir}) + \delta_{zk}\, \chi^{P2}_{ijzz}\, s_i(\omega_s) s_j(\omega_v) s'_z(\omega_{ir}) + \\ + \delta_{zi}\, \chi^{Q}_{zzjk}\, s'_z(\omega_s) s_j(\omega_v) s_k(\omega_{ir}) \Big)\, dz$$

it can be shown that $\chi^{I}_{ijk} = \chi^{I}_{jik}$. Under these same conditions, Kleinman symmetry holds for the dipole susceptibilty and $\chi^{D}_{ijk} = \chi^{D}_{jik}$. Therefore, both the quadrupole and dipole susceptibilities have the same symmetry relations amongst their components. This means that the dipole or quadrupole origin of the interface signal cannot be separated based on the symmetries of the effective surface susceptibilty tensor.

6) Measurement of the phase of $\boldsymbol{\chi}^{S}$; no information : We have discussed earlier how a measurement of the phase of $\boldsymbol{\chi}^{D}$ can be used to determine the absolute orientation of a surface molecule. Can a phase measurement allow us to separate $\boldsymbol{\chi}^{D}$ from the multipole susceptibilities? Unfortunately, the answer is no. As stated previously, the quadrupole susceptibilities are obtained by replacing one of the dipole operators, $\boldsymbol{\mu}$, in Eq. (2) with a quadrupole operator, **q**. For real wave functions, both $\boldsymbol{\mu}$ and **q** have real matrix elements.[8] Therefore, for each of $\boldsymbol{\chi}^{D}$, $\boldsymbol{\chi}^{P}$ and $\boldsymbol{\chi}^{Q}$, their non-resonant components will be real quantities while their resonant components will be pure imaginary at an isolated resonant peak. To compare how

each of these susceptibilities contributes to the radiated field, we refer to the effective surface susceptibilities evaluated in Eq. (16). Here we see that if each of the susceptibilities are in quadrature, then so are their corresponding terms in the effective surface susceptibility. The same is true for the bulk polarization as can be seen in Eq. (18). As for the magnetic dipole contributions, it can be shown that the susceptibility always enters expressions similar to those of the quadrupole susceptibilities through the term $i\chi^M/\omega c$ (see Eq. (9)). Since the matrix elements of the magnetic dipole operator are imaginary for real wavefunctions, these terms will again be in quadrature with the quadrupole terms. Therefore, a measurement of the phase of the surface susceptibility will not provide us with information to separate the surface dipole and multipole contributions.

At this point, we'd like to consider the relative magnitude of the multipole susceptibilities with respect to each other and in comparison with the surface dipole term. For the bulk polarization contribution, $|\chi^B| \sim L_c\, k\, g\, \chi^{MP}/\varepsilon$ where g is a geometrical factor depending on the angles of incidence of the input beams and χ^{MP} is some average multipole susceptibility. Assuming g~1 (it can be much smaller) and the reflection geometry ($L^R_c \sim k^{-1}$), we have $|\chi^B| \sim \chi^{MP}/\varepsilon$. The interface multipole term has the same physical origin as the bulk polarization: it is due to the gradient of the fields. Although the interface field gradient is larger than the bulk field gradient by a factor λ/d where d is the interface thickness, the ratio of the effective thickness of material that contributes in the two cases is $\sim \lambda/d$. This cancelation of factors, along with an inspection of χ^{SD}, shows that the multipole contributions, bulk and interface, are all of order χ^{MP}/ε. How does this compare with the surface dipole contribution χ^D/ε ? In order for the surface contribution to be comparable to the bulk we require, from Eq. (3), $N_s\alpha^D \geq N_b\alpha^{MP}$ where $N_s \sim a^{-2}$ and $N_b \sim a^{-3}$ are the

surface and bulk densities, respectively, and a is the dimension of the molecule, and we have applied Eq. (3) to the multipolar susceptibilities. Since $\alpha^D/\alpha^{MP} \sim 1/r$, with r being an average electron delocalization in the molecule, we have $N_s\alpha^D / N_b\alpha^{MP} \sim a / r$. This quantity is larger than or of order unity so we can expect the surface dipole term to be at least as large as the bulk contribution and possibly dominate in cases of significant surface polar ordering.

In conclusion, we have reviewed the theory of sum frequency generation from an interface, with particular attention paid to the interfaces between media with inversion symmetry. The information obtainable from SFG includes molecular orientation, conformation and interaction, as well as surface density and in plane rotational symmetry of orientation distribution. The unique surface specificity of SFG makes it particularly valuable as a probe of interfaces where the bulk media has resonances similar to those of the interface. In the case where the interface is bounded by centrosymmetric media, the bulk surface dipole contributions are necessarily zero, and the multipole contributions must be considered. We have examined the strategies available for deducing the surface dipole contribution to the total signal from the interface, and have shown from general considerations that it is likely to be at least as large as the multipole contrbutions.

References

[1] Y. R. Shen, Annu. Rev. Mat. Sci. 16, 69 (1986).

[2] Y. R. Shen, Nature, 337, 519 (1989).

[3] Y. R. Shen, Annu. Rev. Phys. Chem. 40, 327 (1989).

[4] For the earliest experiments of this effect see R. W. Terhune, P. D. Maker, and C. M. Savage, Phys. Rev. Lett. 8, 404 (1962); J. A. Giordmaine in *Proceedings of the Third Conference on Quantum Electronics*, P. Grivet and N. Bloembergen, eds. (Columbia University Press, New York, 1964).

[5] N. Bloembergen and P. S. Pershan, Phys. Rev. **128**, 606 (1962).

[6] Y. R. Shen, The Principles of Nonlinear Optics (Wiley, New York, 1984) Chs 6,25.

[7] J. A. Armstrong, N. Bloembergen, J. Ducuing, and P. S. Pershan, Phys. Rev. **127**, 1918 (1962).

[8] E. Adler, Phys. Rev. 134, A728, (1964).

[9] Y. R. Shen, Ref. 6, p. 171.

[10] X. Zhu, Ph. D. Thesis, University of California, 1989, unpublished.

[11] the first attempt was reported in H. W. K. Tom, Ph. D. Thesis, University of California, 1984, unpublished.

[12] X. D. Zhu, H. Suhr, and Y. R. Shen, Phys. Rev. B **35**, 3047 (1987).

[13] J. H. Hunt, P. Guyot-Sionnest, and Y. R. Shen, Chem. Phys. Lett. **133**, 189 (1987).

[14] P. Guyot-Sionnest, J. H. Hunt, and Y. R. Shen, Phys. Rev. Lett. **59**, 1597 (1988).

[15] P. Guyot-Sionnest, R. Superfine, J. H. Hunt and Y. R. Shen, Chem. Phys. Lett. **144**, 1 (1988).

[16] R. Superfine, P. Guyot-Sionnest, J. H. Hunt, C. T. Kao, and Y. R. Shen, Surf. Sci. **200**, L445 (1988).

[17] J. Y. Huang, R. Superfine and Y. R. Shen, Phys. Rev. B, **42**, 3660 (1990).

[18] R. Superfine, J. Y. Huang and Y. R. Shen, Chem. Phys. Lett. **172**,303 (1990).

[19] R. Superfine, J. Y. Huang and Y. R. Shen, Opt. Lett. **15**, 1276 (1990).

[20] R. Superfine, J. Y. Huang and Y. R. Shen, Phys. Rev. Lett. **66**, 1066 (1991)

[21] P. Guyot-Sionnest and A. Tadjeddine, J. Chem. Phys. (1990).

[22] P. Guyot-Sionnest, P. Dumas, Y. J. Chabal and G. S. Higashi, Phys. Rev. Lett. **64**, 2156 (1990).

[23] P. Guyot-Sionnest, Phys. Rev. Lett. **66**,1489 (1991).

[24] A. L. Harris, C. E. D. Chidsey, N. J. Levinos, and D. N. Loicono, Chem. Phys. Lett. **141**, 350 (1987).

[25] A. L. Harris, and N. J. Levinos, J. Chem. Phys. **90**, 3878 (1989).

[26] A. L. Harris, L. Rothberg, L. H. Dubois, N. J. Levinos, and L. Dhar, Phys. Rev. Lett. **64,** 2086 (1990) ; A. L. Harris and L. Rothberg, J. Chem. Phys. **94**,2449 (1991); A. L. Harris, L. Rothberg, L. Dhar, N. J. Levinos, L. H. Dubois, J. Chem. Phys. **94**,2438 (1991).

[27] J. Miragliotta, R. S. Polizzotti, P. Rabinowitz, S. D. Cameron and R. B. Hall, Chem. Phys. **143**, (1990).

[28] H. W. Schrotter and H. W. Klockner, in *Raman Spectroscopy of Gases and Liquids*, A. Weber, ed. (Springer-Verlag, Berlin, 1979).

[29] R. G. Snyder, J. Chem. Phys., **42**, 1744 (1963).

[30] W. Chen, M. Feller, and Y. R. Shen, Phys. Rev. Lett. **63**, 2665 (1989).

[31] T. Heinz, Ph. D. Thesis, University of California, 1982, unpublished.

[32] P. Guyot-Sionnest, W. Chen, and Y. R. Shen, Phys. Rev. B **33**, 8254 (1986).

[33] P. Guyot-Sionnest and Y. R. Shen, Phys. Rev. B **35**, 4420 (1987).

[34] P. Guyot-Sionnest and Y. R. Shen, Phys. Rev. B **38**, 7985 (1988).

[35] N. Bloembergen, R. K. Chang, S. S. Jha, and C. H. Lee, Phys. Rev. **174**, 813 (1968).

[36] P. S. Pershan, Phys. Rev. **130**,919 (1963).

[37] D. C. Hanna, M. A. Yuratich, and D. Cotter, Nonlinear Optics of Free Atoms and Molecules, Springer series in Optical Sciences 17 (Springer-Verlag, Berlin, 1979).

[38] D. S. Bethune, R. W. Smith, and Y. R. Shen, Phys. Rev. A **17**,277 (1978).

[39] L. D. Barron, Molecular Light Scattering and Optical Activity, (Cambridge University Press, Cambridge, 1982) Ch. 4.

[40] H. W. K. Tom, Ph. D. Thesis, University of California, 1984, unpublished.

[41] F. Brown and R. E. Parks, Phys. Rev. Lett. **16**, 507 (1966); N. Bloembergen, R. K. Chang, and C. H. Lee, Phys. Rev. Lett. 16, 986 (1966).

II. Infrared -Visible Sum Frequency Generation: Theory and Practice

B. Practice

In this section we will describe our experimental setup, Fig. 1, for measuring infrared - visible SFG.[1] The oscillator is a Nd:YAG laser with a repetition rate of 10 Hz that is both actively and passively modelocked.[2] The active modelocking is accomplished by an acoustooptic modulator while a flowing dye cell containing Kodak Q-Switch I provides the passive modelocking. This combination provides an ouput pulse train containing approximately 8 pulses FWHM, total energy of 7 mj, with each pulse having a duration of about 35 picoseconds. The largest pulse of the pulse train, selected out by a high speed pockels cell, is then amplified in a two stage amplifier to 20 mj. The beam is then split with 4 mj. of the 1.064 μm light used to produce the visible pulse at .532 μm and the rest used to generate the tunable infrared light.

The visible pulse is generated by frequency doubling the 4 mj pulse in a KD*P crystal using type II phase matching.[3] In practice, we have a conversion efficiency of about 25% and produce about 1mj of .532 μm light. This pulse is then directed onto the sample through a focusing lens, a polarizer and finally a half wave plate to adjust the beam polarization. The rest of the amplified pulse is directed to a two stage optical parametric amplifier which uses $LiNbO_3$ crystals to obtain infrared radiation tunable between 1.4 and 4.0 μm.[4] The OPA is tuned by rotating the $LiNbO_3$ crystals with respect to the beam propagation axis, thereby selecting the infrared frequency according to the phase matching conditions of the crystal. The output energy of the infrared pulses is approx. 400 μj at 3000 cm^{-1} falling to about 200 μj at 3800 cm^{-1}. The infrared pulse then propagates through a Ge brewtser window to filter out the short wavelength beam that is simultaneously generated in the OPA, then a pair of

ZnSe fresnel rhombs acting as a half wave plate for control of the polarization, and finally a focusing lens. The focusing is usually adjusted depending on the concerns of the particular experiment, such as heating effects or alignment sensitivity, but the spot size is usually between 200 and 500 μm in diameter.

The most important part of the detection system, Fig. 2, consists of irises used as spatial filters to block the reflected and scattered light at .532 μm. This is very effective because, unlike spontaneous Raman scattering, the SFG beam radiated from the surface is coherent and therefore highly collimated. Furthermore, it is necessary to spectrally filter the output to remove the remaining scattered .532 μm light. This is accomplished with low pass optical filters and, optionally, a monochromator. The filters typically have a transmittance of 10^{-5} at .532 μm and 70% at the sum frequency wavelength around .455 μm. The monochromator is most useful to check for the presence of flourescence in the scattered light. This can be the most serious problem in degrading the signal to noise ratio (SNR) of the detection system since the flourescence can occur within the frequency band of the SFG signal. After optimizing the spatial filtering to where the accepted solid angle of the detection system equals that of the SFG beam, the SNR can be improved only by narrowing the frequency bandpass of the system to that of the SFG signal. Flourescence was the largest noise source for the liquid surface experiments from methanol and water. Whereas the photomultiplier dark counts was about 1 count in 1000 laser pulses, the flourescence could contribute noise around 40 times larger. Eventually, very careful spatial filtering close to the sample reduced this noise down to about 4 counts in 1000 pulses.

In the cases when a measurement of the polarization of the SFG beam is required, a polarizer is inserted, usually before the spectral filtering. Finally, the SFG signal is detected with a photomultiplier tube. Overall, the detection system

can provide detection efficiencies of over 5%. According to our earlier estimate of the SFG signal level, this should allow us to detect surface molecules at 1% monolayer coverages, in the case where the photomultiplier dark counts dominate the noise.

References

[1] J. H. Hunt, Ph. D. Thesis, University of California, 1988, unpublished.

[2] H. P. Kortz, IEEE J. Quant. Electr. **QE-19**, 578 (1983).

[3] Y. R. Shen, *The Principles of Nonlinear Optics* (Wiley, New York, 1984).

[4] A. Laubereau, L. Greiter and W. Kaiser, Appl. Phys. Lett. **25**, 87, (1974); A. Seilmeier and W. Kaiser, Appl. Phys. **23**, 113 (1980); W. Kranitzky, K. Ding, A. Seilmeier, and W. Kaiser, Opt. Comm. **34**, 483 (1980).

Figure Captions"

Fig. 1. Laser setup including active-passive modelocked laser producing 35 ps pulses at a repetition rate of 10Hz. A single pulse is selected from the Q-switched pulse train with a fast pockels cell in combination with crossed polarizers. The single pulse is amplified in amplifier #1 then double passed through amplifier #2 to obtain 20mj .About 4mj is split off to be doubled in the KD*P crystal to produce about 1mj of .532μm light . The rest is sent to a dual crystal $LiNbO_3$ optrical parametric amplifier to produce infrared pulses of approximately 300μj tunable from 2700 to 3900 cm^{-1}.

Fig. 2. Setup close to sample. After final turning mirror, visible beam goes through polarizer and then halfwave plate to control polarization at sample. Infrared beam goes through Fresnel rhomb which serves as a broadband half wave plate and then a focusing lens. Beams are overlapped on sample to a spot size about 400μm in diameter

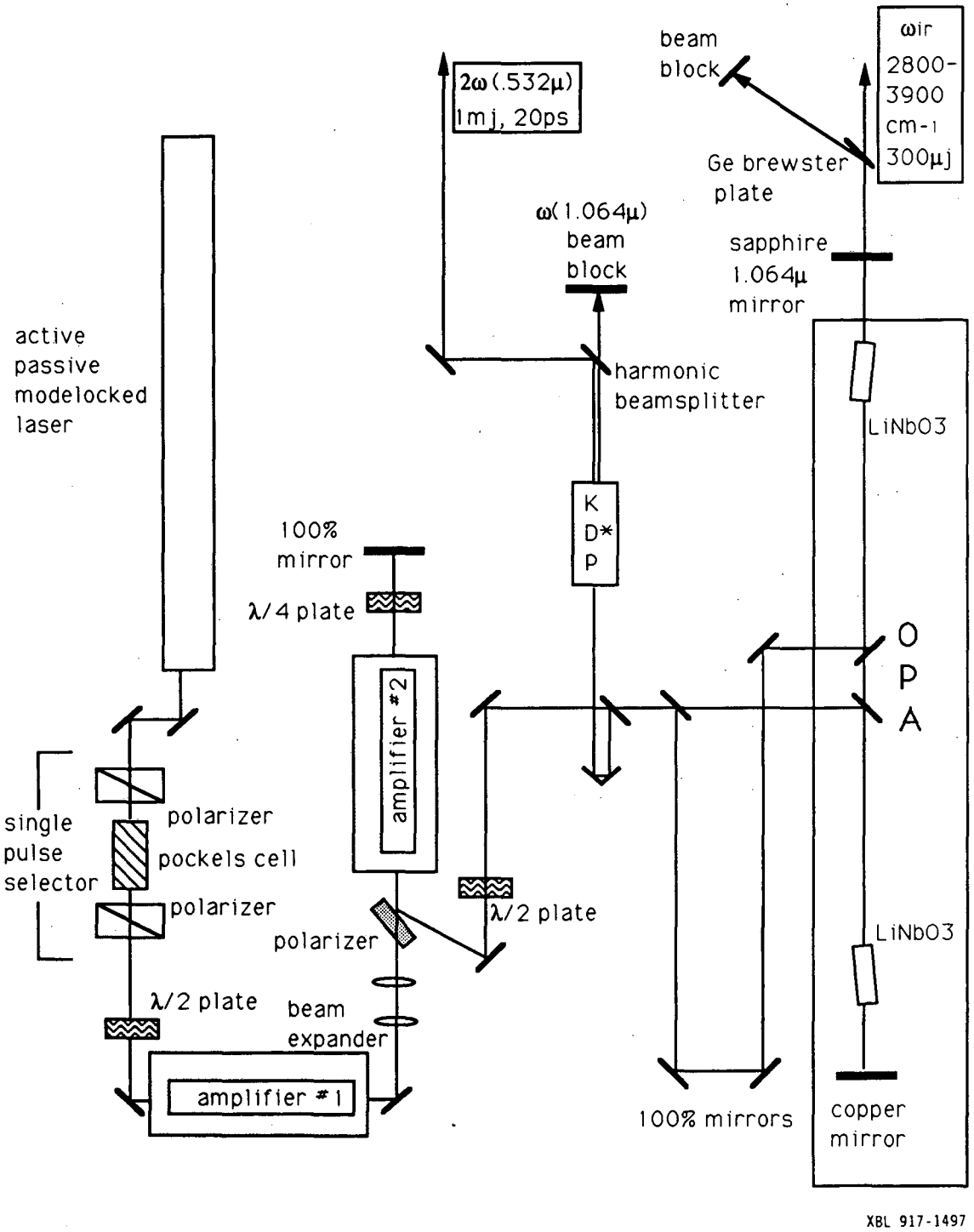
ωir
2800-
3900
cm-1
300μj
beam
block
2ω(.532μ)
1mj, 20ps
Ge brewster
plate
ω(1.064μ)
beam
block
sapphire
1.064μ
mirror
active
passive
modelocked
laser
harmonic
beamsplitter
LiNbO3
K
D*
P
100%
mirror
λ/4 plate
O
P
A
amplifier #2
single
pulse
selector
polarizer
pockels cell
polarizer
λ/2 plate
polarizer
λ/2 plate
beam
expander
amplifier #1
LiNbO3
100% mirrors
copper
mirror
XBL 917-1497

Fig.1

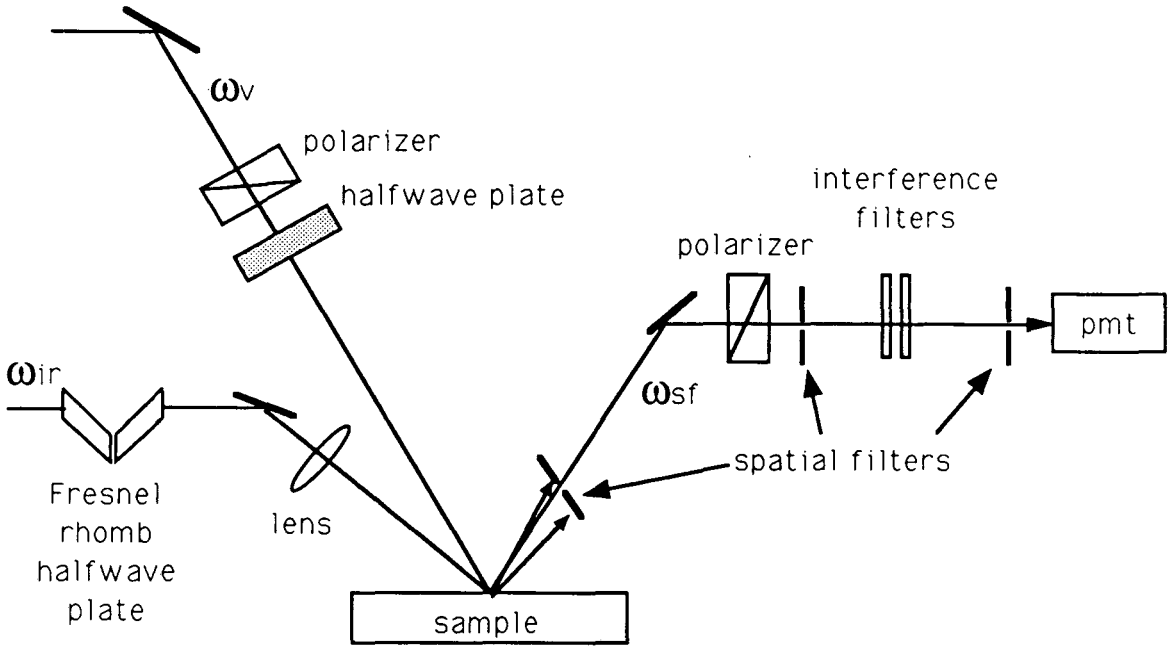

XBL 917-1498

Fig.2

III. A Nonlinear Spectroscopic Study of Coadsorbed Liquid Crystal and Surfactant Monolayers: Conformation and Interaction.

A. Introduction

The interfacial properties of liquid crystals (LC) are of great interest to many researchers for basic science understanding and for practical application to LC devices.[1,2] It is well known that the bulk alignment of a LC in a cell is strongly affected by the surface treatment of the cell walls. The deposition of a single monolayer on the cell wall can determine whether the alignment of the bulk liquid crystal director lies parallel to the cell wall or perpendicular (homeotropic alignment). Until recently, a detailed understanding of this phenomena has been impeded by a lack of microscopic probes of the interface. The purpose of the present study is to use optical second harmonic generation (SHG) and infrared-visible sum frequency generation (SFG) simultaneously to obtain information about the orientation and conformation of the LC and surfactant alkyl chains in pure monolayers and their interaction in mixed monolayers.

We examine monolayers of the liquid crystal 4'n-octyl-4-cyanobiphenyl (8CB) on clean glass and on glass coated with one of two surfactants: n-methylaminoproply-trimethoxysilane [$MeNH(CH_2)_3Si(OMe)_3$, MAP], known to induce bulk LC alignment parallel to the surface as in the clean glass case, and n,n-dimethyl-n-octadecyl-3-aminopropyl-trimethoxysilychloride [$CH_3(CH_2)_{17}(Me)_2N^+(CH_2)_3Si(OMe)_3Cl^-$, DMOAP] for homeotropic bulk alignment.[1] These molecules are depicted in Fig.1 and the surface bonding geometries suggested from NMR studies on high surface area silicas are represented in left hand column of Fig. 2. The two surfactants both have a MAP head group that attaches to the glass. In addition, DMOAP has an 18 carbon alkyl chain that

extends away from the surface.

In a previous SHG experiment,[3] a surprising result was found: the 8CB core had the same orientation on all three surfaces, even though they produced different bulk alignments. In the present study, using SFG spectroscopy, we have found that 8CB deposited on MAP leaves the surfactant monolayer relatively unchanged, consistent with a picture of 8CB adsorbing on top of the MAP molecules. In contrast, the adsorption of 8CB on DMOAP penetrates the DMOAP monolayer and reduces the conformational defects in the DMOAP alkyl chains. This then allows us to identify two competing effects in the surface alignment of the bulk LC.

B. Theory and Experiment

For surface SHG and SFG, the signal is proportional to the square of the effective surface nonlinear polarization[4]

$$\mathbf{P}(\omega_s) = \boldsymbol{\chi}^{(2)}(\omega_s = \omega_1 + \omega_2) : \mathbf{E}_1(\omega_1)\, \mathbf{E}(\omega_2) \qquad (1)$$

with $\omega_1 = \omega_2$ for SHG. In the case of a monolayer of molecules with appreciable second order polarizability deposited on a centrosymmetric insulator, the monolayer dipole susceptibility often dominates other contributions in SHG and SFG. The surface susceptibility can then be related to the nonlinear molecular polarizability by a coordinate transformation averaged over the molecular orientational distribution

$$\chi^{(2)}_{s.ijk} = N \sum_{lmn} < (\mathbf{i}\cdot\mathbf{l})\,(\mathbf{j}\cdot\mathbf{m})\,(\mathbf{k}\cdot\mathbf{n}) > \alpha^{(2)}_{lmn} \qquad (2)$$

where N_s is the surface molecular density and the angular brackets denote the

orientational average. The independent elements of $\chi^{(2)}$ can be deduced by measuring the signal for different polarizations of the incident and output beams. Then if $\alpha^{(2)}$ is known, the parameters of an orientational distribution can be determined.[5]

In the case of infrared-visible SFG, the nonlinear polarizability near vibrational resonances can be written as

$$\alpha^{(2)} = \alpha^{(2)}_{NR} + \alpha^{(2)}_{R} \quad ; \quad \alpha^{(2)}_{R} = \sum_{q} \frac{a_q}{\omega_q - \omega_{ir} - i\Gamma_q} \tag{3}$$

where a_q, ω_q, and Γ_q are the strength, frequency, and damping constant of the q mode, respectively. The resonant enhancement of $\alpha^{(2)}$ as ω_{ir} scans over ω_q then yields the surface vibrational spectrum observed by SFG.

The experimental setup has been described previously. In the present experiment, we are interested in measuring both the SHG and the SFG signals. The direction for the collimated signal radiated from the surface for either process is given by the surface phase matching condition $k_{s,x} = k_{1,x} + k_{2,x}$ where $k_{i,x}$ is the x-component of the wavevector for the beam at frequency ω_i. For SHG, $\omega_s = 2\omega_v$ and $\omega_1 = \omega_2 = \omega_v$ while for SFG $\omega_1 = \omega_v$, $\omega_2 = \omega_{ir}$ and $\omega_s = \omega_v + \omega_{ir}$. When the beams are incident from air at the air/medium interface, the angle of the signal in the reflected direction is given simply by the input beam angles since the dispersion of air is negligible. Then the SHG beam is collinear with the reflected beam at ω_v and color filters are needed to separate the two beams. In our experiment with ω_v and ω_{ir} incident at 47° and 54° with respect to the surface normal, the reflected SFG beam is at 47.9°. At .25 meters from the surface the reflected visible beam and SFG beam are displaced by over 3mm and are easily separated by a mirror. Both signals were then simultaneously measured in separate detection arms (Fig. 3). The peak

positions, strengths and widths of a resonance can be determined by a fit of the SFG spectrum to Eq. (3). For this experiment, the pulse energies and spot diameters at the sample were .6 mj, 700 μm and .2 mj, 250 μm for the visible and infrared beams, respectively. The typical signal levels per pulse from a surface monolayer of 8CB were about 200 photons for SHG and about 100 photons for SFG on resonance.

Our samples were prepared on fused quartz substrates which had been cleaned in chromic acid and rinsed in distilled water. DMOAP and MAP were chemisorbed from solution and polymerized according to the literature.[2] The 8CB monolayers on various surfaces were deposited by evaporation from a heated drop of LC held above the substrate with SHG used as an in situ monitor.[3] The SHG signal as a function of surface density is calibrated from a monolayer deposited on the water surface (Langmuir film) where the surface density can be independenly measured to within 10%.

C. SFG Spectra of Surfactant Coated Surfaces

We will focus on the SFG spectra associated with χ_{yyz} in the CH stretch region because it has been shown to be most sensitive to the conformation of the alkyl chain.[6] They have been obtained with polarizations s, s, and p for the SF, visible and infrared beams, respectively. The spectrum for MAP treated glass (MAP/G) (Fig. 4) is relatively weak with only broad features. Since χ_{yyz} here is most sensitive to the symmetric stretch of CH_2 and CH_3 and should increase with higher polar ordering of these groups along the surface normal, the weakness of the SFG signal indicates that the average orientation of the symmetry axes of the CH_2 and CH_3 groups are tilted far away from the surface normal. MAP is known to attach to the glass surface through a covalent bond between the surfactant Si atom and the surface silanol group. The NH group is expected to hydrogen bond to the surface

leaving the CH_2 chain lying along the surface.[7] A congested spectrum is expected since the CH_2 and CH_3 groups have overlapping resonances between 2850 and 2950 cm^{-1}. A more detailed analysis of the spectral features is, however, difficult because of the lack of IR and Raman studies on this molecule.

In contrast, a significantly stronger spectrum is obtained for DMOAP on glass (DMOAP/G), as displayed in Fig. 5(b) (open circles). Three prominent peaks at 2848 cm^{-1}, 2880 cm^{-1}, and 2933 cm^{-1} are present. The surprising part of the result is that the spectrum looks very much like that of a half-packed pentadecanoic acid (PDA, $CH_3(CH_2)_{13}COOH$) monolayer on water, as shown in Fig. 5(a) for comparison. It was found in a previous study[6] that the SFG spectrum of $|\chi_{yyz}|^2$ for a fully packed PDA monolayer exhibits only peaks at 2875 cm^{-1} and 2940 cm^{-1}, assigned to the symmetric stretch and Fermi resonance of the terminal methyl group. As the monolayer becomes less dense, these two peaks lose intensity while a peak at 2850 cm^{-1}, assigned to the CH_2 symmetric stretch mode, increases and dominates the spectrum at a surface density corresponding to 47 $Å^2$ per alkyl chain. This is because for a full PDA monolayer, all the alkyl chains are straight and upright on the surface so that by symmetry only the terminal CH_3 group contributes to the SFG spectrum, but as the monolayer expands,the chains acquire trans-gauche defects, break the symmetry, and contribute to the CH_2 stretch resonances in the SFG spectrum. We notice that the head group of DMOAP may occupy a surface area of about 40-50 ^{2}. The chain density of a compact DMOAP layer is then about the same as that of a half-packed PDA monolayer and the spectra of the two should be very similar if they are dominated by the contribution from the chains. The apparent lack of contribution from the DMOAP head group can be explained by the local field (dielectric shielding) effect which reduces the field seen by the head group buried beneath the alkane chains by about 2.3 as compared to an exposed head group.

The state of conformation of the alkane chain has been studied by infrared absorption and Raman scattering of liquid alkanes and alkanes bonded to high surface area silica (ABS).[8-11] The C-H bending , scissoring and wagging modes, which appear in the spectral region 1470 to 1350 cm^{-1}, as well as the rocking modes around 650cm^{-1}, have been found to be sensitive to the conformation of the chain. The intensities of the peaks assigned to to the various defects can be analyzed to provide quantitative information on the defect concentration. Some examples of the defects identified are depicted in Fig. 6. It is clear that the gauche and gauche-gauche defects create the most significant lateral disorder and might be most affected by lateral interactions between chains due to packing constraints. In liquid alkanes, for a chain with 16 CH_2 groups, theoretical and experimental studies have determined that the average number of defects per chain is approximately .8, 1.3 and 1.4 for the end gauche (eg), gauche-gauche (gg) and the gauche-trans-gauche (kink) defects, respectively.[8-10,12] Unfortunately, the single midchain gauche defect does not have an independent spectral signature so its concentration is not determined. In a study of ABS with chain lengths ($16CH_2$) and surface densities (50$Å^2$ per chain) similar to DMOAP/G, the defect concentrations per chain were found to be .4 (eg ; note that there are one half the number of end groups for the bonded chain), .6 (gg) and 1.1 (kink).[11] This indicates that substantial disorder is present in the surface layer, although the lateral interactions of the bonded phase and the fixation of one end have already reduced the gg defect concentration from that of the liquid.

D. SFG Spectra of Surface After Deposition of Liquid Crystal Monolayer

We now discuss the SFG spectra of 8CB monolayers on various surfaces. For a full 8CB monolayer on clean glass (8CB/G), the spectrum is shown in Fig. 7. The surface density here is the same as that of a full monolayer on water as measured

by SHG and corresponds to 35 $Å^2$ per molecule.[3] Two peaks at 3070 and 3050 cm^{-1} can be assigned to C-H stretch modes of the biphenyl core.[13] The peaks at 2875 and 2940 cm^{-1} are associated with the symmetric stretch and Fermi resonance of the terminal methyl group, respectively. The weak peak at 2850 cm^{-1} is due to symmetric stretch of CH_2 groups in the alkyl chain and the shoulder at 2920 cm^{-1} is due to either asymmetric stretches or Fermi resonances of symmetric stretches of the same CH_2 groups. The weakness of the 2850 cm^{-1} peak indicates that the 8CB alkyl chain is relatively straight. Furthermore, SHG measurements with different input-output polarizations showed that the biphenyl core of 8CB is tilted at 70° from the surface normal with the cyano group attached to the surface.[3] They, however, cannot determine the orientation of the molecule with respect to rotation about the biphenyl symmetry axis. In an experiment reported in a later section, we have measured the phase of χ_{yyz} for SFG at the 2875 cm^{-1} resonance. The result shows that the methyl group, and hence the alkyl chain, must point away from the surface.

For 8CB monolayers deposited on the surfactant treated glass, our SHG measurements confirmed that the tilt of the biphenyl core on either MAP or DMOAP-coated glass was 70°, the same as 8CB on clean glass.[3] The saturation coverage, as determined by SHG, was found to be 70% of the full monolayer on clean glass. The SFG spectrum for an 8CB monolayer on MAP-coated glass is presented in Fig. 4 together with the spectrum for MAP only. It appears very similar to that for 8CB on clean glass in Fig. 7. In fact, the spectral intensity, about one-half that of 8CB/G, can be explained as originating solely from the .70 monolayer of 8CB with little contribution from the surfactant. This suggests that the MAP contribution must have been reduced by the dielectric shielding effect of the 8CB layer on top of MAP.

In the case of 8CB deposited on DMOAP-coated glass (8CB/D), the SFG

spectrum, given in Fig. 5(b) together with that for DMOAP only, shows clear evidence of interaction between 8CB and DMOAP. The strong peak at 2850 cm^{-1} in the DMOAP/G spectrum is greatly reduced in the 8CB/D spectrum. The ratio of the susceptibility of the 2850 cm^{-1} mode before and after the deposition of 8CB is 19. This is far too large to be attributed to changes in the local field, which at most can account for a change on the order of the 8CB dielectric constant, about 2.5. The spectrum of 8CB/D in the spectral region above 2850 cm^{-1} can be understood from $|\chi_{yyz}(\omega_{ir})|^2$, with $\chi_{yyz}(\omega_{ir})$ obtained from the sum of the susceptibility of DMOAP/G and that of 8CB/G weighted for the lower coverage. In the present case, the 8CB molecules must have penetrated the alkyl chain layer to adsorb on the head groups of DMOAP or glass. Thus, no dielectric shielding of the spectral contribution from the alkyl chain methyl group of DMOAP by the 8CB layer can be expected. The most likely explanation for the decrease at 2850 cm^{-1} is that the increase in steric interaction would remove defects in the DMOAP chains and hence reduce the CH_2 peak at 2850 cm^{-1}, as has been demonstrated in the previous study on PDA monolayers.[6] The ability of an adsorbate to affect the conformation of a surface species has also been seen in the IR absorption studies on the bonded phases of alkane chains on high surface area silicas discussed earlier.[11] When the C_{16}/silica samples were immersed in methanol liquid, the chain defect concentrations dropped by a fact of two for the kink defects and a factor of three for the gg defects. This was presumably due to the interpenetration of the liquid into the chains, a similar picture to the coadsortion of 8CB on the DMOAP surface.

E. Surface Interactions and Bulk Alignment

Our results here provide insight into the microscopic mechanisms responsible for the effect of the surface treatment on the bulk LC alignment. In the case of glass

treated with surfactant octadecyltrichlorosilane (OTS), deposited 8CB forms a nonpolar rather than a polar layer and the bulk alignment is perpendicular to the surface.[3] OTS has the same long alkyl chain as DMOAP but has a much simpler and smaller headgroup in that it bonds to the surface through the Si atom that terminates the alkyl chain. The SFG spectrum of a full monolayer of OTS on glass is nearly identical to that of a full PDA monolayer, indicating that the chains are well ordered and that the monolayer is compact.[6] We can consider DMOAP as an intermediate case between clean glass, MAP, and OTS. Both DMOAP and OTS lead to homeotropic alignment of the LC bulk, while clean glass and MAP yield parallel alignment. Clean glass, MAP/G, and DMOAP/G allow the adsorption of a polar layer of 8CB, but OTS does not.[3] The similarity of DMOAP/G to clean glass and MAP/G is due to the large headgroup of DMOAP which spaces the chains and permits access of 8CB to surface polar sites. However, once 8CB fills in the DMOAP chains, the subsequent 8CB sees a compact alkyl monolayer similar to OTS. It appears that in order for the monolayer surface treatment to induce parallel alignment of the bulk LC, the second 8CB layer must have access to the biphenyl cores of 8CB molecules bound at surface polar sites. Though DMOAP permits the presence of these strongly bound molecules, its long alkyl chain prevents their biphenyl cores from interacting with subsequent layers.

In conclusion, we have demonstrated that SHG and SFG can provide a detailed picture of the interfacial structure of LC systems. We have observed the existence of interaction between the LC monolayer and the surfactant treated glass which reveals the importance of the competing effects of surface polar adsorption sites and surfactant alkyl chains in aligning the bulk LC.

References

[1] J. Cognard, Alignment of Nematic Liquid Crystals and their Mixtures (Gordon and Breach, London, 1982).

[2] F. J. Kahn, Appl. Phys. Lett.**22**,386 (1973).

[3] C. S. Mullin, P. Guyot-Sionnest, and Y. R. Shen, Phys. Rev. **A 39**, 3745 (1989).

[4] Y. R. Shen, Ann. Rev. Phys. Chem. **40**, 327 (1989).

[5] W. Chen, M. Feller, and Y. R. Shen, Phys. Rev. Lett. **63**, 2665 (1989).

[6] P. Guyot-Sionnest, J. H. Hunt, and Y. R. Shen, Phys. Rev. Lett. **59**, 1597 (1988).

[7] G. S. Caravajal, D. E. Leyden, G. R. Quintig, and G. E. Maciel, Anal. Chem. **60**, 1776 (1988).

[8] R. G. Snyder, J. Chem. Phys. **47**, 1316 (1967).

[9] M. Maroncelli, H. L. Strauss, and R. G. Snyder, J. Chem. Phys. **82**, 2811 (1985).

[10] M. Maroncelli, H. L. Strauss, and R. G. Snyder, J. Phys. Chem. **89**, 4390 (1985).

[11] L. C. Sander, J. B. Callis, and L. R. Field, Anal. Chem. 55, 1068 (1983).

[12] P. J. Flory, *Statistical Mechanics of Chain Molecules*,(Interscience, New York, 1969).

[13] L. J. Bellamy, **The Infrared Spectra of Complex Molecules** (Wiley, New York, 1975).

Figure Captions

Fig. 1. The molecules used in this study: n-methylaminoproply-trimethoxysilane [$MeNH(CH_2)_3Si(OMe)_3$, MAP]; n,n-dimethyl-n-octadecyl-3-aminopropyl-trimethoxysilychloride [$CH_3(CH_2)_{17}(Me)_2N^+(CH_2)_3Si(OMe)_3Cl^-$, DMOAP]; 4'n-octyl-4-cyanobiphenyl (8CB) and octadecyltrichlorosilane [$CH_3(CH_2)_{17}SiCl_3$ (OTS)].

Fig. 2. Sample surfaces after surface treatment and after deposition of 8CB monolayer. (a) clean glass: There is most certainly some adsorbed water on the surface which can effect the subsequent surface chemistry and adsorption of liquid crystal. (b) MAP/glass: Molecule adsorbs with nitrogen weakly hydrogen bonded to surface. 8CB most likely adsorbs at polar sites on surface. (c) DMOAP/glass: Monolayer with chain defects due to large interchain distance. 8CB lies with same angle as on clean glass and MAP/glass, though not depicted here. With the view of surface presented here, molecule would perhaps lie down into page. (d) OTS/glass: Monolayer is close packed with chain defects limited to chain ends. 8CB monolayer does not form on this surface.

Fig. 3. Experimental setup for simultaneous detection of SHG and SFG. SHG is used as in situ deposition monitor and surface density calibration for liquid crystal molecule 8CB.

Fig. 4. SFG spectrum of MAP on clean glass (open circles) compared with spectrum of same sample taken after deposition of .70 monolayer of 8CB (filled circles). Spectra are normalized to a quartz crystal reference.

Fig. 5. (a) Spectrum of PDA monolayer on water surface at density of 47 /molecules. (b) Comparison of SFG spectrum of DMOAP on clean glass (open circles) and spectrum of same sample after deposition of .7 monolayer of 8CB (filled circles).

Fig. 6. Representative alkane chain conformational defects. The chain end gauche and kink defects dominate in high density phases due to steric constraints, but at low densities, the gauche and gauche-gauche defects become substantial.

Fig. 7. SFG spectrum of 8CB monolayer on clean glass. Note change in horizontal scale from the previous spectra.

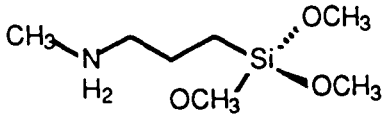

MAP

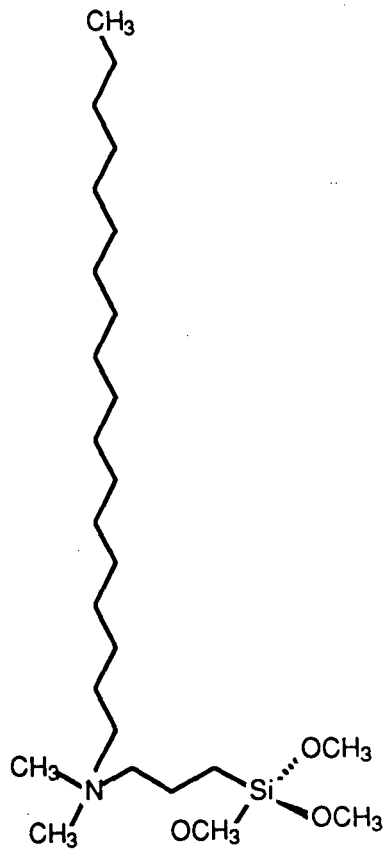

DMOAP

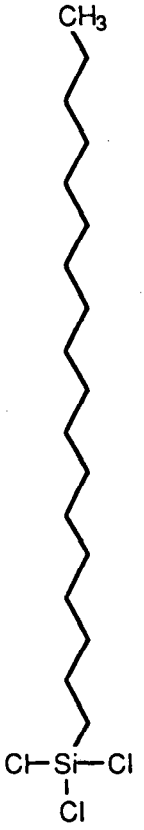

OTS

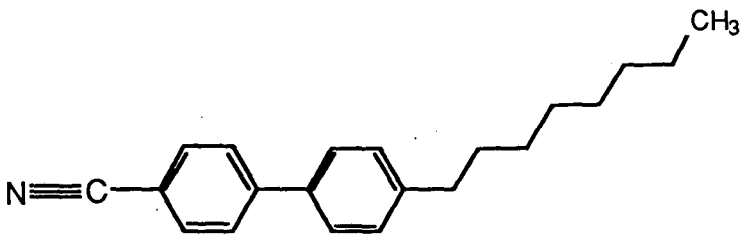

8CB

XBL 917-1499

Fig.1

After surface treatment

After 8CB deposition

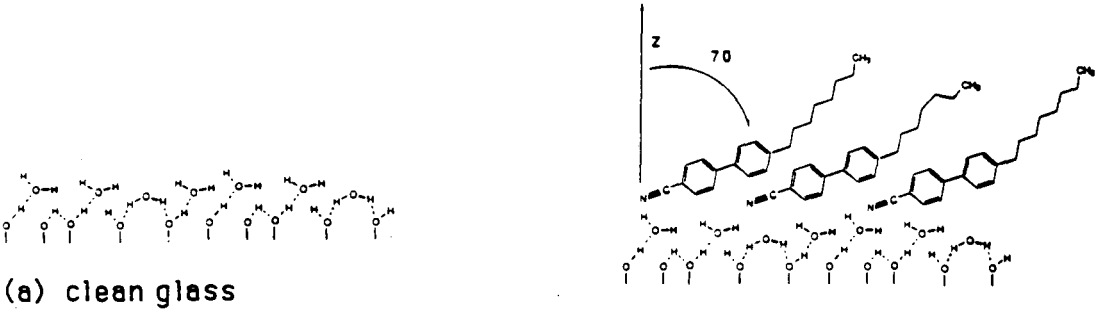

(a) clean glass

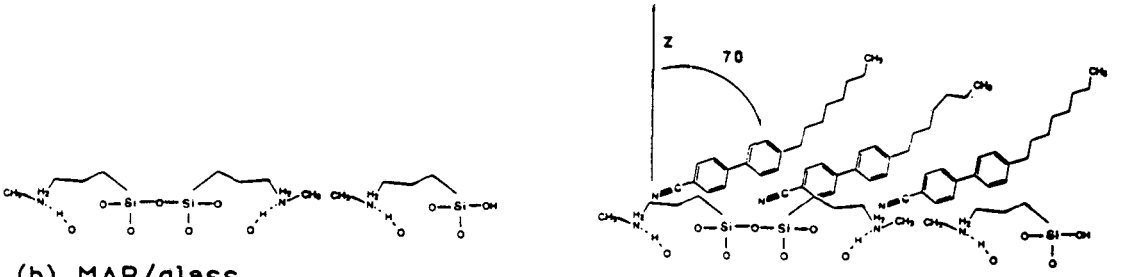

(b) MAP/glass

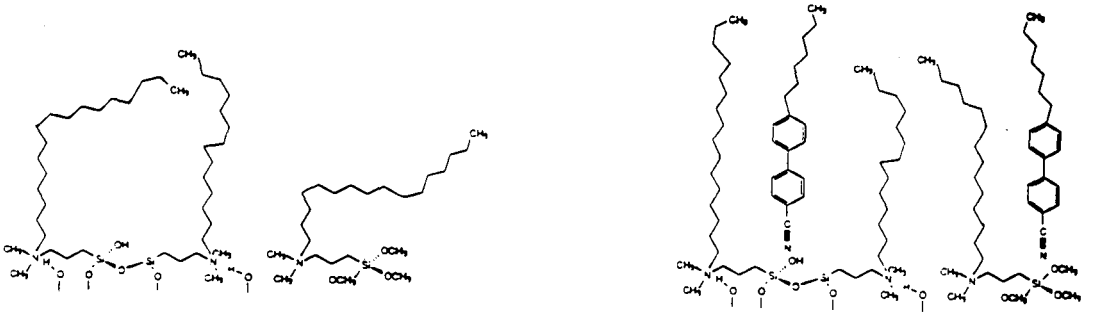

(c) DMOAP/glass

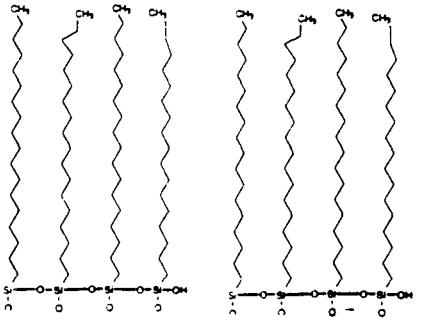

(d) OTS/glass

XBL 917-1500

Fig.2

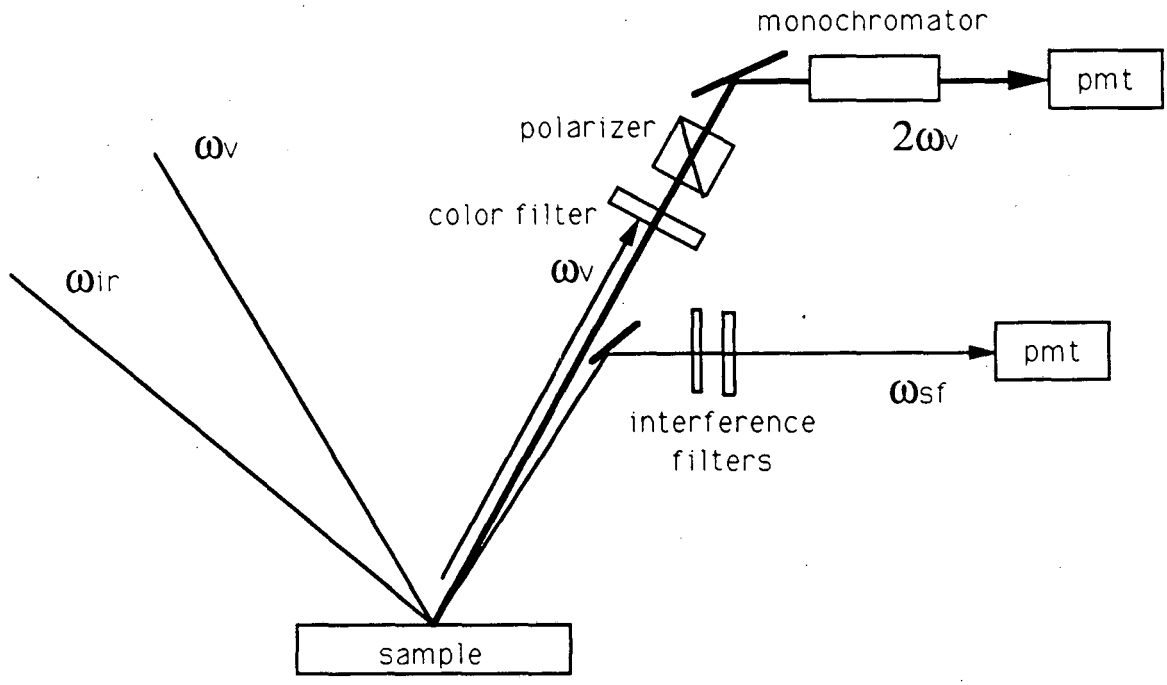
monochromator
pmt
polarizer
2ωv
ωv
color filter
ωir
ωv
pmt
ωsf
interference
filters
sample
XBL 917-1501

Fig.3

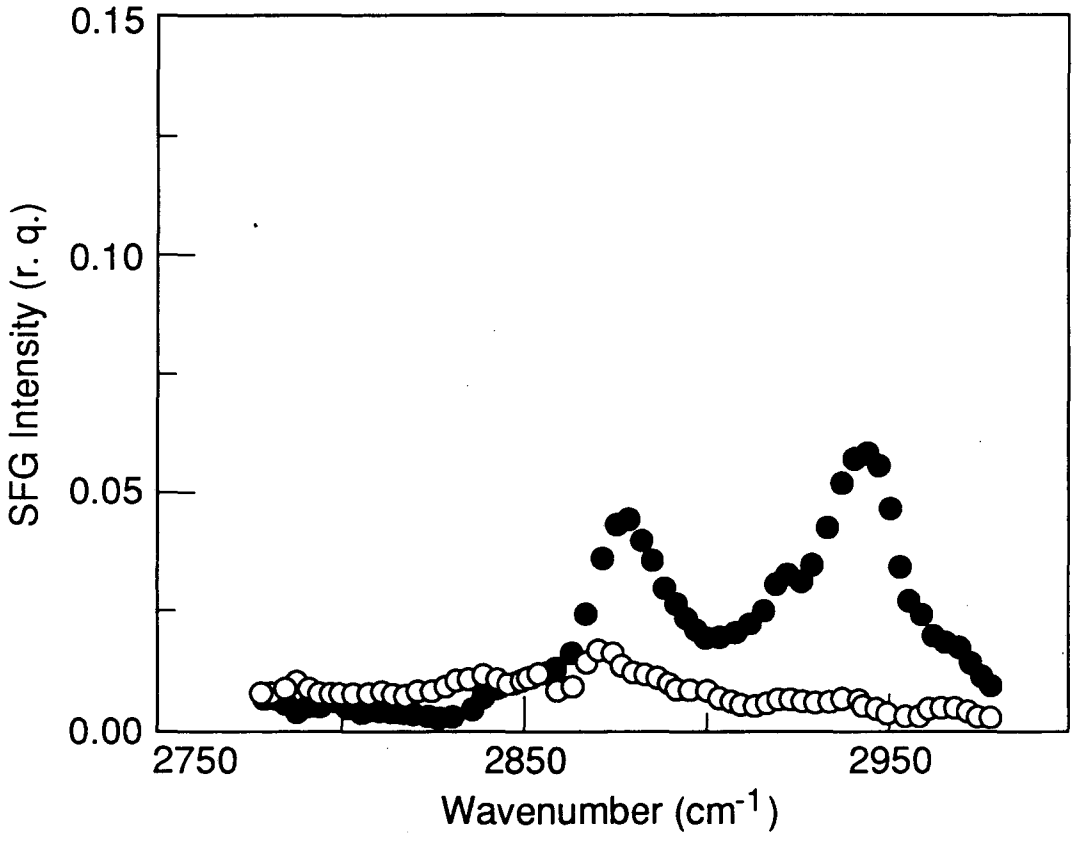

XBL 903-5458

Fig. 4

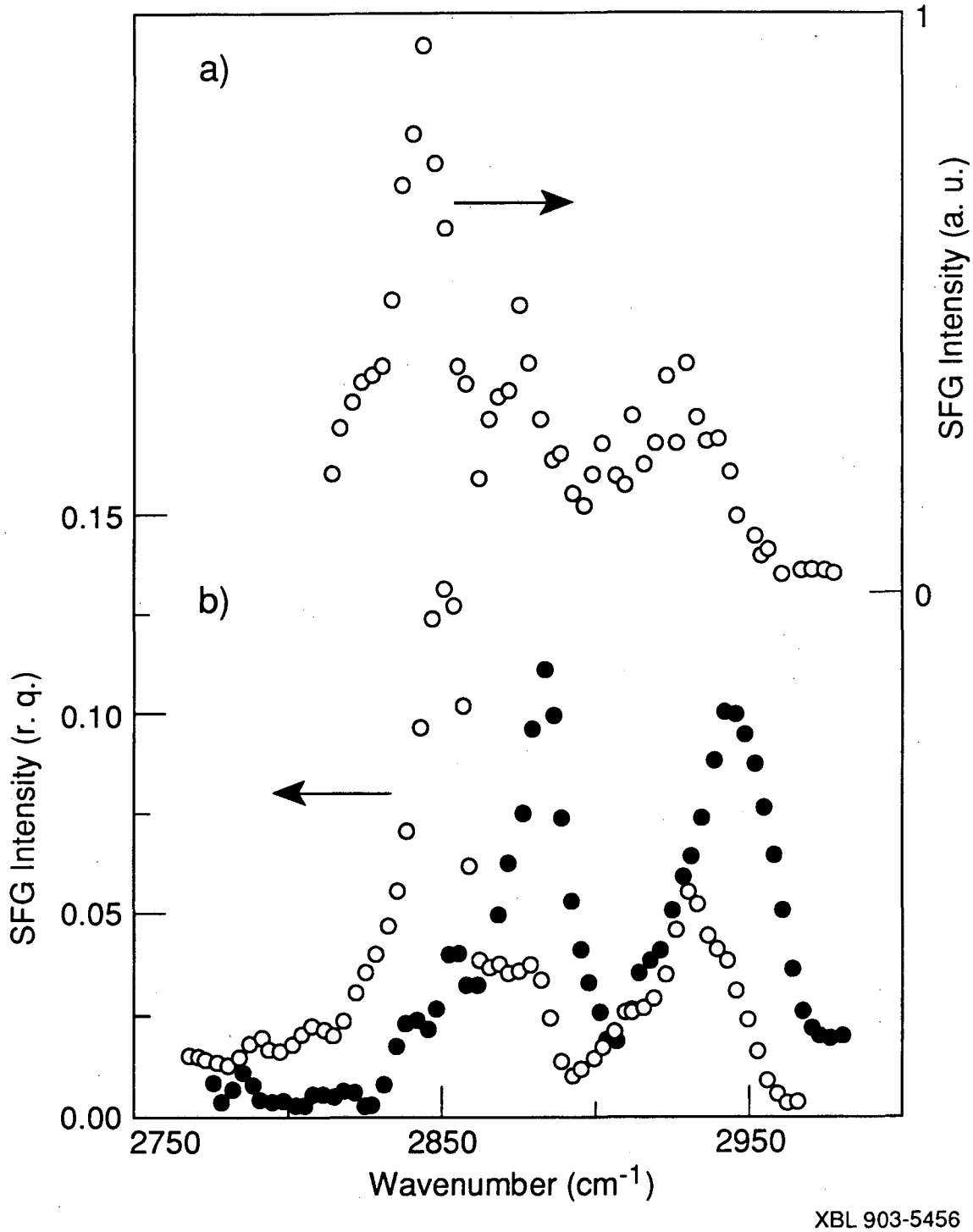

XBL 903-5456

Fig.5

Alkane Chain Conformational Defects

(a) all trans

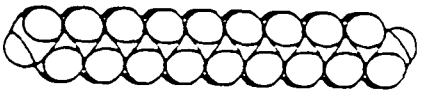

(b) end gauche

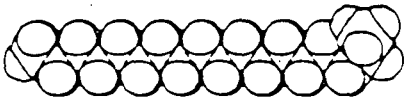

(c) gauche

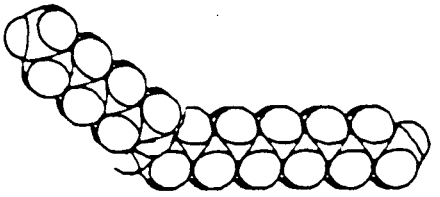

(d) kink

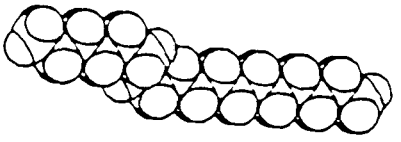

(e) gauche gauche

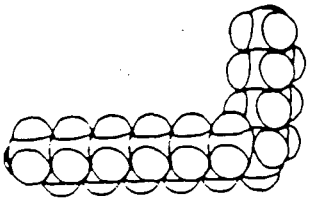

XBL 917-1502

Fig.6

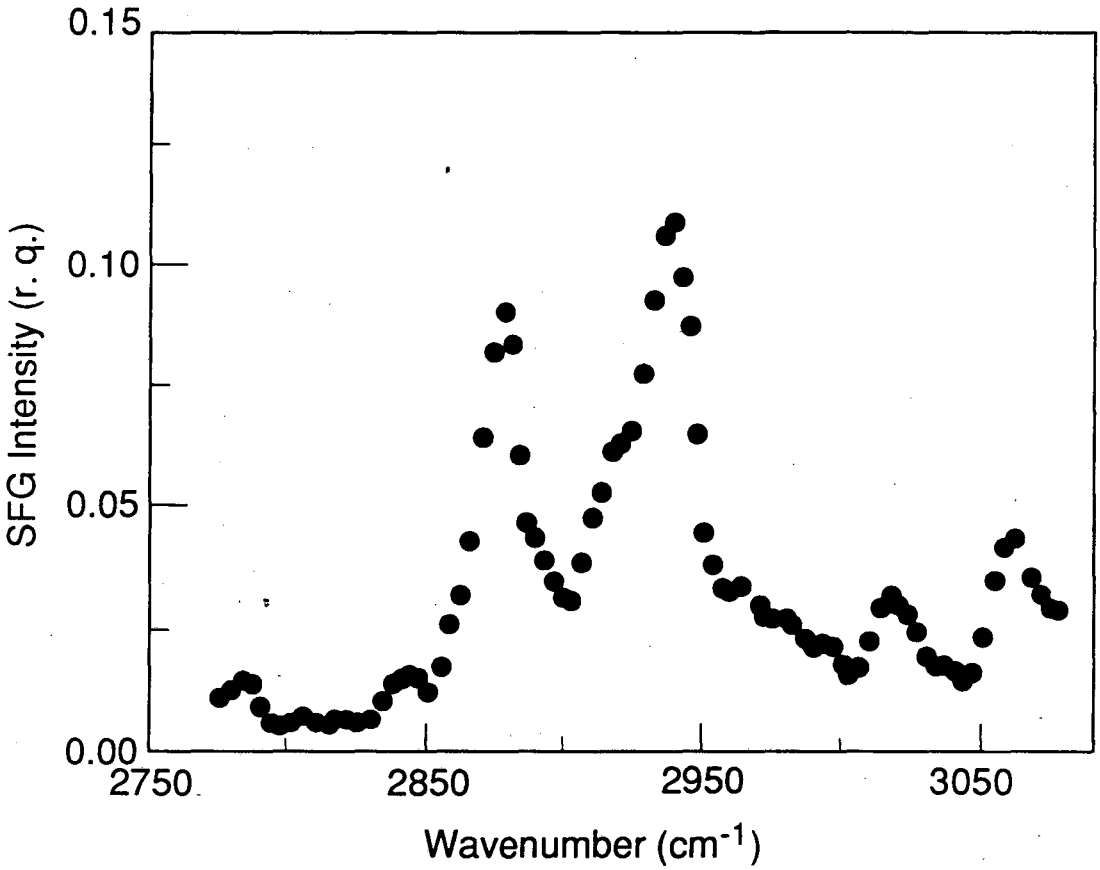
0.15
0.10
0.05
0.00
SFG Intensity (r. q.)
2750
2850
2950
3050
Wavenumber (cm-1)
XBL 903-5455

Fig.7

IV. Phase Measurement For Surface Infrared Visible Sum-Frequency Generation.

Coherent nonlinear optical measurements allow us to deduce separately the amplitude and phase of a nonlinear susceptibility χ^{NL} of a material system, both of which carry useful information about the material.[1] For example, infrared-visible sum frequency generation (SFG) spectroscopy[2-9] can yield the vibrational spectrum of a surface monolayer of molecules and the orientation of a group of atoms in these molecules via χ^{NL}, and the phase of χ^{NL} determines the polarity of the orientation of the atomic group. The latter information, though important for the understanding of many problems in surface science, cannot be obtained by the more conventional techniques. While phase measurements on surface χ^{NL} have been reported with surface second harmonic generation by a number of researchers,[10-13] none has so far been attempted in surface SFG. In this paper, we describe two techniques that can determine the phases of χ^{NL} in surface SFG and hence the polar orientations of specific atomic groups in the adsorbed molecules.

A. Introduction - Theory and Experiment

Consider surface SFG in the reflection geometry. The effective nonlinear polarization has the form[1]

$$\mathbf{P}(\omega_s) = \chi^{NL}(\omega_s = \omega_1 + \omega_2) : \mathbf{E}_1(\omega_1)\, \mathbf{E}(\omega_2) \qquad (1)$$

where χ^{NL} is the effective surface nonlinear susceptibility, and $\mathbf{E}_1$ and $\mathbf{E}_2$ are the fields at the visible and infrared frequencies, ω_v and ω_{ir}, respectively. We can write

$$\chi^{NL} = \chi^{S} + \chi^{B} \qquad (2)$$

with χ^S and χ^B referring to contributions coming from the surface (assuming the surface molecular monolayer) and the bulk, respectively. The frequency dependence of the total susceptibility can be written as

$$\chi^{(2)}(\omega_{ir}) = \chi^{NR} + \chi^{R}(\omega_{ir}) \tag{3}$$

where χ_{NR} and χ_R are the non-resonant and resonant contributions, respectively. Both the surface and bulk can contribute to χ^{NR} and χ^R.

The surface dipole term is related to the nonlinear polarizability $\alpha^{(2)}$ by a coordinate transformation averaged over the molecular orientation distribution (denoted by the angular brackets below)[6]

$$\chi^S = N \langle \alpha^{(2)} \rangle \tag{4}$$

with

$$\alpha^{(2)} = \alpha^{NR} + \alpha^{R} \tag{5}$$

$$\alpha^R = \sum_q \frac{A_q}{\omega_q - \omega_{ir} - i\Gamma_q} \tag{6}$$

where A_q, ω_q and Γ_q are, respectively, the strength, frequency, and damping of the near-resonant ($\omega_{ir} \sim \omega_q$) vibrational mode Q, and N is the surface density of the molecules. The local field effect has been neglected. We note that the phase of $\langle \alpha^{(2)} \rangle_{ijk}$ varies with ω_{ir} as it scans through the vibrational resonance. Since SFG is a second order process, the susceptibility is described by a third rank tensor and an

inversion of the orientational distribution will change the sign of the susceptibility. The determination of the sign of this susceptibility to establish the orientation of a molecular group is the subject of this section.

The bulk contribution, on the other hand, can be written as[14]

$$\chi^B = i L_c \chi \tag{7}$$

with the coherence length in reflection $L_c = (k_{ir,z} + k_{v,z} + k_{s,z})^{-1}$, χ being the bulk nonlinear susceptibility of the substrate, and $k_{i,z}$ the z component of the wavevector at ω_i inside the substrate. For example, for a Y-cut crystalline quartz substrate, the bulk susceptibility is from a dipole contribution, and we have

$$\chi^B{}_{yyx} = i L_c \chi_{XXX} \sin^2\theta \cos\theta \tag{8}$$

where X, Y, Z are the crystal axes, x, y, z are the lab coordinates with z normal to the surface, and θ is the angle between x and X (Fig.1). In this case, χ^B has a negligible frequency dependence over the wavelengths of interest and contributes only to the non-resonant susceptibility χ_{NR}. We note here that the magnitude and the sign of χ^B in this case can be varied by a rotation of the quartz crystal.

Since the radiated electric field is proportional to the polarization described by Eq.(1), the equations (2) and (3) above can be interpreted as the interference between fields generated by the surface and bulk susceptibilities or by the resonant and nonresonant susceptibilities, respectively. The field radiated from an interface can also interfere with a field generated somewhere along the beam path. In this case, the SF signal is given by

$$S(\omega_s) \propto |\, \mathbf{E}_I(\omega_s) + A\, \mathbf{P}^{(2)}(\omega_s)\,|^2$$

$$\propto |\, 1 + |B|\, \boldsymbol{\chi}^{NL} \exp(i\phi)\,|^2 \qquad (9)$$

where A and B are constants, ϕ is the relative phase between $\mathbf{E}_I$ and $A\,\mathbf{P}^{(2)}$,and $\mathbf{E}_I$ is the SF field generated somewhere along the beam path that can interfere with the SF output from the surface. We will later discuss a method for generating this field.

From Eqs. (2), (3) and (9) above, we can identify three ways of determining the phase of $\boldsymbol{\chi}^S$ on a resonance. In the presence of a nonzero $\boldsymbol{\chi}^B$ (Eq. (2)), the phase of $\boldsymbol{\chi}^S$ at a particular frequency can be determined by noting the interference pattern obtained as $\boldsymbol{\chi}^B$ is varied. The relative phase between the susceptibilities of two resonances can be obtained from the SFG spectrum, either directly, if the two peaks overlap (Eq.(6)), or from the interference of each peak with a nonresonant background (Eq.(3)). This last method will be used to determine the relative orientation of surface species in the last section on SFG from the water surface. The first example we present below is the interference of the surface signal with the field generated from a remote nonlinear crystal (Eq.(9)). This is the most general (and not surprisingly, the most difficult) technique in that it can be applied to any surface resonance and allow one to obtain the relative phases of the susceptibilities for different samples.

The experimental setup is the same as presented in previous sections. The polarizations, s, s, and p, were chosen for the SF output, visible and infrared beams, respectively. This allows us to measure the surface susceptibility component $\chi^{NL}{}_{yyz}$. As an example, the sum-frequency spectrum, $|\,\chi^{NL}{}_{yyz}\,|^2$ versus ω_{ir}, for the symmetric stretch of the terminal CH_3 groups of a full monolayer of pentadecanoic acid (PDA, Fig.2) on water[6] is shown in Fig. 3. In this case, $\mathbf{E}_I = 0$ and $\boldsymbol{\chi}^B$ is

negligible, so that $\chi^{NL}{}_{yyz} = \chi^{S}{}_{yyz}$. The spectrum can then be fit using Eqs. (4) and (6). Although the relative phase of $<\boldsymbol{\alpha}^{R}>$ and $<\boldsymbol{\alpha}^{NR}>$ can be deduced from the fit, the absolute phase of either $\boldsymbol{\chi}^{S}$ or $<\boldsymbol{\alpha}^{R}>$ cannot be determined.

B. Technique I: Interference with Remote Crystal Susceptibilty

The phase of $\chi^{S}{}_{yyz}$ for the PDA monolayer can be measured directly. As seen in Fig. 4, three fields, the reflected visible and infrared beams ($\mathbf{E}_v$ and $\mathbf{E}_{ir}$, respectively) and the radiated sum frequency field ($\mathbf{E}_s$) , come off of the sample surface in the reflection direction. If they are directed into a remote nonlinear crystal, it can be shown using the coupled wave approach that the field at the sum frequency exiting the crystal, E_s^f, is given by [15]

$$E_s^f = E_s^c + C\, E_v^c\, E_{ir}^c \tag{10}$$

where E_ω^c is the complex amplitude of the field at the entrance face of the crystal and C is a constant which depends on the particular crystal used. In this case, the interference is occuring between the sum frequency field from the sample and the sum frequency field which would have been radiated from the remote crystal in the absence of the sample field. The fields E^c can be written as

$$E_s^c = F\, \chi^s\, E_v^i\, E_{ir}^i\, \exp(i k_s l_s) \tag{11}$$

$$E_v^c = r_v\, E_v^i \exp(i k_v l_v) \qquad E_{ir}^c = r_{ir}\, E_{ir}^i \exp(i k_{ir} l_{ir})$$

where F is obtained from Eq. (6) of chapter II, r_i is the amplitude reflection coefficient of the sample, k_i is the free space wavevector and l_i is the optical pathlength from the sample to the remote crystal. The exponential factors describe

the change in the phase of the field due to the propagation from the sample to the crystal. Equation (10) can now be put into the form of Eq. (9) with

$$E_s^f \propto 1 + B_s \chi^s \exp[i(k_s l_s - k_v l_v - k_{ir} l_{ir})] \quad (12)$$

where $B_s = (F/C\, r_v\, r_{ir})_s$ is a complex coefficient particular to the sample. The sum frequency signal intensity, $I_s \propto |E_s^f|^2$, will vary sinusoidally with the change in the phase $\phi = (k_s l_s - k_v l_v - k_{ir} l_{ir})$ of the exponential function. We then replace the sample with a reference with susceptibility χ^r at the sample position and repeat the measurement. The shift in the interference patterns for the sample and the reference as a function ϕ measures the relative phase of χ^r and χ^s. If the phase of χ^r is known, this measurement then provides us with the phase of χ^s.

In our experiment, the reflected visible, infrared and radiated sum frequency fields are collected by a lens placed after the sample and focused into a y-cut quartz crystal. The contrast of the interference pattern obtained when varying ϕ depends on the overlap of the three beams in the remote quartz crystal. Equation (10) above applies to the regions of the crystal where the beams are overlapped, outside of which there can be no interference of the fields. Therefore it is important to calculate the beam profiles to ensure that the beam waists at the remote quartz crystal are approximately equal. We have typically obtained contrasts of 50%, quite sufficient for the measurement. The relative phases of the fields at the surface of this remote quartz crystal, ϕ, was varied by the use of a fused silica compensator consisting of two wedges of glass. As one wedge is translated across the other, the pathlength of the three fields in the glass is changed. This phase can be written as

$$\phi = (k_s - k_v - k_{ir})\, l_a + (k_s n_s - k_v n_v - k_{ir} n_{ir})\, l_g = \phi_o + (k_s n_s - k_v n_v - k_{ir} n_{ir})\, \Delta l_g \quad (13)$$

where l_a and l_g are the total pathlengths in air and in the glass, respectively, and n_ω is the index of refraction of the glass. With $n_s = 1.4649$, $n_v = 1.4608$ and $n_{ir} = 1.4087$, we find that Δl_g, the change in the glass pathlength produced by the translation of the glass wedges, needs to be equal to 38 μm in order to obtain a 2π phase change. This calculation has been done for the infrared frequency of 2875 cm^{-1}, at the CH_3 symmetric stretch resonance peak. With a measured wedge angle for our homemade compensator of 1.2°, the translation of the wedge to produce the 2π shift is 1.9 mm, in good agreement with the periodicity seen in the interference patterns in Fig. 5.

At each ω_{ir}, an interference pattern is obtained from the translation of the compensator. Then the phase measurement was calibrated at each ω_{ir} using a second oriented crystalline quartz as a reference that is placed in the sample position. Figure 5 shows the observed interference patterns at several frequencies through the resonance peak. They are compared with patterns obtained when a quartz reference is placed in the sample position. The results allow us to find the phase ϕ of $\chi^S{}_{yyz}$ at the chosen frequencies. The data are plotted in Fig. 3 together with the theoretical curve calculated from Eqs. (4) and (6). Since we have characterized our quartz reference to determine the absolute sign of χ_{XXX}, and hence χ^r, our measurement determines the absolute phase of $\chi^S{}_{yyz}$ on resonance to be $+\pi/2$. The importance of the absolute phase of α^R will be discussed in the next chapter.

C. Technique II: Interference with Substrate Susceptibility

We can also find the phase of $\chi^S{}_{yyz}$ for a PDA monolayer by depositing the monolayer directly on a Y-cut crystalline quartz substrate. In this case, we have $\mathbf{E}_I = 0$, but $\boldsymbol{\chi}^{NL}$ now contains a nonvanishing $\chi^B{}_{yyx}$ given by Eq. (8). Again, the SF signal of Eq. (9) will exhibit an interference pattern if the angle θ in Eq. (8) can be

varied . This can be achieved simply by rotating the quartz substrate about its surface normal, pictured in Fig.1. In the simplest case, the monolayer will have an isotropic azimuthal distribution and therefore χ^S_{yyz} will be independent of rotation. This is thought to be the case for our sample where the Langmuir-Blodgett film of fatty acid is deposited at high surface pressure. Our experimental results are depicted in Fig. 6. For a clean quartz substrate, we have $S(\omega_s) \propto |\chi^B_{yyz}|^2 \propto \sin^4\theta \cos^2\theta$, which should show two peaks symmetric with respect to $\theta = \pi/2$. This is confirmed by the experiment. For the PDA monolayer on quartz, with ω_{ir} off resonance, the experimental data still showed two peaks symmetric about $\theta = \pi/2$ as one would expect from a real χ^S_{yyz}. On resonance, however, the peaks became asymmetric about $\theta = \pi/2$, as illustrated in Fig. 6. The higher peak appearing on the $\theta < \pi/2$ side indicates that A^Q_{yyz} is positive. The data are well fit by a χ^S_{yyz} that is independent of θ, demonstrating that the monolayer is indeed isotropic. In general, the technique is applicable to anisotropic monolayers. Since the bulk susceptibility as a function of rotation is known, the interference pattern for an anisotropic monolayer could reveal the rotational symmetry of $\boldsymbol{\chi}^S$ in addition to the phase of $\boldsymbol{\chi}^S$ as a function of rotation.

We have also plotted in Fig. 6 the result on a liquid crystal monolayer of 4'-(n-octyl)-4-cyanobiphenyl (8CB, Fig. 2) on the Y-cut quartz substrate. The same asymmetry is observed, although compared to the PDA case the degree of asymmetry is less, indicating a smaller A^Q_{yyz} with the same sign. It is reasonable to assume that $\boldsymbol{\alpha}^{(2)}$ is nearly the same for the two molecules since their methyl groups are both attached to alkane chains. Therefore, the relative sign of A^Q_{yyz} gives the relative orientation of the CH_3 groups for the two molecules. Since it is well known that the PDA molecules are adsorbed on water or quartz with the CH_3 terminal group pointing away from the surface, we can then conclude that 8CB molecules

adsorbed on quartz also have their CH_3 terminal group of the alkane chain pointing away from the surface.

D. Phase Measurement for Spectroscopy

While in this section we have focused on the use of the determination of the phase of a susceptibility on resonance in order to determine the orientation, up or down, of a molecular group, the measurement of the phase of χ^{NL} as a function of frequency can also be used to clarify the spectrum and identify peak positions. In detecting the signal strength, we measure the square of the absolute magnitude of the susceptibility χ^{NL}. This spectrum can be misleading, with dips appearing instead of peaks,or peaks being apparently displaced. Though often the signal strength is sufficient to determine a unique fit to Eq.(6), thereby determining the parameters of the resonance, there are cases where the lineshape can be obscure. A simple example of this can be seen by considering the signal from a surface in the case of a single peak with a nonresonant background that is pure imaginary, as in the case of the surface of a dielectric with a bulk dipole nonlinearity (i.e. quartz). In this case the signal is written as

$$S(\omega_{ir}) \propto |i\chi^{NR} + \frac{A_q}{\omega_q - \omega_{ir} - i\Gamma_q}|^2 = |\chi^{NR}|^2 + \frac{2\chi^{NR} A' + A'^2}{\Delta\omega^2 + 1} \qquad (14)$$

where $A' = A_q/\Gamma_q$ and $\Delta\omega = (\omega_q - \omega_{ir})/\Gamma_q$. If we consider the special case where $\chi^{NR} = -A'/2$, the second term is zero, and the signal is given by the first term, which is just the signal of the surface without the resonance. This means that one could take a surface, deposit a monolayer which by itself had a signal at the resonance peak equal to four times that of the bare surface, and see no change in the signal from the surface! However, the phase of the susceptibility of the monolayer together

with the substrate is given by $\phi = \tan^{-1}\{-.5(\Delta\omega-1)^2\}$ which changes dramatically through the resonance. In this case, the only way to detect the monolayer resonance is to measure the phase as a function of ω_{ir}. Although this case is somewhat specific, it serves as an example of how the phase of the susceptibility can also be helpful in establishing peak positions and strengths.

In conclusion, we have discussed the various ways in which one can obtain the phase of the resonant part of a surface susceptibility. We have demonstrated two interference methods for accomplishing the phase measurement of a surface nonlinear susceptibility involved in surface SFG spectroscopy. They then enable us to determine the absolute or polar orientation of a selected group of atoms in molecules adsorbed at an interface.

References

[1] Y. R. Shen, The Principles of Nonlinear Optics (Wiley, New York, 1984).

[2] Y. R. Shen, Ann. Rev. Phys. Chem. **40**, 327 (1989).

[3] Y. R. Shen, Nature **337**,519 (1989).

[4] X. D. Zhu, H. Suhr, and Y. R. Shen, Phys. Rev. **B35**, 304 (1987).

[5] J. H. Hunt, P. Guyot-Sionnest, and Y. R. Shen, Chem. Phys. Lett. **133**, 189 (1987).

[6] P. Guyot-Sionnest, J. H. Hunt, and Y. R. Shen, Phys. Rev. Lett. **59**, 1597 (1988).

7 A. L. Harris, C. E. D. Chidsey, N. J. Levinos, and D. N. Loiacono, Chem. Phys. Lett. **141**, 350 (1987).

[8] R. Superfine, P. Guyot-Sionnest, J. H. Hunt, C. T. Kao, and Y. R. Shen, Surf. Sci. **200**, L445 (1988).

[9] P. Guyot-Sionnest, R. Superfine, J. H. Hunt, and Y. R. Shen, Chem. Phys. Lett. **144**, 1 (1988).

[10] R. K. Chang, J. Ducuing, and N. Bloembergen, Phys. Rev. Lett. **15**, 6 (1965).

[11] H. W. K. Tom, T. F. Heinz, and Y. R. Shen, Phys. Rev. Lett. **51**, 1983 (1983).

[12] K. Keminitz, K. Bhattacharyya, J. M. Hicks, G. R. Pinto, K. B. Eisenthal, and T. F. Heinz, Chem. Phys. Lett. **131**, 285 (1986).

[13] G. Berkovic, Y. R. Shen, G. Marowsky, and R. Steinhoff, J. Opt. Soc. Am. B **6**, 205 (1989).

[14] H. W. K. Tom, Ph.D. Thesis (University of California, Berkeley, California, 1985).

[15] Ref. 1, p.71.

Figure Captions

Fig. 1. Experimental arrangement for the phase measurement using the bulk nonlinearity of the substrate, Y-cut crystalline quartz.

Fig. 2. Diagrams of the two molecules used in this study, pentadecanoic acid (PDA) and the liquid crystal molecule 8CB, and their orientation after being deposited on glass.

Fig. 3. SFG spectrum (circles) of CH_3 symmetric stretch of PDA monolayer on water surface. Solid line is obtained from a fit to Eqs. (3) and (6). Dashed curve is the phase of χ^{NL} obtained from the fit to the intensity while the data points from the interference measurement are represented by bars.

Fig. 4. Experimental setup for the phase measurement using a remote nonlinear crystal. Three beams, the radiated sum frequency and the reflected visible and infrared, are collected by a lens and focused through a compensator into a nonlinear crystal. A simple compensator has been constructed from two wedges of fused silica. One wedge is translated across a fixed wedge changing the relative optical pathlength of the three beams.

Fig. 5. Comparison of the interference patterns from quartz (squares) and PDA monolayer (circles) obtained at ω_{ir} = 2859 cm^{-1} (top), 2876 cm^{-1} (middle) and 2889 cm^{-1} (bottom). The data have been normalized and shifted vertically for the sake of comparison. Note the horizontal shift in the interference patterns as ω_{ir} changes.

Fig. 6. Rotational dependence of SFG intensity for crystalline quartz off resonance

(triangles), at CH_3 symmetric stretch resonance for PDA deposited monolayer (circles) and 8CB monolayer (squares). Curves are fits of data to Eqs. (2) and (8).

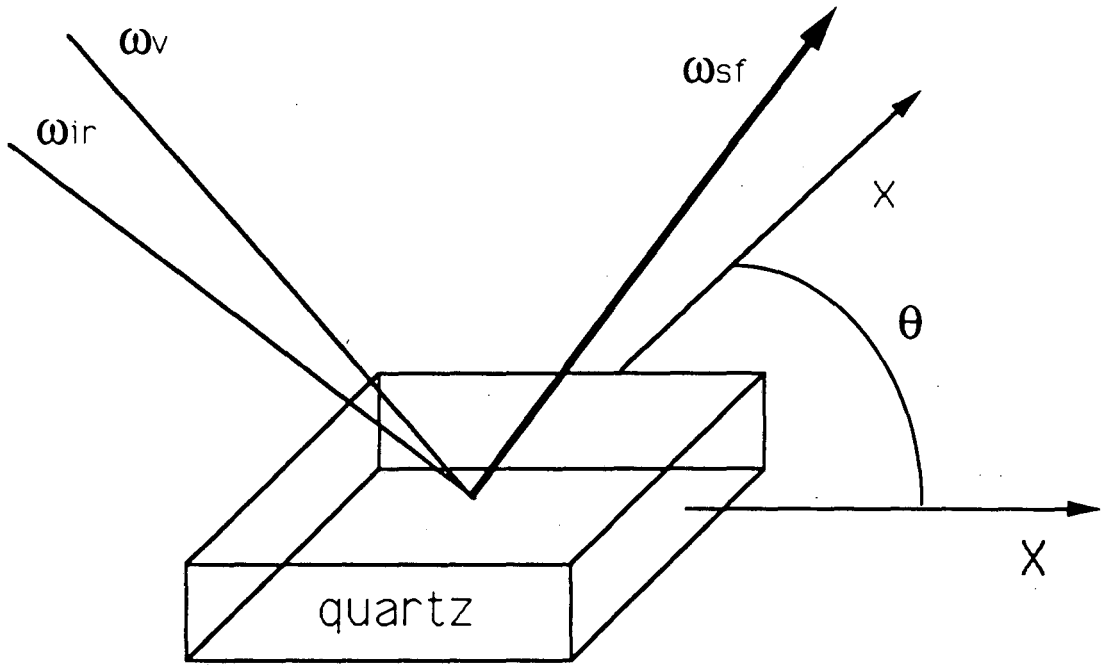

XBL 917-1503

Fig.1

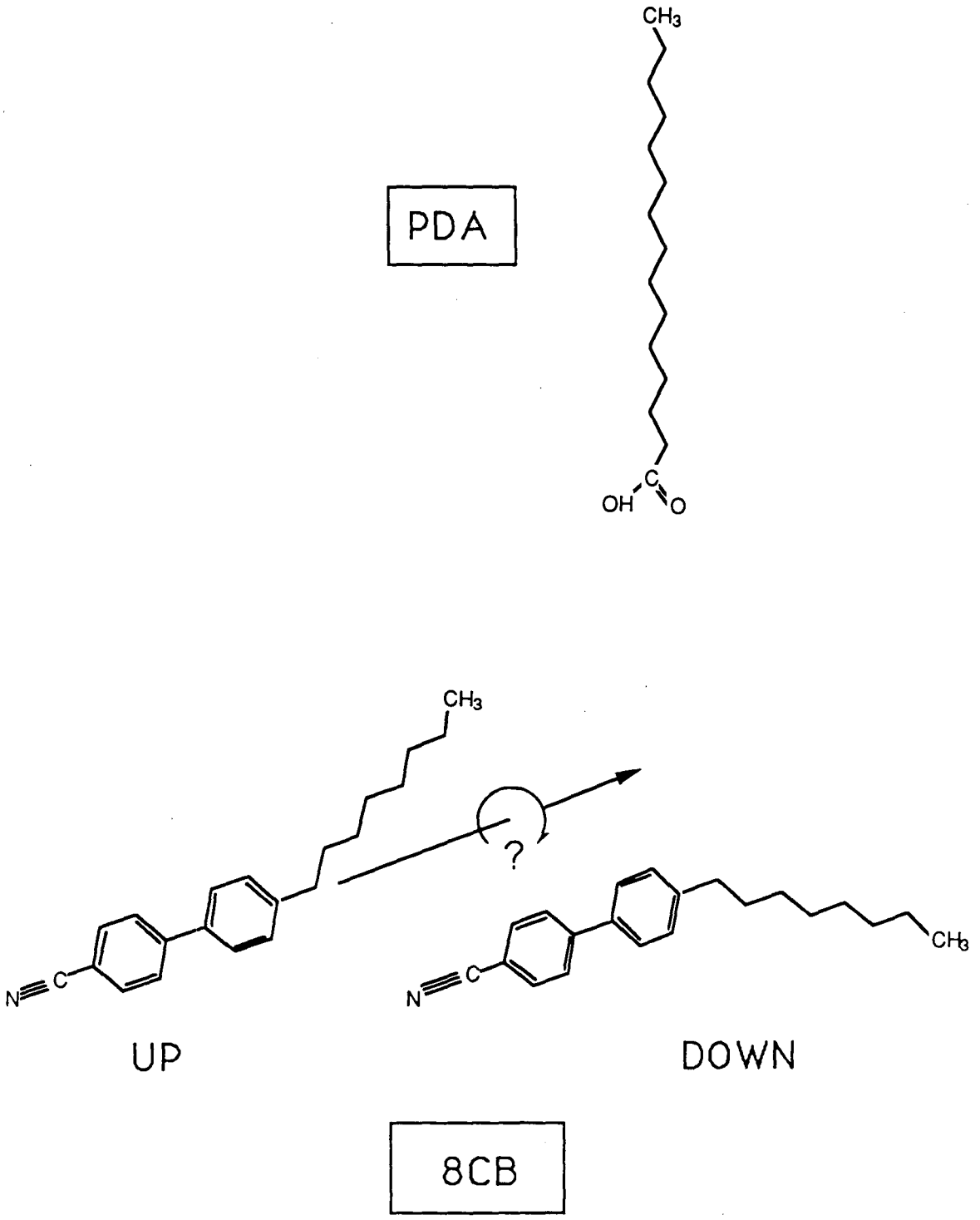

XBL 917-1504

Fig.2

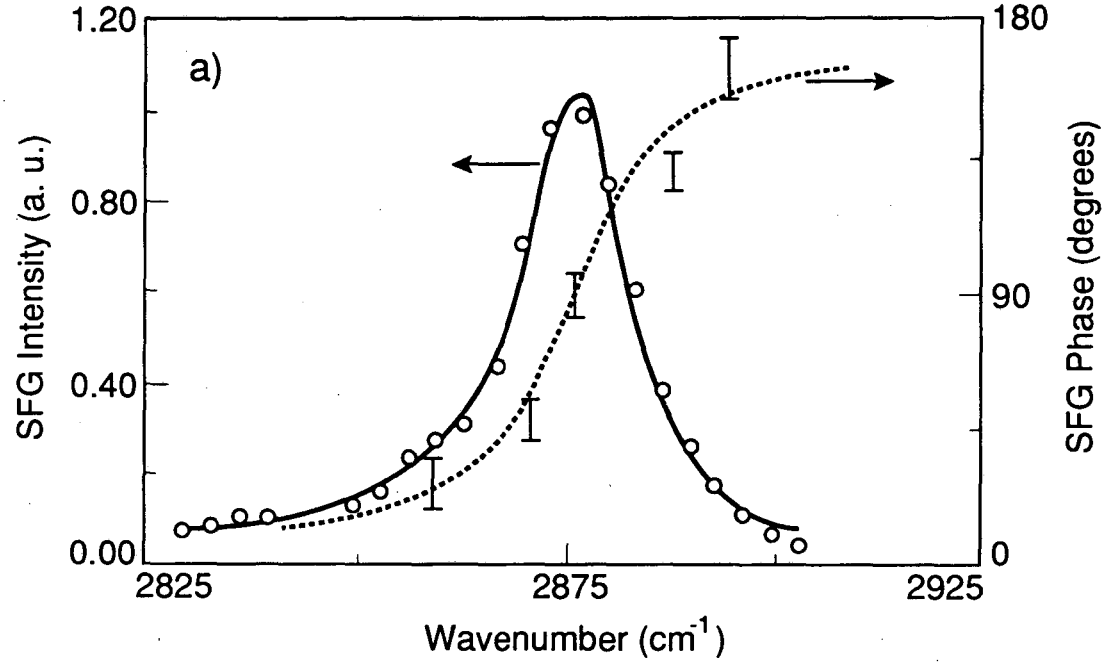
a)
1.20
0.80
0.40
0.00
SFG Intensity (a. u.)
180
90
0
SFG Phase (degrees)
2825
2875
2925
Wavenumber (cm-1)
XBL 903-5464

Fig.3

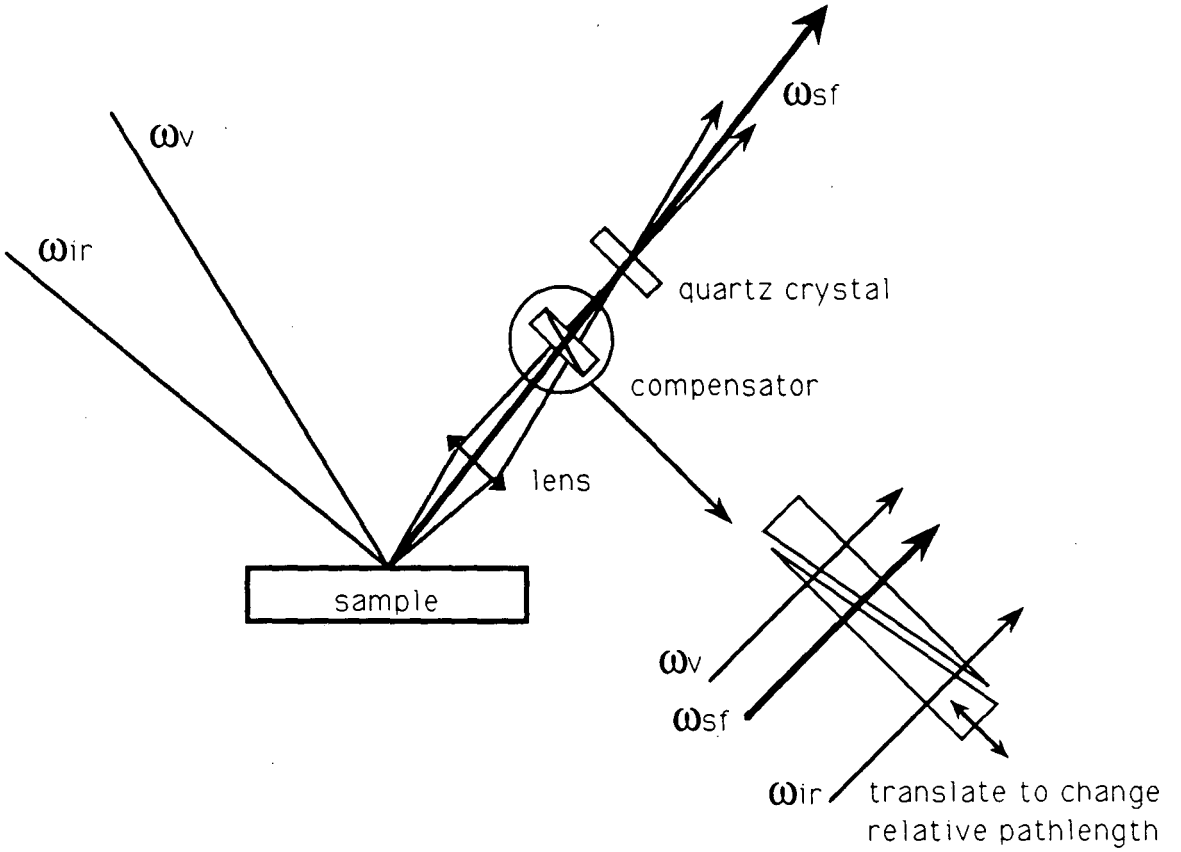
ωsf
ωv
ωir
quartz crystal
compensator
lens
sample
ωv
ωsf
ωir
translate to change
relative pathlength
XBL 917-1505

Fig.4

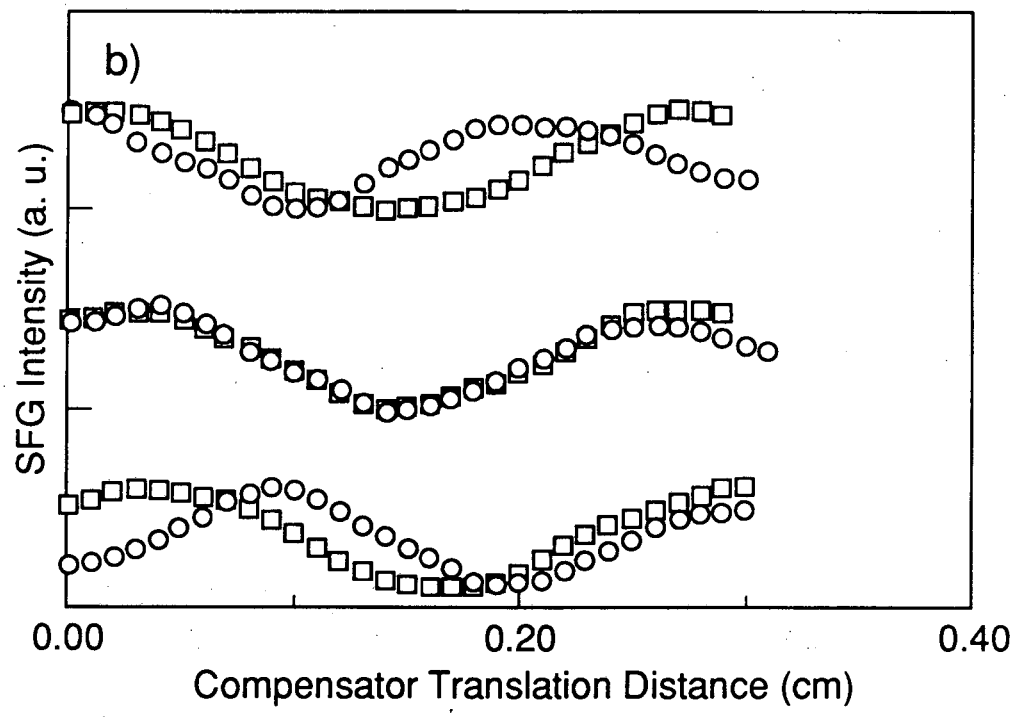

XBL 903-5454

Fig.5

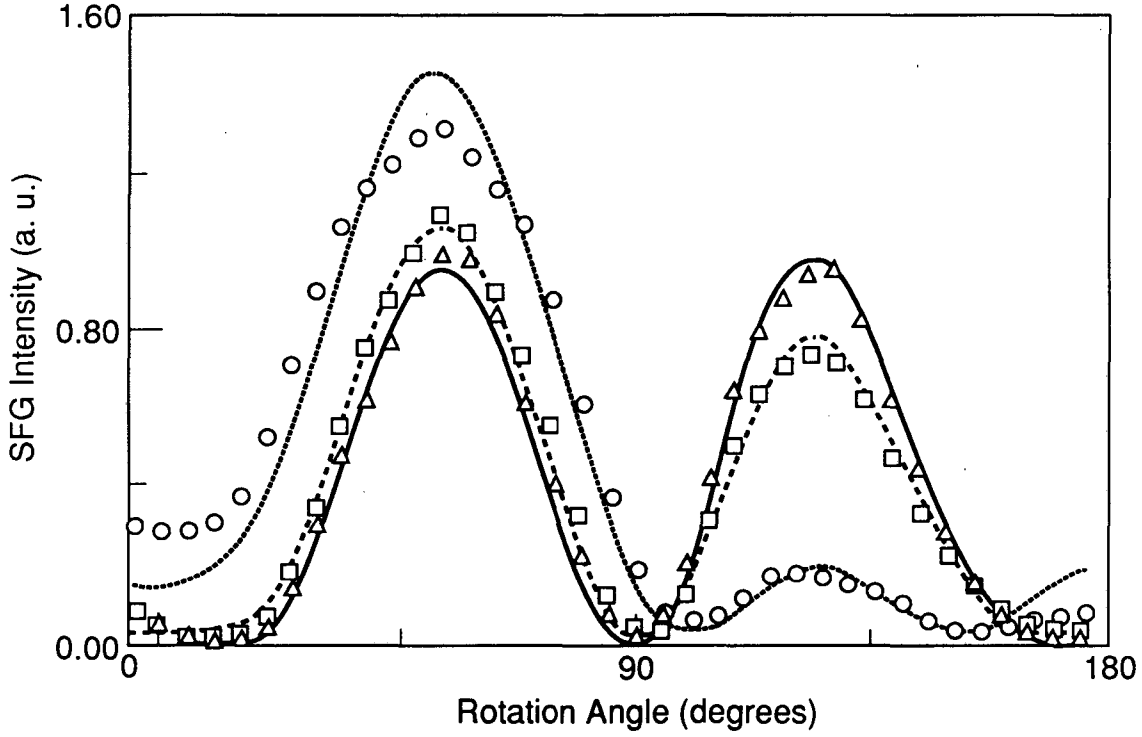
1.60
0.80
0.00
SFG Intensity (a. u.)
0
90
180
Rotation Angle (degrees)
XBL 903-5451

Fig.6

V. Experimental Determination of the Sign of Molecular Dipole Moment Derivatives: An Infrared Visible Sum Frequency Generation Absolute Phase Measurement Study.

Knowledge of the bond dipole, bond polarizability, and their derivatives with respect to the normal mode coordinates is important for the understanding of molecular structure. They have been intensely studied in the past.[1] Although the magnitudes of these quantities are accessible through standard techniques, the experimental determination of their sign has proven much more difficult. However, it is well known that coherent nonlinear optical techniques can measure the phase of a material response.[2-4] In particular, we have recently demonstrated the ability to measure the sign of the nonlinear susceptibility $\boldsymbol{\chi}^{(2)}_s$ of an oriented molecular monolayer at a vibrational resonance using infrared-visible sum frequency generation (SFG). Knowing the polar orientation of the monolayer, the sign of $\boldsymbol{\chi}^{(2)}_s$ directly determines the relative sign of the derivatives of the dipole moment and polarizability with respect to that normal mode. When the sign of one of these quantities is well established, the sign of $\boldsymbol{\chi}^{(2)}_s$ allows us to determine the sign of the unknown quantity. We present our results for the CH stretch vibration mode for two different molecules.

A. Theory

For surface SFG, the signal is generated by the surface nonlinear polarization[5]

$$\mathbf{P}^{(2)}_s = \boldsymbol{\chi}^{(2)}_s : \mathbf{E}_1(\omega_v)\, \mathbf{E}(\omega_{ir}) \qquad (1)$$

where $\mathbf{E}_1$ and $\mathbf{E}_2$ are the fields at the visible and infrared frequencies, respectively, and $\boldsymbol{\chi}_s^{(2)}$ is the surface nonlinear susceptibility. In the case where $\boldsymbol{\chi}_s^{(2)}$ is dominated by adsorbed molecules, it is related to the molecular nonlinear polarizability $\boldsymbol{\alpha}^{(2)}$ through a coordinate transformation averaged over the molecular orientational distribution, denoted by the angular brackets ,

$$\chi_{s,ijk}^{(2)} = N \sum_{lmn} < (\mathbf{i}\cdot\mathbf{l})\,(\mathbf{j}\cdot\mathbf{m})\,(\mathbf{k}\cdot\mathbf{n}) > \alpha_{lmn}^{(2)} \qquad (2)$$

where N is the surface density. With ω_{ir} near vibrational resonances, we can write $\boldsymbol{\alpha}^{(2)} = \boldsymbol{\alpha}_{nr}^{(2)} + \boldsymbol{\alpha}_{r}^{(2)}$ with the resonant part given by[6-8]

$$\alpha_{r,lmn}^{(2)} = \sum_q \frac{1}{2\omega_q} \frac{1}{\omega_q - \omega_{ir} - i\Gamma_q} \frac{\partial \mu_n}{\partial Q} \frac{\partial \alpha_{lm}^{(1)}}{\partial Q} \qquad (3a)$$

$$\frac{\partial \mu_n}{\partial Q} = \left(\frac{2\omega_q}{\hbar}\right)^{1/2} < g \,|\, \mu_n \,|\, q > \qquad (3b)$$

$$\frac{\partial \alpha_{lm}^{(1)}}{\partial Q} = \left(\frac{2\omega_q}{\hbar}\right)^{1/2} \sum_q \frac{1}{\hbar} \left(\frac{< g \,|\, \mu_l \,|\, n >< n \,|\, \mu_m \,|\, q >}{\omega_s - \omega_{ng} + i\Gamma_{ng}} - \frac{< n \,|\, \mu_l \,|\, q >< g \,|\, \mu_m \,|\, n >}{\omega_s - \omega_{qn} + i\Gamma_{qn}} \right) \qquad (3c)$$

where $\boldsymbol{\mu}$ and $\boldsymbol{\alpha}^{(1)}$ are the molecular dipole moment and linear polarizability, respectively, and Q is the normal mode vibrational coordinate. In addition, |q> is a ground electronic but excited vibrational state, |n> is an excited electronic state, μ_i is a component of the dipole moment operator including both electrons and ions, and we have assumed that all of the molecules are initially in their ground state. While infrared absorption and Raman scattering can yield the magnitudes of $\partial\boldsymbol{\mu}/\partial Q$ and $\partial\boldsymbol{\alpha}^{(1)}/\partial Q$, they do not determine their signs. In our SFG measurements, we can measure the phase of $\boldsymbol{\chi}_s^{(2)}$, which for molecules of known orientation determines the

phase of $\boldsymbol{\alpha}^{(2)}$ and hence the relative sign of $\partial\boldsymbol{\mu}/\partial Q$ and $\partial\boldsymbol{\alpha}^{(1)}/\partial Q$ for the molecules.

We have studied the symmetric CH stretch mode of the methyl group of adsorbed molecules. We assume C_{3v} symmetry for the methyl group and a bond polarizability model where only the dipole matrix elements along the C-H bonds contribute to $\partial\boldsymbol{\mu}/\partial Q$ and $\partial\boldsymbol{\alpha}^{(1)}/\partial Q$ in Eq. (3). Raman scattering[9,10] and infrared absorption[11] measurements have shown these to be reasonable assumptions. For an orientational distribution isotropic in the surface plane, we then find

$$\chi^{(2)}_{s.yyz} = N\,(0.275 \langle\cos\theta\rangle + 0.165 \langle\cos^3\theta\rangle)\,\frac{1}{2\omega_q}\,\frac{1}{\omega_q - \omega_{ir} - i\Gamma_q}\,\frac{\partial\mu_\xi}{\partial r}\,\frac{\partial\alpha^{(1)}_{\xi\xi}}{\partial r} \qquad (4)$$

where θ is the angle between the surface normal z and the methyl group symmetry axis, ξ is the C-H bond axis and r is the local mode coordinate for the separation of the CH nuclei. If the polar orientation i.e., $\langle\cos\theta\rangle$, of the methyl group is known, the absolute phase measurement of $\chi^{(2)}_{s.yyz}$ at $\omega_{ir} = \omega_q$ allows us to determine the relative sign of $\partial\mu_\xi/\partial r$ and $\partial\alpha^{(1)}_{\xi\xi}/\partial r$. In our experiment, we studied a pentadecanoic acid (PDA, $CH_3C_{13}H_{27}COOH$) monolayer on water[8] and a methoxy (CH_3O) monolayer on glass, depicted in Fig. 1.[12] In both cases, the methyl group is known to be oriented away from the surface with $\langle\cos\theta\rangle$ being negative.

B. Experimental Results

The details of the phase measurement for $\boldsymbol{\chi}^{(2)}_s$ have been presented in the previous section. The susceptibility $\chi^{(2)}_{s.yyz}$ is measured with s, s and p polarizations for the visible, infrared and sum frequency, respectively. The phase measurement is accomplished as in the previous section using the remote nonlinear crystal (quartz) to produce a field to interfere with the sum frequency signal radiated from the

surface. The orientation of the reference quartz is calibrated by a piezoelectric measurement, thereby allowing us to determine the absolute sign of $\chi_s^{(2)}$.[4,13]

Figure 2 shows the SFG spectrum and the phase of $\chi_{s.yyz}^{(2)}$ with ω_{ir} around the CH_3 symmetric stretch (ν_s) resonance for a compact monolayer of PDA spread on water.[8] The results are well described by Eq. (3) with phase of $\chi_{s.yyz}^{(2)}$ on resonance equal to $+\pi/2$. Therefore, we find $(\partial\mu_\xi/\partial r)(\partial\alpha_{\xi\xi}^{(1)}/\partial r) > 0$.

The methoxy sample was prepared from the adsorption of tetramethoxysilane [$(CH_3O)_4Si$, TMS] onto acid-cleaned fused silica from a dry hexadecane solution. The SFG spectrum (Fig. 3) shows a strong signal at the CH_3 ν_s resonance at 2850 cm^{-1},[14] with $|\chi_{s.yyz}^{(2)}|$ greater than 80% of that from the compact monolayer of PDA. This indicates that the methoxy groups form a packed layer with high polar ordering. The dense packing and tetrahedral geometry favor the orientation of the methoxy with the CH_3 group pointing away from the surface. This was confirmed with a contact angle measurement testing the wettability of the surface by water. We found a contact angle of ~ 50°, consistent with results on model methoxy monolayer systems studied with alkylthiols [$CH_3O(CH_2)_{16}SH$] adsorbed on glass.[15] If the oxygen atoms of methoxy were exposed the surface would be modeled by that of poly (ethylene glycol) [$H(OCH_2CH_2)_nOH$], for which the contact angle of water is zero. The measurement on the phase of $\chi_{s.yyz}^{(2)}$ for the methoxy sample, however, gave $-\pi/2$ with ω_{ir} on the ν_s resonance, just opposite in sign to that of PDA. This indicates that for methoxy, $(\partial\mu_\xi/\partial r)(\partial\alpha_{\xi\xi}^{(1)}/\partial r) > 0$.

C. Sign of Raman Polarizability

What can we say about the signs of $\partial\mu_\xi/\partial r$ and $\partial\alpha_{\xi\xi}^{(1)}/\partial r$ separately for the two molecules? For the C-H bond of either molecule, the Raman polarizability $\alpha_{\xi\xi}^{(1)}/\partial r$ is expected to be positive, meaning that $\alpha^{(1)}$ increases with increasing C-H

distance. This can be derived from the molecular orbital theory of covalent bonds.[16,17] In the solid state, it is found for diamond, silicon and germanium that the linear susceptibility decreases with increasing pressure. Within the bond polarizability model, where the crystal susceptibility is calculated by summing over the bond polarizabilities, this implies that $\partial\alpha^{(1)}_{\xi\xi}/\partial r$ is positive. In the case of molecules, the sign has been directly measured for H_2 by determining the temperature dependence of the refractive index of H_2 gas.[18] As the temperature is increased, higher vibrational states are occupied and due to anharmonicity in the interatomic potential, the average distance between atoms increases. Therefore, the larger refractive index at high temperatures implies that the polarizability increases with internuclear distance, i.e $\partial\alpha^{(1)}_{\xi\xi}/\partial r$ is positive.

Yoshino and Bernstein extended these results by a simple argument to other molecules containing H (NH_3, H_2S, etc.).[19] They assumed that the polarizability is a monotonic function of the separation of the hydrogens from the central atom (C for CH_4, for example). Although this assumption seems rather unsophisticated, this work is widely cited in experimental and ab inition theoretical studies. With this assumption, the sign of $\partial\alpha^{(1)}_{\xi\xi}/\partial r$ depends on whether the sum of the polarizabilities of the individual atoms (α_0) is larger than the polarizability of the composite atom, α_∞. For molecules of the type X-H_n, the composite atom is the inert gas atom for the row belonging to the central atom X (e.g. Ne for CH_4). For example, the polarizability of Ne, $\alpha_{Ne} = 4.0\times10^{-25}$ cm^3, while the polarizability of the separated atoms is $\alpha_\infty = \alpha_C + 4\alpha_H = 51.4\times10^{-25}$ cm^3. Therefore, the sign of $\partial\alpha^{(1)}_{\xi\xi}/\partial r$ is again positive. This simple analysis holds true for H_2, consistent with the experimental results. In recent years, ab initio calculations[9] have concluded that the sign of /∂r for C-H bonds is positive in hydrocarbons for all hybridizations (sp_3, sp_2, sp). With $\partial\alpha^{(1)}_{\xi\xi}/\partial r > 0$ well established,the sign of $(\partial\mu_\xi/\partial r)(\partial\alpha^{(1)}_{\xi\xi}/\partial r)$ is just the sign of

$\partial\mu_\xi/\partial r$.

D. Sign of Dipole Moment Derivative

We can gain insight into the physical significance of $\partial\mu_\xi/\partial Q$ by explicitly writing the dipole moment of the molecule as a function of the normal modes.[20] The total dipole moment operator, $\boldsymbol{\mu}_T$ is written as

$$\boldsymbol{\mu}_T = \boldsymbol{\mu}_e + \boldsymbol{\mu}_N = \sum_i q_e \mathbf{r}_i + \sum_N q_N \mathbf{R}_N \qquad (5)$$

where $\boldsymbol{\mu}$, q and $\mathbf{r}$ are the dipole moment operators, charge and position operators, respectively, for the valence electrons (e) or the ion cores (N). The Born-Oppenheimer states for the molecule are written as $\Psi(\mathbf{r},Q) = <\Theta(\mathbf{r},Q)\,\Phi(Q)|$ where Φ is the nuclear wavefunction and Θ is the electronic wavefunction which depends parametrically on the nuclear coordinates, $\mathbf{r}$. The transition moment is taken between the ground and first vibrational level, both belonging to the ground electronic manifold:

$$\boldsymbol{\mu}_T^{0i} = <\Theta_g^Q \Phi_0|\,(\sum_i q_e \mathbf{r}_i + \sum_N q_N \mathbf{R}_N)\,|\Theta_g^Q \Phi_i>. \qquad (6)$$

This can be evaluated by expanding the electronic states about the equilibrium nuclear coordinates, Q_0 ,

$$<\Theta_g^Q| = <\Theta_g^0| + \sum_s <\Theta_s^0| \left(<\Theta_g^0|\partial H/\partial Q|\,\Theta_s^0> E_{gs}^{-1}\, Q \right) \qquad (7)$$

where Θ_s^0 is an excited electronic state also evaluated at Q_0, $E_{gs} = \hbar(\omega_s - \omega_g)$, and H is the full Hamiltonian for the molecule. We can then write the transition moment

as

$$\boldsymbol{\mu}_T{}^{0i} = \frac{\partial \boldsymbol{\mu}_T}{\partial Q_i} Q_i \; ; \quad \frac{\partial \boldsymbol{\mu}_T}{\partial Q_i} = \frac{\partial \boldsymbol{\mu}_e}{\partial Q_i} + \sum_N q_N \frac{\partial \mathbf{R}_N}{\partial Q_i} \tag{8}$$

$$\frac{\partial \boldsymbol{\mu}_e}{\partial Q} = \sum_s \langle \Theta_g^0 | \boldsymbol{\mu}_e | \Theta_s^0 \rangle \left(\langle \Theta_g^0 | \partial H / \partial Q | \Theta_s^0 \rangle E_{gs}^{-1} \right). \tag{9}$$

From this expression, it is clear that $\partial \boldsymbol{\mu} / \partial Q$ has contributions from the change in both the electron distribution and the positions of the ion cores during the vibrational motion. This is sometimes written as[21]

$$\frac{\partial \boldsymbol{\mu}_T}{\partial Q_i} = \sum_N \frac{\partial q_N^{eff}}{\partial Q_i} \mathbf{R}_N + q_N^{eff} \frac{\partial \mathbf{R}_N}{\partial Q_i} \tag{10}$$

where q_N^{eff} is an effective charge located on the nuclear site that describes the equilibrium charge distribution. Then the first term describes a flow of charge between sites during the nuclear motion while the second term is due to the motion of the original site charges. We can now see that the sign of $\partial \mu_\xi / \partial Q$ can provide important information about the equilibrium and dynamic charge distribution within a molecule.

In contrast to the Raman polarizability, the sign of $\partial \mu_\xi / \partial r$ has been predicted to change with C-H hybridization and with the electronegativity of X in X-H or X-C-H. Usually, it can only be obtained through theoretical fits of parameterizations to infrared absorption intensities (FPI)[22,23] or, more recently, from ab initio calculations.[24] It is therefore of great interest to have a technique that can directly - measure this quantity. For the alkane methyl group (C-C-H, sp_3), our result of $\partial \mu_\xi / \partial r < 0$ is in agreement with the ab initio calculations.[24] For the methoxy group

(O-C-H, sp_3), we have $\partial\mu_\xi/\partial r > 0$, but the corresponding ab initio calculation is not yet available. However, the different signs of $\partial\mu_\xi/\partial r$ in the two cases are consistent with the trend noted in studies of FPI of $\partial\mu_\xi/\partial r$ becoming more positive with the increasing electronegativity of the substituent X in X-C-H.[22] To our knowledge, this represents the most direct determination of the sign of $\partial\boldsymbol{\mu}/\partial Q$ by experiment.

In conclusion, we have shown that the phase of the SFG susceptibility together with the known polar orientation of the molecules determines the relative sign of the derivatives of the bond dipole moment and polarizability, $\partial\boldsymbol{\mu}/\partial Q$ and $\partial\boldsymbol{\alpha}^{(1)}/\partial Q$ for the molecules. With the sign of the polarizability derivative well established, this then yields the sign of $\partial\boldsymbol{\mu}/\partial Q$. We have experimentally determined that $\partial\mu_\xi/\partial r$ is negative for the C-H stretch of the alkane methyl group, but positive for the C-H stretch of methoxy.

References

[1] W. B. Person and G. Zerbi, eds., *Vibrational Intensities in Infrared and Raman Spectroscopy*, (Elsevier, Amsterdam, 1982).

[2] R. K. Chang, J. Ducuing, and N. Bloembergen, Phys. Rev. Lett. **15**, 6 (1965).

[3] H. W. K. Tom, T. F. Heinz, and Y. R. Shen, Phys. Rev. Lett. **51**, 1983 (1983).

[4] K. Keminitz, K. Bhattacharyya, J. M. Hicks, G. R. Pinto, K. B. Eisenthal, and T. F. Heinz, Chem. Phys. Lett. **131**, 285 (1986).

[5] Y. R. Shen, Ann. Rev. Phys. Chem. **40**, 327 (1989).

[6] X. D. Zhu, H. Suhr, and Y. R. Shen, Phys. Rev. **B35**, 304 (1987).

[7] J. H. Hunt, P. Guyot-Sionnest, and Y. R. Shen, Chem. Phys. Lett. **133**, 189 (1987).

[8] P. Guyot-Sionnest, J. H. Hunt, and Y. R. Shen, Phys. Rev. Lett. **59**, 1597 (1988).

[9] E. Norby Svendsen and T. Stroyer-Hansen, Mol. Phys. **56**, 1025 (1985); K. M. Gough, W. F. Murphy, T. Stroyer-Hansen, and E. Norby Svendsen, J. Chem. Phys. **87**, 3341 (1987); K. Gough, J. Chem. Phys. **91**, 2424 (1989).

[10] T. Yoshino and H. J. Bernstein, J. Mol. Spec. **2**, 241 (1958).

[11] M. L. Sage, J. Chem. Phys. **80**, 2872 (1984).

[12] D. W. Sindorf and G. E. Maciel, J. Amer. Chem. Soc. **105**, 3767 (1983); D. W. Sindorf and G. E. Maciel, J. Amer. Chem. Soc. **103**, 4263 (1981); J. P. Blitz, R. S. Shreedhara Murthy, and D. E. Leyden, **109**, 7141 (1987).

[13] S. Singh in *Handbook of Lasers*; J. JH. Wynne and N. Bloembergen, Phys. Rev. **188**, 1211 (1969); D. F. Nelson and E. H. Turner, J. Appl. Phys. **39**, 3337 (1968); W. L. Faust and C. H. Henry, Phys. Rev. Lett. **17**, 1265 (1966).

[14] R. S. McDonald, J. Phys. Chem. **62**, 1168 (1958).

[15] G. M. Whitesides and P. E. Laibinis, Langmuir **6**, 87 (1990).

[16] J. C. Phillips, *Covalent Bonding in Crystals, Molecules, and Polymers* (University of Chicago Press, Chicago, 1969).

[17] W. A. Harrison, *Electronic Structure and the Properties of Solids* (W. H. Freeman, San Francisco, 1980) p. 120.

[18] R. P. Bell. Trans. Faraday Soc. **38**, 422 (1942).

[19] T. Yoshino and H. J. Bernstein, J. Mol. Spec. **2**, 213 (1958).

[20] G. Herzberg, Molecular Spectra and Molecular Structure, II. Infrared and Raman Spectra of Polyatomic Molecules. (Van Nostrand, New York, 1956).

[21] G. Longhi, G. Zerbi, L. Ricard and S. Abbate, J. Chem. Phys. **88**,6733 (1988) and references therein.

[22] B. Galabov, T. Dudev, J. R. Durig, and W. J. Orville-Thomas, J. Mol. Struct. **173**, 111 (1988).

[23] S. Kondo, T. Nakanaga, and S. Saeki, J. Chem. Phys. **73**, 5409 (1980).

[24] K. B. Wiberg, and J. J. Wendoloski, J. Phys. Chem. **88**, 586 (1984).

Figure Captions

Fig. 1. Pentadecanoic acid (PDA) and tetramethoxysilane (TMS) and their orientation when adsorbed (PDA) or bonded (TMS) to glass.

Fig. 2 SFG spectrum at CH_3 ν_s resonance for PDA monolayer on water. Both curves are from a fit of the SFG intensity to Eq. (3).

Fig. 3 SFG spectrum in CH stretch region of monolayer of tetramethoxysilane bonded to fused silica. The CH_3 ν_s resonance is located at 2850 cm^{-1}.

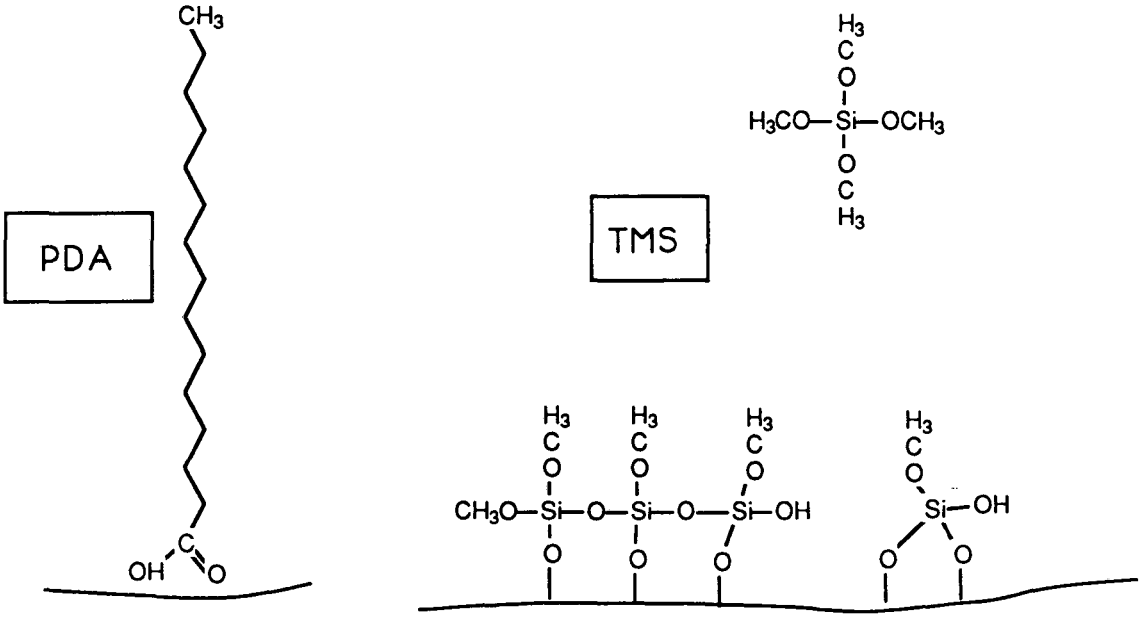

Definition of molecular coordinates

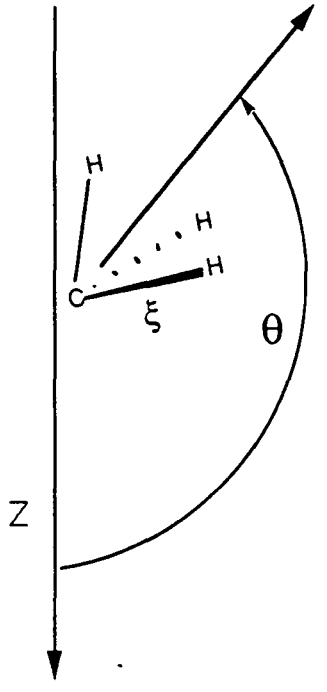

XBL 917-1506

Fig.1

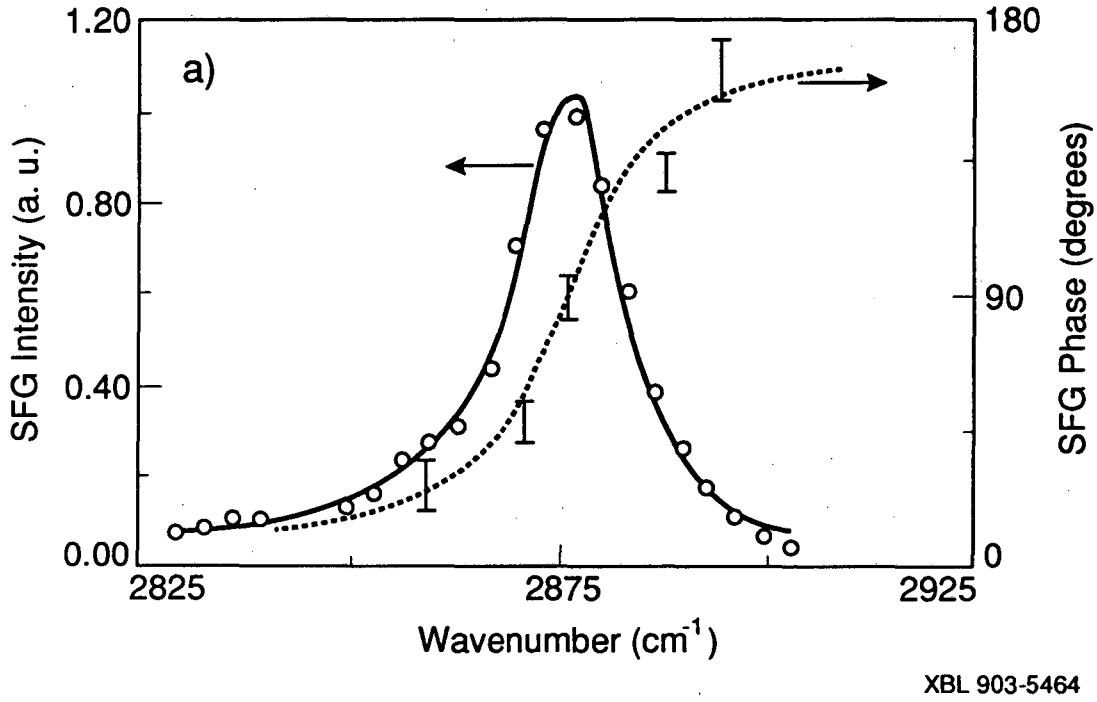
a)
1.20
0.80
0.40
0.00
SFG Intensity (a. u.)
180
90
0
SFG Phase (degrees)
2825
2875
2925
Wavenumber (cm-1)
XBL 903-5464

Fig.2

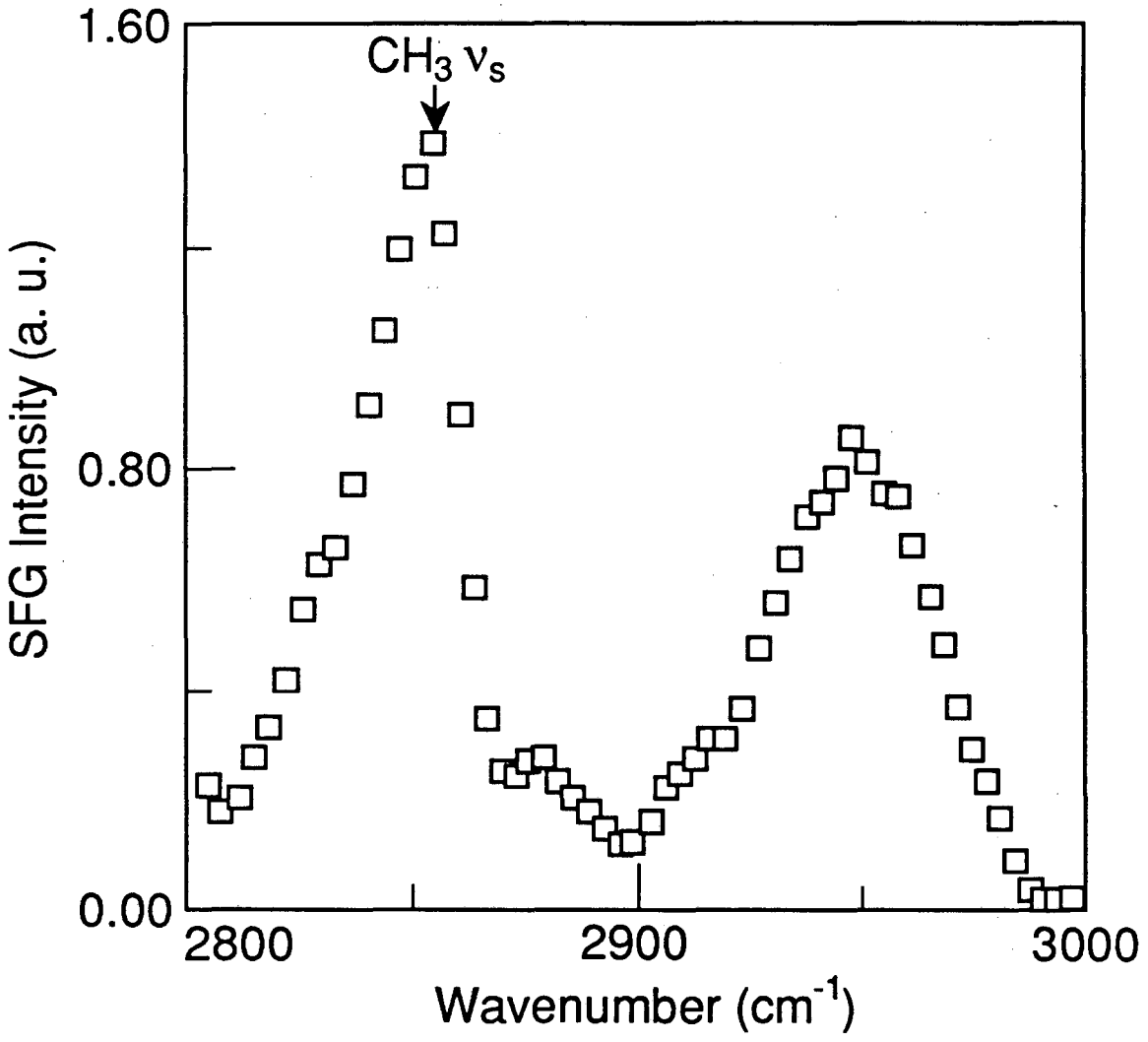
1.60
0.80
0.00
SFG Intensity (a. u.)
CH_3 ν_s
2800
2900
3000
Wavenumber (cm^{-1})
XBL 903-5457

Fig.3

VI. Molecular Ordering at the Pure Liquid/Vapor Interface: Part I. Introduction

The liquid/vapor interface is of fundamental interest as the transition region between two phases of a pure substance. It is also an important starting point for the understanding of heterogeneous interfaces, such as the liquid/solid interface. In the bulk of the liquid or gas phases, the molecules are randomly oriented. Our question is: Do the molecules at the interface react to the asymmetry of their surroundings and establish specific orientations? The experimental evidence from the measurement of macroscopic thermodynamic quantities argues that, in some cases, the answer is yes . For example, the presence of a surface potential in non-ionic liquids establishes the presence of surface polar ordering. The calculation of the surface potential has dominated theoretical studies of aqueous interfaces,[1-4] even though measurement of this quantity is problematical.[5] The ordering of the molecules at the interface should also be manifested in the molar surface entropy, which can be measured by the derivative of the surface tension with respect to temperature.[6] Good has pointed out that low molecular weight liquids can be separated into two classes: In one class, the non-polar and polar non-hydrogen bonding liquids with molar surface entropies averaging about 24 J/deg, and , in a distinct group, the hydrogen bonded liquids with surface entropies around 11 J/deg. It was then argued that the difference between the surface entropies of the two groups was due to increased orientational ordering of the molecules at the interface.[6] Lastly, in the case of alcohols, the surface tension itself suggests surface ordering. The surface tension of alcohols is similar to that of hydrocarbons, implying CH groups, and not OH, are exposed at the interface.[7]

A. Experimental Techniques

The question of liquid interfacial molecular ordering presents many

challenges to both theoretical and experimental studies. The quantity of interest is the density - orientational profile, $f(z,\Omega)$, the probability of finding a molecule at position z in the interface with an orientation Ω. This is a very difficult quantity to measure experimentally.[8] The experimental probe with the greatest spatial resolution is x-ray scattering. It has recently been applied to liquid surfaces in the specular reflection geometry to measure the electron density profile through the interface.[9] In principle, with a molecule with sufficient electron density asymmetry, x-ray scattering should be able to provide information about molecular orientation. However, at this point, x-ray scattering has been used to obtain the surface density profile, i.e. the roughness of the surface, with no conclusions about molecular orientation. It is well known from surface science that the scattering of massive probes such as in electron energy loss spectroscopy, Auger and UV photoelectron spectroscopy can be highly surface specific. The surface specificity of these probes relies on the high scattering cross section of the electrons with matter which also necessitates that the experiments be performed in high vacuum to reduce background scattering. Remarkably, these techniques have been applied to liquid surfaces by the use of a liquid jet in a vacuum chamber.[10] Although the studies have been limited to date, these techniques have been used to obtain the polar orientation of molecules at pure liquid surfaces. However, no experiments have been done on the simple molecules water or methanol as yet.

Optical probes, both linear and nonlinear, have also provided detailed information about liquid surfaces. Whereas x-ray reflectivity meassures the electron density profile, the linear scattering of light as measured in ellipsometry measures the dielectric constant profile.[8] However, since the linear polarizability tensor is symmetric, this technique cannot tell which end of the molecule is up, although it could, in principle, measure the tilt of the molecular axis. To date, ellipsometry has been used to obtain only surface density profiles. We have previously discussed the

surface specificity of the second order nonlinear optical techniques of second harmonic generation (SHG) and sum frequency generation (SFG). In the nonresonant case, SHG has been applied to the liquid/vapor interface of water.[11] However, there is much less information available in SHG as compared to SFG and the separation of bulk and surface contributions as well as the subsequent interpretation of the data is much more difficult in the former.

B. Theory

The theoretical difficulties are as challenging as the experimental problems. The system lacks the translational symmetry of a crystal while retaining solid state densities which necessitate detailed intermolecular potentials[12] and the consideration of many body corrections.[13,14] In addition, the interface is highly inhomogeneous with the density changing by three orders of magnitude over a distance of only several molecular diameters.[15]

We can roughly divide the theoretical approaches into two types. First, there is the analytical approach, which starts from statistical mechanics to obtain a general expression for the orientational distribution function by evaluating the total energy, then the Boltzman factor, as a function of the orientation of the molecule.[3,16] The most useful solutions involve a perturbation expansion in the intermolecular potential which is assumed to be pairwise additive. The zero order potential is spherically symmetric so the zero order $f(z,\Omega)$ is simply the density profile, with no orientation dependence. The first order potential includes the anisotropic part and so the first order $f(z,\Omega)$ now contains information on the polar ordering at the interface. We should also mention the influential, though short lived, attempt by Stillinger to derive the surface potential and the molecular orientation distribution from electrostatics.[1] We will have more to say about this method later. In the

second camp, there are the molecular dynamics (MD) simulations. These start with some spatial distribution of molecules, each with an attached interaction potential. The motions of the molecules are then calculated step by step from the forces due to the interactions between molecules along with some randomness added to simulate temperature. The system is allowed to "age" and then "measurements" are done on the various physical quantities of interest, such as the density, diffusion constant, or orientational distribution. These computer calculations have become increasingly useful in obtaining insight into the problem, especially in conjunction with analytical work and in the case of complex systems.[4,17-19]

1. Analytical Results

The analytical approaches provide the first insight into the mechanisms causing orientation at the liquid/vapor interface.[16] First, of course, an anisotropic intermolecular potential is required. The potentials generally used (for the MD simulations, as well) are Lennard-Jones potentials ($V_{LJ} = 4\varepsilon[(\sigma/r)^{12} - (\sigma/r)^{6}]$; LJ) centered on sites within the molecule, which take into account the short range repulsion due to electron cloud overlap and long range attraction due to induction and dispersion. The electrostatic interactions are accounted for with electric multipoles. Calculations have been carried out for the homonuclear, two site Lennard-Jones (AALJ) potential, where identical 6-12 potentials are centered on two sites, the AALJ with a point quadrupole (AALJQ), and a single site Lennard-Jones potential plus point dipole (SLJD). Even for these relatively simple potentials, surprising complexity in the orientation distribution is found. The orientation of the molecules is seen to change as the transition region between the vapor and liquid is traversed. For AALJ, there is a tendency for the molecules on the liquid (high density) side of the interfacial density profile to stand perpendicular to the surface while they lie parallel on the vapor (low density) side. This trend is reversed for both

AALJQ and SLJD. However, there is no polar orientation at the surface, i.e. $< \cos\theta >$ is zero, for all of these potentials. This can be understood for AALJ and AALJQ from the inversion symmetry of the Lennard-Jones part of the potential and the quadrupole distribution. For SLJD, it is seen that adding a dipole moment to a spherically symmetric potential does not produce polar ordering. This can perhaps be accounted for by the fact that the lateral interaction between dipoles favors an antiparallel orientation.

The simplest potential to display polar ordering is the heteronuclear Lennard-Jones model (ABLJ). It is interesting to note that the effect of adding a point dipole (ABLJD) is to make the molecules lie flat at the interface, reducing the polar ordering that is obtained in its absence. In the electrostatic model of Stillinger, polar ordering requires the molecule to possess both a point dipole and a point quadrupole in the presence of a gradient of the dielectric constant.[1] The combination of multipoles produces an asymmetry in the magnitude of the electric field about the molecule, depending on the relative sign of the dipole and quadrupole. The molecule will then orient to immerse the high field part of the molecule in the high dielectric constant region to minimize the total energy. Within this model, the dipole moment alone will not produce polar ordering since the absolute magnitude of the field about the molecule is symmetric with respect to inversion, so that either polar orientation is energetically identical.[1]

2. Molecular Dynamics Simulations

While the analytic results have established important features of surface ordering, notably the importance of the molecular quadrupole moment, their application to real systems has been limited to the inert gases and diatomic species. One problem, which also arises in MD simulations, concerns the use of only the dipole and quadrupole multipole moments to represent the interaction between

actual molecular charge distributions. This is questionable since the interaction distance is of the order of the size of the charge distribution itself and higher order multipoles might be important. To handle more complicated molecules at this point in time requires MD calculations. Over the past decade, a great deal of effort has gone into understanding the intermolecular potential of water,[12] and several MD simulations of the water liquid/vapor interface have been performed. We will discuss the successes of these simulations in comparison with our SFG spectra in the next two sections. At this point, lest the later success of MD simulations inspire undue confidence, we will review some of the problems with the MD calculations.

A molecular dynamics simulation can only be as realistic as the intermolecular potential it employs. The systems we will be studying are the hydrogen bonded liquids methanol and water. How can an interaction potential model the hydrogen bond? The hydrogen bonds of water[20] and methanol,[21] with enthalpies of about 5 kcal/mol, are of moderate strength and neither charge transfer nor covalency is considered significant.[22] Therefore, the interaction between molecules results mostly from the charge distribution within each molecule, an electrostatic interaction, along with some distortion of this distribution due to the polarizability of the molecule. This is the basis for the use of distributions of point charges within each molecule to produce the hydrogen bonding interaction. For example, a positive charge is placed on each hydrogen atom and compensating negative charges are placed in the molecule to account for the oxygen lone pairs. Unfortunately, because of the complexity, most models do not include the molecular polarizability explicitly.

In the case of water, there are two classes of intermolecular potentials in use. Both rely on similar analytic functions, with free parameters, for the interaction between molecules. The difference between the two groups is that one (i.e. Carravetta-Clementi (CC)) fits the free parameters to ab initio interaction

potentials,[23] which are presently only available for the dimer, while the other group (i.e. ST2,[24] SPC,[25] TIP4P [26]) fits to various experimental values obtained for the bulk liquid, such as the molecular dipole and quadrupole moments, or the oxygen pair distribution function which can be obtained from X-ray scattering. Herein lies the major criticism. As noted before, the interfacial density varies from bulk liquid to vapor and the use of an interaction potential derived from either density relies on the density independence of the interactions. However, this is known to be untrue for water.[20] For example, the dipole moment of water in the vapor is 1.85 D while in the condensed phases it is estimated to be 2.6-3.0 D. Quantum mechanical calculations on trimers and tetramers indicate that the strength of the hydrogen bonding is ~ 25% larger per hydrogen bond than in the dimer. It is not surprising then that the CC potential, derived from the dimer interaction, fails to reproduce bulk liquid quantities. For example, it calculates a bulk density that is 13% too low, a great change for a condensed matter system. The problem is that these potentials explicitly assume pairwise additivity for the interaction energy, mostly due to the neglect of a molecular polarizability. This leaves them without the flexibility to adequately deal with the density variations of the interface. While some attempts to include these effects have been made, they are not yet well developed.[13,14]

Perhaps these difficulties account for the lack of success of the calculations in reproducing the surface potential or the surface tension of water. The analytical approaches have focused on calculating the surface potential. While the original electrostatic model obtained the correct sign and magnitude, it used a value of the water quadrupole moment that was three times too small and of the wrong sign.[1] If we insert the presently accepted value of Q_{zz} = -0.13 D Å ,[27] this treatment yields the wrong sign and is too small by an order of magnitude. Croxton, using a local free energy formalism, obtained the correct sign for the surface potential but was too large by an order of magnitude.[3] The MD simulations have similar problems. For

the surface potential, the TIP4P[18] model predicts the wrong sign and Wilson et. al. have argued that this quantity is rather sensitive to the details of the molecular charge distribution and might necessitate the inclusion of a molecular polarizability.[4] The surface tension has also faired poorly, with the CC potential predicting 25 dyn/cm,[17] the ST2 model obtaining 97 dyn/cm [28] and TIP4P calculating 149 dyn/cm[4,29] while the experimental value is 68 dyn/cm.[30] However, the CC potential is quite accurate in determining the molar surface entropy, an indication that the molecular ordering might be realistic.

Much less theoretical work has been done on the liquid/vapor interface of methanol. The single MD simulation available uses a model of three sites, one for the CH_3 group and two for the OH, interacting with those of another molecule through Coulomb and Lennard -Jones potentials.[31] The calculated surface tension and bulk liquid density differ from the experimental values by 25% and 14% respectively, while the surface entropy, as in the case of water, is reproduced quite well.

The analytical understanding of molecular orientational ordering at liquid interfaces is in an early stage, as are the computer simulations which can provide very detailed information, albeit with intermolecular potentials that require improvement. Clearly, an experimental technique to probe the molecular orientation distribution directly would fulfill a great need in the understanding of the liquid/vapor interface.

References

[1] F. H. Stillinger, Jr. and A. Ben Naim, J. Chem. Phys. **47**,4431 (1967).

[2] N. H. Fletcher, Philos. Mag. **18**, 1287 (1968).

[3] C. A. Croxton, Physica **106A**, 239 (1981).

[4] M. A. Wilson, A. Pohorille, and L. R. Pratt, J. Chem. Phys. **88**, 3281 (1988).

[5] J. E. B. Randles, Phys. Chem. Liq. **7**, 107 (1977).

[6] R. J. Good, J. Phys. Chem. **61**,810 (1957).

[7] A. W. Adamson, *Physical Chemistry of Surfaces* (Wiley, New York, 1990), p. 69.

[8] D. Beaglehole in Fluid Interfacial Phenomena, C. A. Croxton, ed. (J. Wiley, New York, 1986), Ch. 11.

[9] for a review, see J. Als-Nielsen, in Physiochemical Hydrodynamics, Interfacial Phenomena, M. G. Velarde, ed. (Plenum Press, New, York,198).

[10] E. M. Lee and R. K. Thomas, Physica B **156**, 525 (1989); R. E. Ballard et. al., Chem. Phys. Lett. **147**, 629 (1988); R. E. Ballard et. al., Chem. Phys. Lett. **151**, 477 (1988); R.E. Ballard, Jimmy Jones and D. Read, Chem. Phys. Lett. **121**, 45 (1985); W. Keller, H. Morgner and W. A. Muller, Molecular Physics **57**, 623 (1986).

[11] M. C. Goh, J. M. Hicks, K. Keminitz, G. R. Pinto, K. Bhattacharyya, K. B. Eisenthal, and T. F. Heinz, J. Phys. Chem. **92**, 5074 (1988).

[12] for a recent review see K. Watanabe and M. L. Klein, Chem. Phys. **131**, 157 (1989).

[13] P. Barnes, J. L. Finney, J. D. Nicholas, and J. E. Quinn, Nature **282**, 459 (1979).

[14] S. L. Carnie and G. N. Patey, Mol. Phys. **47**, 1129 (1982).

[15] A. Braslau, M. Deutsch, P. S. Pershan, A. H. Weiss, J. Als-Nielsen, and J. Bohr, Phys. Rev. Lett. **54**, 114 (1985).

[16] K. E. Gubbins in *Fluid Interfacial Phenomena*, C. A. Croxton, ed. (J. Wiley, New

York, 1986), Ch. 10.

[17] M. Matsumoto and Y. Kataoka, J. Chem. Phys. **88**, 3233 (1988).

[18] M. A. Wilson, A. Pohorille, and L. R. Pratt, J. Phys. Chem. **91**, 4873 (1987).

[19] R. M. Townsend and S. A. Rice, J. Chem. Phys. **94**, 2207 (1991).

20 D. Eisenberg and W. Kauzmann, The Structure and Properties of Water (Oxford, New York, 1969).

[21] U. Liddel and E. D. Becker, Spectrochimica Acta **10**, 70 (1957).

[22] M. D. Joesten and L. J. Schaad, *Hydrogen Bonding* (Dekker, New York, 1974).

[23] O. Matsuoka, E. Clementi, and M. Yoshimine, J. Chem. Phys. **64**, 1351 (1976); V. Carravetta and E. Clementi, J. Chem. Phys. **81**, 2646 (1984).

[24] F. H. Stillinger and A. Rahman, J. Chem. Phys. **60**, 1545 (1974).

[25] H. J. Berendsen, J. P. M. Postma, W. F. van Gunsteren, and J. Hermans, in Intermolecular Forces, B. Pullman, ed. (Reidel, Dordrecht, 1981) p. 331.

[26] W. L. Jorgensen, J. Chandrasekhar, J. D. Madura, R. W. Impey, and M. L. Klein, J. Chem. Phys. **79**, 926 (1983).

[27] J. Verhoeven and A. Dymanus, J. Chem. Phys. **52**, 3222 (1970).

[28] F. H. Stillinger and A. Rahman, J. Chem. Phys. **60**, 1545 (1974).

[29] This researcher commented that it is remarkable it comes this close. L. R. Pratt, private communication.

[30] G. J. Gittens, J. Colloid Interface Sci. **30**, 406 (1969).

[31] M. Matsumoto and Y. Kataoka, J. Chem. Phys. **90**, 2398 (1989).

VII. Molecular Orientational Ordering at the Pure Liquid/Vapor Interface: Part II. Methanol

We report here our study on the air/methanol surface using SFG. Methanol was chosen since it is a strongly hydrogen bonded liquid and shows the same low surface entropy of other hydrogen bonded molecules, including water.[1] It is expected to order at the surface because it contains the essential elements of a surfactant, a hydrophobic group, CH_3, and a hydrogen bonding group, OH.[2] In this sense it can be thought of as the simplest surfactant. In addition, a molecular dynamics simulation on the surface molecular orientation is available.[3] Our result shows that the surface methanol molecules are polar-oriented with CH_3 groups facing away from the liquid, in agreement with the theoretical prediction.

A. Introduction - Theory and Experiment

We have discussed the theory of sum frequency generation at the interface of isotropic media. The process is allowed in the electric-dipole approximation only in a medium without inversion symmetry. In the case of a molecular liquid, we expect that the surface contributes to the SFG spectrum significantly only if the molecules at the surface are polar-oriented. The polarization dependence of the SFG spectrum then allows us to deduce the average polar orientation of the surface molecules (or atomic groups in the molecules). This however assumes that the quadrupole and bulk contributions to SFG can be neglected or subtracted.[4] Therefore the other important task of our present work is to show that by properly designing the experiments, one can find the relative magnitudes of the various contributions to the observed SFG spectrum. In the methanol case, the spectrum is actually dominated by the polar-oriented surface molecular layer.

The material property that can be deduced from the measurement of SFG in reflection from a surface is the effective surface nonlinear susceptibility $\chi_S^{(2)}(\omega_2 = \omega_v + \omega_{ir})$ which generally consists of three parts[4]

$$\chi_S^{(2)} = \chi_D + \chi_I + \chi_{SB} \tag{1}$$

where χ_D is the electric-dipole contribution from the polar-oriented surface layer, χ_I is the electric-quadrupole contribution from the surface region due to the rapid field variation at the interface, and χ_{SB} is the electric-quadrupole contribution originating from the bulk. With the input infrared frequency ω_{ir} near resonances and the input visible frequency ω_v off resonance, each term in Eq. (1) can be decomposed into a resonant and nonresonant part; for example,

$$\chi_D = \chi_D^{NR} + \chi_D^{R} \tag{2a}$$

$$\chi_D^{R} = \sum_q \frac{A_q}{\omega_q - \omega_{ir} - i\Gamma_q} \tag{2b}$$

Here, A_q, ω_q, and Γ_q are the strength, frequency, and damping constant for the q^{th} vibrational mode of the molecules. Note that for the same mode q, the resonant frequency ω_q in χ_D, χ_I and χ_{SB} may be different.

We are particularly interested in the electric-dipole term χ_D, as it carries information about the polar orientation of the surface molecules. We can write

$$\chi_{D,ijk} = s_i(\omega_i)\, s_j(\omega_j)\, s_k(\omega_k)\, \chi'_{D,ijk} \tag{3a}$$

$$\chi'_{D,ijk} = N_s \sum_{lmn} < (\mathbf{i}\cdot\mathbf{l})\,(\mathbf{j}\cdot\mathbf{m})\,(\mathbf{k}\cdot\mathbf{n}) > \alpha^{(2)}_{lmn} \qquad (3b)$$

where N_S is the surface density of the polar-oriented molecules at the surface, $s_i(\omega_i)$ $= E_Z(z=0,\omega_i) / D_Z(z=0,\omega_i)$ for i = z and is equal to unity for i = x or y, $\boldsymbol{\alpha}^{(2)}$ is the second-order nonlinear polarizability, and the angular brackets denote an average over the orientational distribution. In our SHG experiment on methanol, the CH_3 stretch modes are probed. As a simple model for the molecular polarizability of the symmetric stretch mode, we assume that the CH_3 group of methanol has C_{3v} symmetry, and the second-order polarizability of each CH bond can be characterized by a single component $\alpha^{(2)}_{\xi\xi\xi}$ along the bond (Fig. 1). For an isotropic surface, there are three independent dipole susceptibilities, $\chi'_{D,yyz} = \chi'_{D,xxz}$, $\chi'_{D,yzy}$ $= \chi'_{D,zyy} = \chi'_{D,xzx} = \chi'_{D,zxx}$, and $\chi'_{D,zzz}$. We then find, for future analysis of molecular orientation, the following explicit expressions for two elements of $\boldsymbol{\chi}_D$

$$\chi^R_{D,yyz} = N_S\,\varepsilon(\omega_{ir})^{-1}\,\alpha^{(2)}_{\xi\xi\xi}\,(0.275 < \cos\theta > + 0.165 < \cos^3\theta >) \qquad (4a)$$

$$\chi^R_{D,yzy} = N_S\,\varepsilon(\omega_{v})^{-1}\,\alpha^{(2)}_{\xi\xi\xi}\,(-0.165 < \cos\theta > + 0.165 < \cos^3\theta >) \qquad (4b)$$

$$\alpha^{(2)}_{\xi\xi\xi} = a_{CH}/(\omega_{CH} - \omega_{ir} - i\Gamma) \qquad (4c)$$

where $\varepsilon(\omega_{ir})^{-1}$ and $\varepsilon(\omega_{v})^{-1}$ are the dielectric constants of methanol at the infrared and visible frequencies, respectively, z is the surface normal and θ is the angle between the symmetric axis of the CH_3 group and the surface normal. We assume that the dipole susceptibility is effectively due to a monolayer of methanol molecules, although recognizing that in detail, both N and the orientational distribution are expected to have a z dependence through the interfacial region.[5] In order to deduce

χ_D from $\chi_s^{(2)}$, we must also know χ_I and χ_{SB}. We have shown in chapter II from a crude estimate that $|\chi_D|$ for a polar-oriented monolayer should be significantly larger than $|\chi_I| \sim |\chi_{SB}|$ (knowing that the quadrupole bulk contribution comes from the electric quadrupole polarizability of the molecules).[4] We shall discuss how we can conclude experimentally that the yyz and yzy components of χ_I and χ_{SB} are negligible.

The experimental setup has been described previously. In the present experiment, the .6 mj visible pulse at .532 μm (dia. 700μm) and the .1 mj infrared pulse tunable about 3.3 μm (dia. 300 μm) were overlapped at the vapor/liquid interface of methanol in a Teflon trough enclosed in a cell (Fig. 2). This was necessary to limit the evaporation of the liquid during the experiment and to reduce contamination. The absorption of the incident infrared beam in the methanol vapor was kept well below 5% by making the beam path in the vapor less than 2 mm. All measurements were performed at room temperature. The frequency of the IR beam was calibrated to within ± 1.5 cm^{-1} with a polystyrene reference and all spectra were normalized to the SFG spectrum from a quartz crystal. The SF signal from $\chi_{S.yyz}^{(2)}$ at the CH_3 symmetric stretch frequency was about 50 photons per pulse, corresponding to $|\chi_{S.yyz}^{(2)}| = 3.5 \times 10^{-16}$ esu.

B. SFG Spectrum and Peak Assignments

Figure 4 shows the SFG spectrum from the air/methanol liquid (L/V) interface for the ssp (SF output, visible input, and IR input are s-, s-, and p-polarized, respectively) polarization combination. The signal from the sps polarization combination was at the noise level $|\chi_{S.yyz}^{(2)}| < .5 \times 10^{-16}$ esu. A fit of the ssp spectrum to Eq. (2) gives vibrational resonances at 2832 cm^{-1}, 2925 cm^{-1}, and 2951 cm^{-1}. The 2832 cm^{-1} comes from the symmetric (ν_s) CH_3 stretch.[6,7] The peaks

at 2925 and 2951 cm^{-1} have been assigned in Raman scattering studies to two Fermi resonances of the CH_3 ν_s mode with overtones of the CH_3 bending modes.[8,9] The spectrum in Fig. 4 is at least partly due to a surface susceptibility because the same measurement at a glass/methanol liquid (G/L) interface (Fig. 3, top) yielded hardly detectable SFG spectra. If the bulk contribution dominated the spectrum of the L/V interface, then there should be an appreciable signal from the G/L interface since the bulk contributions in the two cases are identical. We now want to show that the observed spectrum is actually dominated by χ_D.

C. Multipole Contributions

The bulk contribution to the effective surface susceptibility, χ_{SB}, has in fact two separate parts. One arises from the true electric quadrupole contribution from the bulk, χ_{SB1}, while the other, χ_{SB2}, is a bulk-like surface contribution originating from the difference between the quadrupole nonlinear susceptibilities of the two sides of the interface.[4] The absence of the reflected SFG from the glass/methanol liquid interface indicates that the total contribution from χ_{SB} is small ($|\chi_{SB}| < 8 \times 10^{-17}$esu). The quadrupole susceptibility χ_{SB1} for the ssp polarization combination can be written as

$$\chi_{SB1,ssp} = L_c\, k_v\, (\varepsilon(\omega_{ir})\, \sin\theta_{ir})^{-1}\, (\chi^{P1}_{yzzy} - \chi^{Q}_{zyyz})\, \sin(\theta_v - \theta_{ir}) \qquad (8)$$

where k_v is the magnitude of the wavevector in methanol for the visible beam, θ is the angle between the wavevector and the surface normal projected into the bulk and the bulk quadrupole susceptibilities χ^{P1} and χ^{Q} have been defined in chapter 2. The coherence length is given by $L_c = (k_{z,v} + k_{z,ir} \pm k_{z,sf})^{-1}$, with the plus sign for the reflected signal and the minus sign for the transmission geometry.[10] If SFG in

transmission through a methanol cell (Fig. 3, bottom) is measured, then the χ_{SB1} contribution is expected to dominate because of the associated long coherence length for SFG in transmission, ~ 15 μm, as compared to ~ 330Å for SFG in reflection. This should allow us to find χ_{SB1}. In Fig. 5, we present the SFG spectrum of the CH_3 ν_s mode from such a measurement using the ssp polarization combination. The cell length was about .1mm, much longer than the absorption depth (~ 5 μm) of methanol at the CH_3 ν_s resonance, so that SFG from the far side of the cell is negligible. The double humps instead of a single resonant peak for the CH_3 ν_s mode can be understood by taking into account the strong resonant IR absorption which adds an imaginary component to the wavevector $\mathbf{k}_{ir}$. This acts to shorten L_c at the resonance peak where $\mathrm{Im}(\mathbf{k}_{ir})$ reaches a maximum, thereby producing a dip in the spectrum. A fit to this spectrum by including $\mathrm{Im}(\mathbf{k}_{ir})$ and assuming that χ_{SB1} dominates the signal yields $|\chi_{SB1,yyz}| = 7 \times 10^{-19}$ esu at resonance. We therefore have $|\chi_{SB1,yyz}| / |\chi^{(2)}_{S,yyz}| \sim 0.02$. For the sps polarization combination, the lack of detectable SF signal in transmission in our experiment gives $|\chi_{SB1,yzy}| < 3 \times 10^{-20}$ esu.

We can further establish that the χ_{SB} contribution is negligible in reflected SFG from methanol. In the experiment at the G/L interface, we altered the methanol surface while leaving the bulk unchanged. We can perform another experiment in which we change the methanol bulk. If the SFG signal originates from the bulk, the change in the bulk signal should appear as a change in the SFG spectrum. It is known that the resonant frequency of the CH_3 ν_s mode of bulk methanol shifts +7 cm^{-1} upon dilution of the methanol to a 1:1 aqueous solution.[8,11] We have confirmed this frequency shift by taking the IR absorption spectra of pure and mixed methanol in a separate detection arm simultaneously with the SFG measurement. As shown in Fig. 6, while the IR absorption spectra do exhibit the

shift, the SFG spectra remain essentially unchanged. This clearly indicates that the SFG spectra are dominated by the surface. By fitting the aqueous solution spectrum with two peaks, the original one from the pure methanol surface plus a peak shifted as in the bulk, we can determine the contribution from the bulk to the signal from the aqueous solution surface. Then, by assuming that χ_{SB} is proportional to the bulk density of methanol, we estimate the bulk contribution to the pure methanol surface to be $|\chi_{SB,yyz}| < 8\% |\chi^{(2)}_{s.yyz}|$ or $|\chi_{SB,yyz}| < 2.7 \times 10^{-17}$ esu at the resonant peak.

The χ_I term comes from the electric quadrupole contribution due to the rapid variation of the input fields at the interface. We could estimate its magnitude by measuring SFG from the methanol molecules adsorbed at various liquid/glass interfaces with different dielectric constant ratios.[4] However, methanol does not adsorb strongly on glass. Instead, we used methoxy (CH_3O) chemically bonded to glass and measured the SFG signal in reflection with carbon tetrachloride ($\varepsilon = 2.12$, equal to glass), acetonitrile ($\varepsilon = 1.79$)[12] and air as the contacting dielectrics. We found that the susceptibility in the CH_3 symmetric stretch frequency region was essentially independent of the dielectric constant of the surrounding medium, which allows us to conclude that, $|\chi_{I,yyz}| < 10\% |\chi^{(2)}_{S.yyz}| \sim 3.4 \times 10^{-17}$ esu and $|\chi_{I,yzy}| < 5 \times 10^{-17}$ esu.

From the above results, we can then establish the fact that $\chi_{D,yyz}$ from a polar-oriented methanol molecular layer at the air/ methanol interface actually dominates the SFG spectrum in Fig. 4. It is the first vibrational spectra ever recorded from a neat liquid surface. The lack of signal for the sps polarization combination sets the limit that $|\chi_{D,yyz}| < .8 \times 10^{-16}$ esu.

D. Orientation of Surface Molecules

It is interesting and important to know whether the polar-oriented surface methanol molecules have their CH_3 groups facing up or down. As we have discussed in a previous section, this information can be obtained from the sign of $\chi^{(2)}_S$ for methanol relative to that of a methoxy monolayer adsorbed on glass. The latter is known to have the CH_3 groups pointing away from the glass. By measuring the phases of $\chi^{(2)}_{S,yyz}$ in the two cases, we found that the two $\chi^{(2)}_{S,yyz}$ at the CH_3 symmetric stretch resonance have the same sign, and therefore the surface methanol molecules , on average, must be oriented with the CH_3 groups projecting out of the liquid. This is consistent with the theoretical prediction: the methanol molecules are oriented to maximize the number of hydrogen bonds among them at the interface.[1-3]

From the measured values of $\chi_{D,yyz}$ and $\chi_{D,yzy}$, we can find $\langle\cos\theta\rangle$ and $\langle\cos^3\theta\rangle$ from Eq. (4) if N_s and $\alpha_{\xi\xi\xi}$ are known. Then with the assumption of a Gaussian distribution for θ, the average tilt angle θ_0 and the width of the distribution $\Delta\theta$ can be determined. We take $N_S = \rho^{2/3}$, where ρ is the methanol liquid density, and obtain $\alpha_{\xi\xi\xi}$ from Eq. (4) by assuming that a_{CH} for methanol is the same as the one for the terminal CH_3 group of a fatty acid molecule. We can determine a_{CH} by measuring the SFG signal from a monolayer of fatty acid spread on the water surface where the surface density and molecular orientation can be determined accurately.[13] Because the result of the analysis is very sensitive to the uncertainty in the data, the uncertainties in the values of θ_0 and $\Delta\theta$ are large. We can only conclude that our data are consistent with a range of values between ($\theta_0 = 0$, $\Delta\theta = 110°$) and ($\theta_0 = 60°$, $\Delta\theta = 70°$). Between these extremes, as the average tilt angle increases, the distribution becomes narrower. Undoubtedly, the orientational distribution is very broad. This is consistent with the turbulent nature of the air/liquid interface, and is in agreement with the recent molecular dynamics calculation.[3]

In conclusion, we have shown that SFG allows us to measure the surface vibrational spectrum of a pure liquid and determine the polar orientation of the surface molecules. No other technique has the same capability. We have found that at the pure methanol liquid/vapor interface, the methanol molecules are oriented with their CH_3 groups facing away from the liquid with a very broad orientational distribution.

References

[1] R. J. Good, J. Chem. Phys. 61, 810 (1957).

[2] A. W. Adamson, *Physical Chemistry of Surfaces* (Wiley, New York, 1990), p. 69.

[3] M. Matsumoto and Y. Kataoka, J. Chem. Phys. **90**, 2398 (1989).

[4] P. Guyot-Sionnest and Y. R. Shen, Phys. Rev. B **38**, 7985 (1988); P. Guyot-Sionnest and Y. R. Shen, Phys. Rev. B **35**, 4420 (1987); Y. R. Shen, *The Principles of Nonlinear Optics* (J. Wiley and Sons, New York, 1984), p.497.

[5] K. E. Gubbins in *Fluid Interfacial Phenomena*, C. A. Croxton, ed. (J. Wiley, Chichester, 1986), Ch. 10.

[6] M. Falk and E. Whalley, J. Chem. Phys. **34**,1554 (1961).

[7] L. J. Bellamy, *The Infrared Spectra of Complex Molecules* (Wiley, New York, 1975).

[8] M. Schwartz, A. Moradi-Araghi and W. H. Koehler, J. Mol. Struct. **63**, 279 (1980).

[9] M. Schwartz, A. Moradi-Araghi and W. H. Koehler, J. Mol. Struct. **81**, 245 (1982).

[10] Y. R. Shen, *The Principles of Nonlinear Optics*, (J. Wiley and Sons, New York, 1984) Ch. 6.

[11] R. E. Hester and R. A. Plane, Spectrochim. Acta **23A**, 2289 (1967).

[12] *Handbook of Chemistry and Physics*, 55th ed., R. C. Weast (CRC, Cleveland, 1974).

[13] P. Guyot-Sionnest, J. H. Hunt, and Y. R. Shen, Phys. Rev. Lett. **59**, 1597 (1988).

FIGURE CAPTIONS

Fig. 1. Methanol molecular coordinates as defined in text, along with schematic of liquid surface.

Fig. 2. Experimental cell for liquid/vapor SFG spectrum. Liquid contacts only teflon which has been acid cleaned and the pathlength of the IR beam in vapor is kept to less than 2mm.

Fig. 3. Experimental cells for (top) the liquid/glass interface and (bottom) the bulk liquid transmission geometry.

Fig. 4. SFG spectrum obtained from the liquid/vapor interface of pure methanol. The beam polarizations are s,s and p for the sum frequency, visible (.532μm) and infrared beams, respectively.

Fig. 5. SFG spectrum for pure methanol obtained in transmission geometry. The solid line is a fit to the data for a single resonant peak including the effect of absorption of the infrared beam in the bulk liquid. The dotted line is obtained from a similar calculation without taking into account the IR absorption.

Fig. 6. Comparison of the bulk IR absorption spectra (top) with the reflected surface SFG spectra for pure methanol (circles) and for a 1:1 water/methanol solution (squares). All spectra are normalized and the two SFG spectra are shifted vertically from each other for clarity .

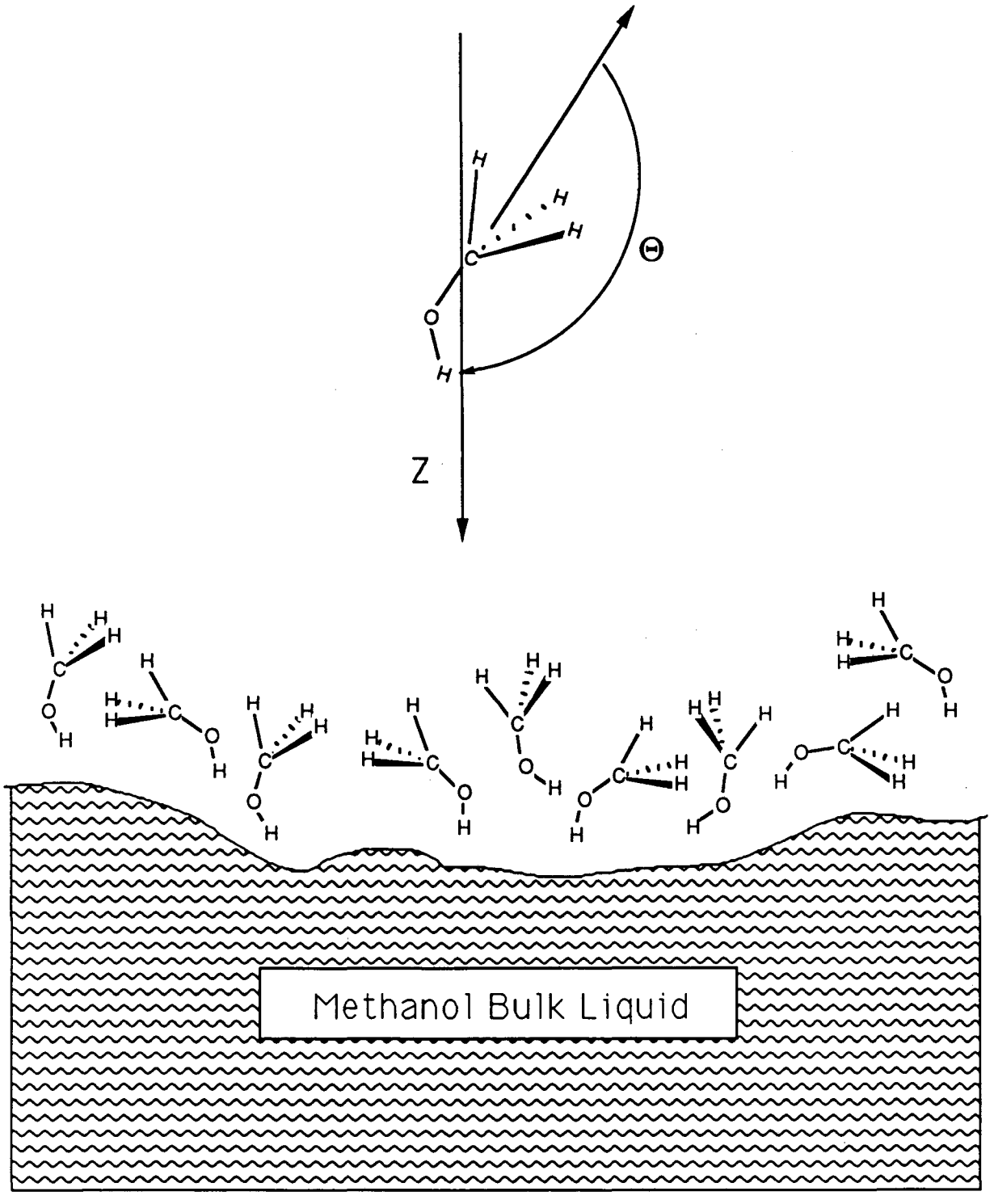

XBL 917-1507

Fig.1

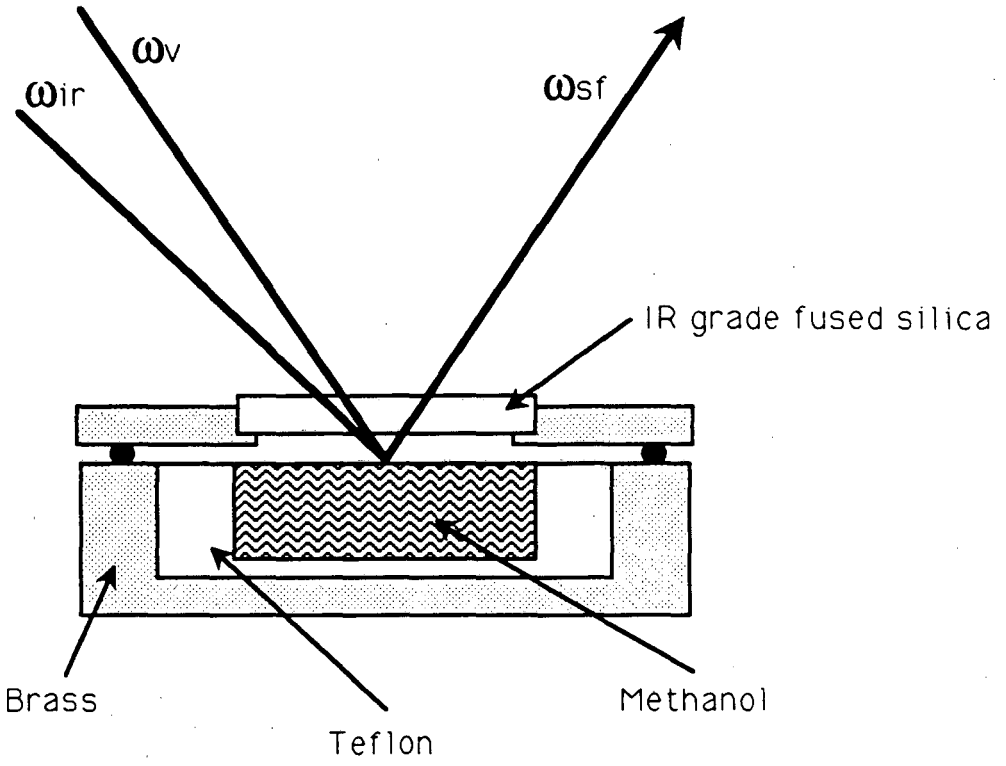

XBL 917-1508

Fig.2

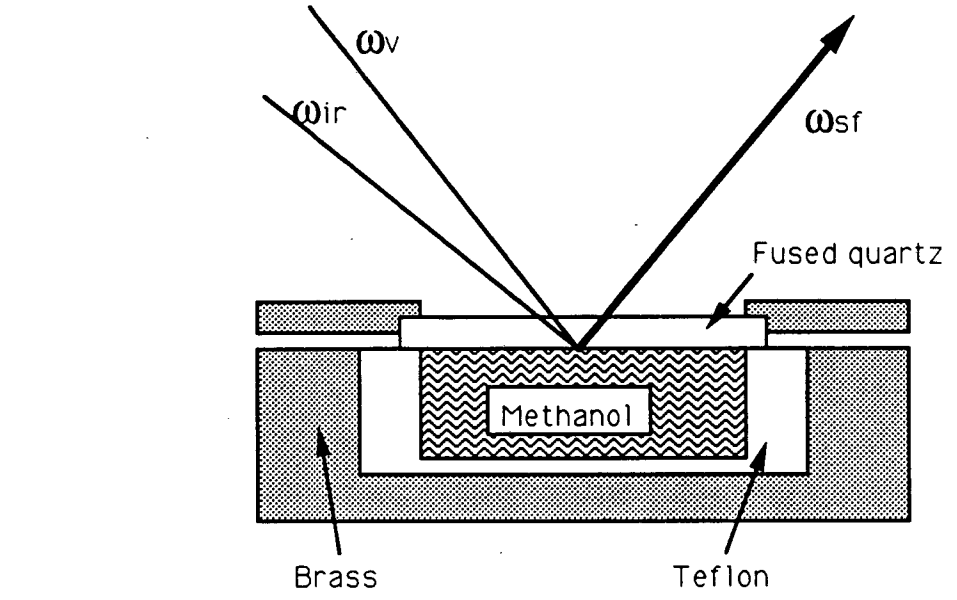

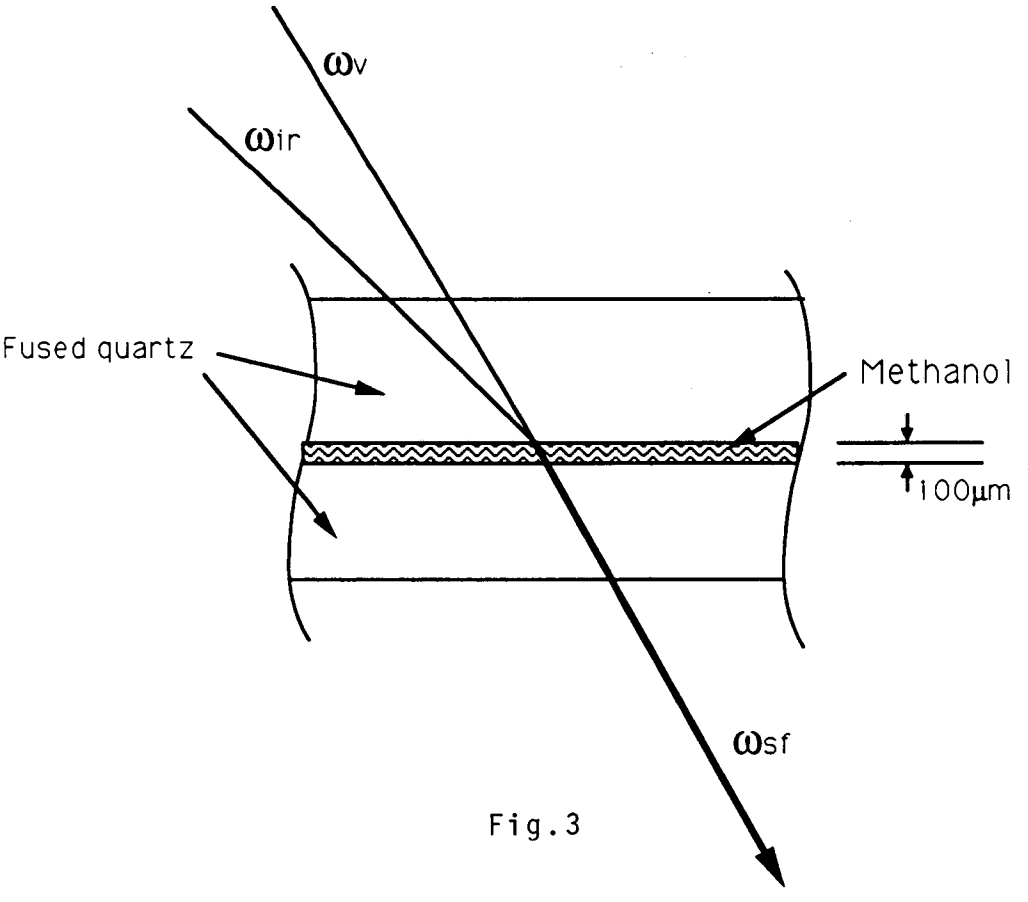

Fig.3

XBL 917-1509

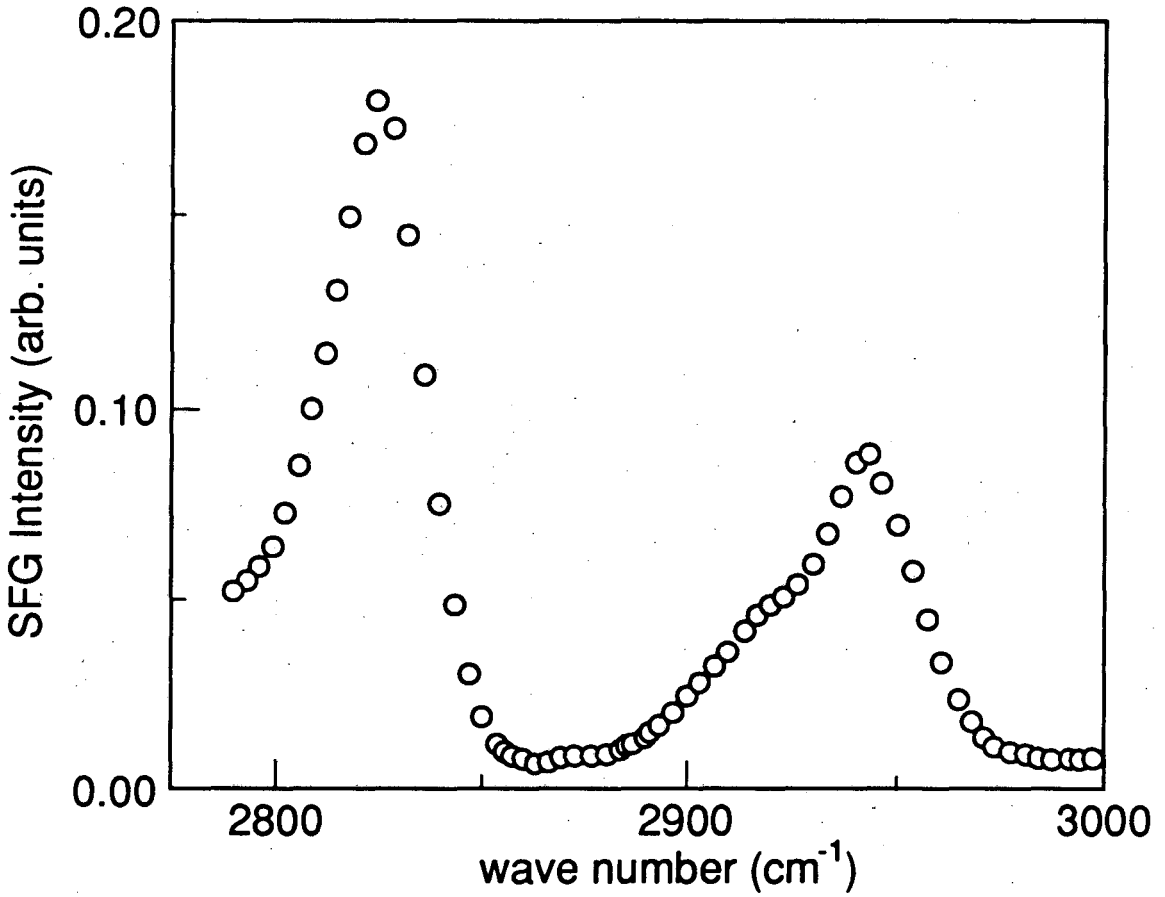
0.20
0.10
0.00
SFG Intensity (arb. units)
2800
2900
3000
wave number (cm-1)
XBL 904-5471A

Fig.4

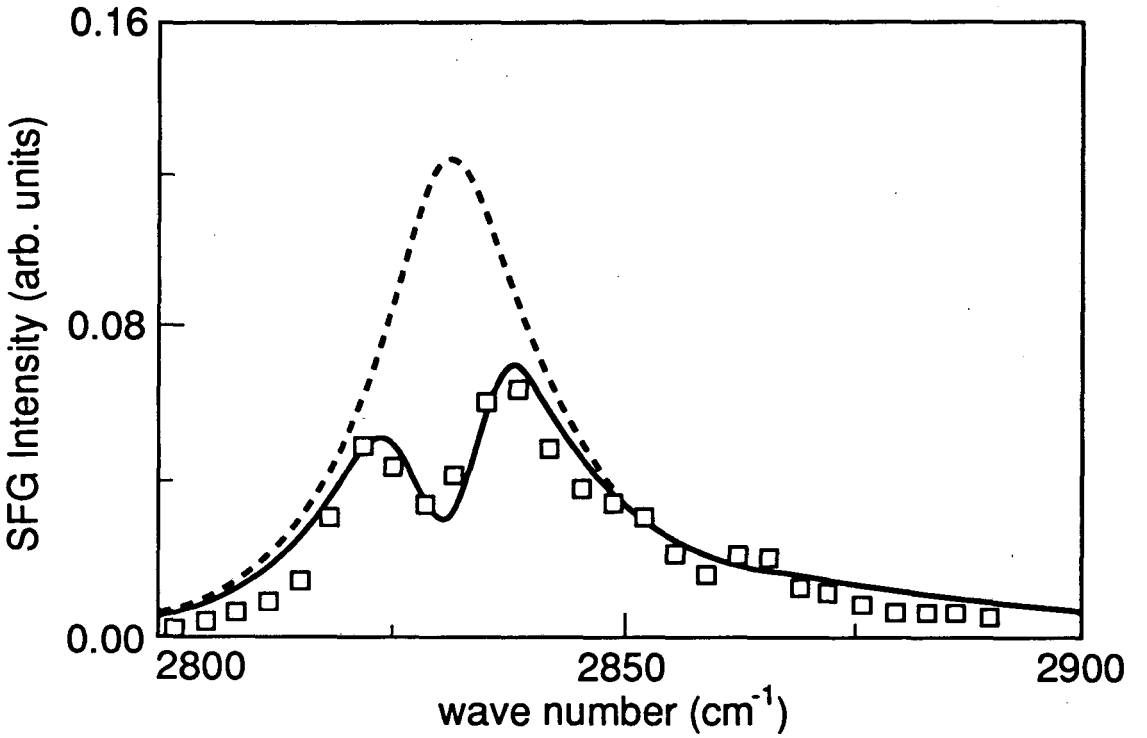

XBL 904-5472A

Fig.5

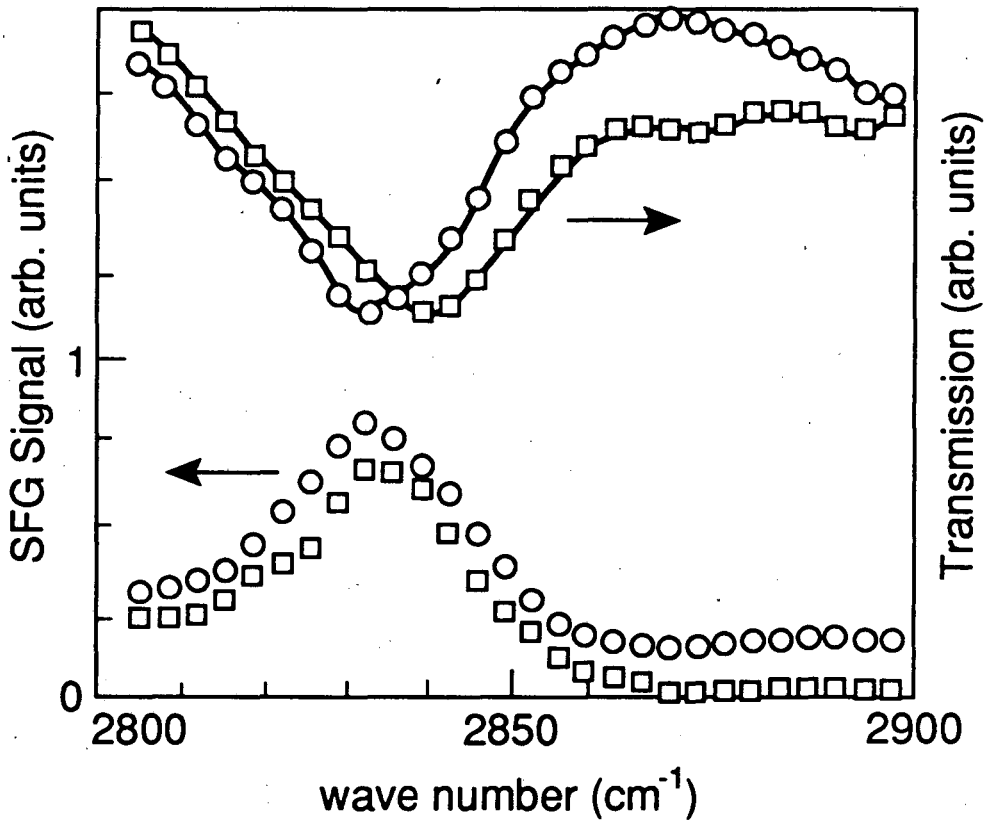

XBL 904-5473A

Fig.6

VIII. Molecular Orientational Ordering at the Pure Liquid/Vapor Interface: Part III. Water

Water is certainly the most studied liquid. Understanding its interfacial properties is important for fundamental studies in chemistry and biology as well as the control of many technological processes.[1] The structure of the pure liquid/vapor interface has had a long history[2] and a substantial literature has developed based on theoretical studies and measurements of macroscopic thermodynamic quantities such as the surface tension and the surface electric potential.[3,4] However, these measurements only give indirect information on surface orientational ordering. In this section, we present the SFG spectrum from the liquid/vapor interface of pure water. It provides the most detailed picture yet obtained of the orientation of the molecules at the neat water surface.

A. Experimental Results

The experimental setup is essentially identical to that described in the previous section. For studying the vibrational spectra in the OH stretch region, the optical parametric amplifier is scanned from 2700 to 3900 cm^{-1}. The bandwidth of the infrared beam varies from about 8 cm^{-1} in the CH stretch region around 2900 cm^{-1} to about 45 cm^{-1} at 3700 cm^{-1}. Calibration is accomplished with a polystyrene reference and an infrared spectrometer.

The SFG spectrum from the water surface is presented in Fig. 1. The polarizations of the input and output beams were sum frequency - s, visible - s, and infrared - p (ssp). The signal in the sps polarization combination was about 10% of the peak ssp signal and showed no resonant features. The SFG signal is

proportional to the square of the absolute magnitude of the nonlinear susceptibility which can be written as

$$\chi_s = \chi_s^{NR} + \chi_s^{R} \tag{1a}$$

$$\chi_s^{R} = \sum_q \frac{A_q}{\omega_q - \omega_{ir} - i\Gamma_q} \tag{1b}$$

where, A_q, ω_q, and Γ_q are the strength, frequency, and damping constant for the q^{th} vibrational mode of the molecules. The peak parameters obtained from a fit of the spectrum to Eq.(1) are collected in Table 1. It should be noted that Eq.(1b) assumes a Lorentzian lineshape for the resonances, and that it has been argued in the literature that the bulk water spectrum (3100 - 3600 cm^{-1}) is more accurately described with more complicated forms.[5] However, we will assume the Lorentzian lineshape and restrict our interpretation to the gross features of the spectrum.

The spectrum in Fig. 1 shows two major features: a broad band between 3100 and 3500 cm^{-1} and a relatively sharp peak at 3690 cm^{-1}. This peak is certainly resolution limited. As in the experiment on the methanol surface, part of our task is to determine the surface or bulk origin of the features of the spectrum. We begin with the 3690 cm^{-1} peak. Two observations help us establish that it originates from the surface. First, the peak lies well outside the range of the bulk water absorption which is confined between 3100 and 3640 cm^{-1} as shown in Fig. (3g). Second, the peak disappears upon modification of the surface, as seen in the spectrum of the water surface after the deposition of a lipid monolayer, Fig.(2), table 2, which will be discussed in detail later.

B. Spectral Assignments from Previous Studies

1. Introduction

The SFG spectrum for the water surface can be understood from the infrared absorption spectra of water clusters,[6-9] which will include molecules with truly unbonded (free) hydrogens, and from the long list of vibrational studies of bulk water,[5,10-15] where all of the hydrogens are interacting, at least weakly, to a neighboring molecule. We will first dicuss the theoretical framework common to the interpretations of the vibrational spectra of both types of water. Then we will present the general conclusions drawn from studies of the water clusters, followed by those of bulk water.

The vibrational spectra are understood, in both the clusters and in the bulk liquid, by starting from the vibrations of the "isolated" molecule and adding perturbations from intramolecular and intermolecular interactions. Loosely speaking, the "isolated" molecule is either in a configuration where the hydrogens are symmetric (either both non hydrogen bonded (NHB) or both hydrogen bonded (HB)) and the molecule retains its C_{2v} symmetry, or the molecule is asymmetric and only one of the hydrogens is NHB. In the first case, a normal mode description is most useful and the vibrational modes correspond to the symmetric (ν_s) and antisymmetric (ν_{as}) stretch modes with ν_{as} at the higher frequency. In the second case, the individual hydrogen stretch frequencies are different enough so that they remain uncoupled from each other and a local mode picture with individual oscillators is used. In this case the NHB OH will have a higher frequency than that of the HB OH group. The bond of the oxygen lone pair only weakly affects the OH frequency.[5] Then couplings are added between vibrational modes. First, an intramolecular coupling can occur from a Fermi resonance between the symmetric stretch mode and the overtone of the bending mode since they both have the same symmetry. Second, an intermolecular coupling is postulated to exist between

neighboring molecules. In this case there would be, for example, a splitting in the "isolated" symmetric stretch frequency with the lower frequency mode described by a coordinated motion with neighboring molecules having their symmetric stretch modes in phase. All of this has been invoked to explain the change in the vibrational spectra in going from the gas phase, with resonances at 3756 cm^{-1} (ν_{as}) and 3657 cm^{-1} (ν_s), to the condensed phase which has a complex broad band centered at 3400cm^{-1} with a full width of about 400cm^{-1}. Clearly, the situation is quite complicated and caution must be exercised in specific peak assignments, particularly in the hydrogen bonded OH stretch region below 3620 cm^{-1}.

2) Water Cluster Spectra

We begin the discussion of the specific peak assignments with the infrared absorption measurements that have been performed on H_2O clusters by infrared predissociation spectroscopy. Several representative geometries, including the calculated lowest energy structure, are presented in Fig. 4.[8,16] The peak assignments for the dimer[7,8] and trimer[6,8] clusters provide insight into the features expected to be present for partially hydrogen bonded water at an interface. There have been a number of experimental and theoretical studies of the dimer which seem to have converged on the geometry and assignments for the vibrational modes. In the dimer, the hydrogen of one molecule, the donor, is hydrogen bonded to the oxygen of the second molecule, the acceptor (Fig. 4(a)). The acceptor molecule, with two free hydrogens, retains its C_{2v} symmetry and the stretch vibrational modes are described by normal modes, with a symmetric stretch at 3610 cm^{-1} and the asymmetric stretch at 3715 cm^{-1}. The donor molecule vibrational modes are separated into the individual stretch modes of the free and hydrogen bonded hydrogens with the free stretch at 3721 cm^{-1} and the bonded stretch at 3535 cm^{-1}. Although the trimer is less

well understood, both infrared absorption measurements in a molecular beam and calculations have been performed. The experiments show a sharp peak at 3715 cm^{-1}, and a broad band between 3200 and 3600 cm^{-1} containing substructure with widths of about 150 cm^{-1} (Fig. 3(a)).[6] The calculations have predicted a cyclic geometry with each molecule having one hydrogen free and one hydrogen bound to the oxygen lone pair of a neighbor, with slightly different geometries for each molecule (Fig. 4(b)).[6,8,17,18] The local mode analysis provides vibrational frequencies for the stretch mode of each hydrogen.[8] The hydrogen stretch frequencies for each molecule have been calculated to be (free hydrogen frequency quoted first) 3740 and 3630 cm^{-1}, 3725 and 3380 cm^{-1} , and 3620 and 3430 cm^{-1} Unfortunately, the calculations fail to reproduce the 3200 cm^{-1} peak seen in the experiments, as well as predicting peaks around 3630 cm^{-1} that are not experimentally observed, so the calculation should only be used as a rough guide to what frequencies may be expected. The 3200 cm^{-1} peak is also rather difficult to assign in bulk water spectra where it is thought to be partially due to a Fermi resonance of the bending overtone with the symmetric stretch mode of a symmetrically (fully) hydrogen bonded water molecule. It is interesting to see how the absorption spectrum changes from the isolated OH groups of the dimer to the spectrum of the fully interacting molecules of bulk water. While the dimer vibrational frequencies are confined to the region greater than 3550 cm^{-1}, the trimer already shows the general features of bulk water that is continued in the spectra of clusters of increasing size. As the cluster size increases in size from $(H_2O)_3$ to $(H_2O)_{19}$, the region from 3100 to 3600 cm^{-1} becomes progressively featureless and fills in to the smooth band that is seen for bulk water (Fig. 3(a-d,g)). Remarkably, the peak at 3715 cm^{-1} persists in the largest cluster, $(H_2O)_{19}$, Fig. 3(d), with its integrated strength relative to the region between 3100 and 3600 cm^{-1} decreasing as the cluster surface to bulk ratio decreases.

3) Bulk Water Spectra

The discussion of the spectra of bulk water inevitably relies on a model to describe its structure.[19] The models are generally recognized as being variations on two extremes, the mixture model and the continuum model. The mixture model postulates a limited number of different types of water molecules differentiated by their interactions with their nearest neighbors (i.e. 3-bonded or 4-bonded molecules) while the continuum model starts from a continuous distribution of strengths of molecular interactions. We will present the general conclusions without pursuing the detailed arguments. The assignments are largely based on the shift of spectral intensity as the temperature of the water is raised. At low temperature, less than 10°, the spectral peak falls below 3300 cm^{-1}. As the temperature is raised, the peak shifts to higher frequencies until finally it is above 3400 cm^{-1} at 90°. Overall, this indicates that the high frequency end of the broad spectrum of bulk water is due to less strongly interacting molecules, while the low frequency part arises from fully hydrogen bonded water. Specifically, the shoulder at 3620 cm^{-1} is assigned to the local stretch mode of the weakly interacting OH group of a partially hydrogen bonded molecule while the region around 3500 cm^{-1} is attributed to the hydrogen bonded OH group of both the partially and fully hydrogen bonded molecules. The region below 3450 cm^{-1} is assigned to the hydrogen bonded OH groups of fully hydrogen bonded molecules and include the effects of Fermi resonance and intermolecular coupling.[5] The conclusion that the low frequency region is due to water that is relatively more structured is also drawn from the infrared absorption spectra of ice (Fig. 3(h)) where the peak is shifted down 200 cm^{-1} from that of liquid water.[14]

C. SFG Spectrum of Neat Water Surface

1) Free OH Peak - Orientation

These studies allow us to unambiguously assign the peak at 3690 cm^{-1} to the stretch mode of an unbonded hydrogen on a water molecule that has its second hydrogen bonded. There are two important questions to answer: What is the surface density of free OH groups and what are their orientation? We can obtain an estimate on the orientation of the unbonded OH group by analyzing the SFG signal for the polarization combinations which access different independent susceptibility components. For an isotropic surface there are three independent surface susceptibility components $\chi_{s,yyz}$, $\chi_{s,yzy}$ and $\chi_{s,zzz}$. The ssp polarization combination measures $\chi_{s,yyz}$, the sps polarization combination measures $\chi_{s,yyz}$ while the ppp combination measures a linear combination of the three independent susceptibilities. From the lack of resonant signal at 3700 cm^{-1} for the sps and ppp polarizations, our measurements have established that

$$\frac{\chi_{s.yzy}}{\chi_{s.yyz}} < .3$$

$$.5 < \frac{\chi_{s.zzz}}{\chi_{s.yyz}} < .75 .$$

In order to understand what these susceptibility ratios can tell us about the orientation distribution, we assume a local moment description of the mode responsible for the peak and assume that the mode is dominated by the motion of the non-hydrogen bonded OH oscillator. We further assume that the SFG signal at 3700cm^{-1} arises entirely from a surface dipole contribution, χ_D. Then the susceptibility can be written as

$$\chi_{D,ijk} = s_i(\omega_i)\, s_j(\omega_j)\, s_k(\omega_k)\ \chi'_{D,ijk} \tag{2a}$$

$$\chi'_{D,ijk} = N_s \sum_{lmn} < (\mathbf{i}\cdot\mathbf{l})\,(\mathbf{j}\cdot\mathbf{m})\,(\mathbf{k}\cdot\mathbf{n}) > \alpha^{(2)}_{lmn} \tag{2b}$$

$$\alpha^{(2)}_{lmn} = \sum_q \frac{1}{2\omega_q} \frac{1}{\omega_q - \omega_{ir} - i\Gamma_q} \frac{\partial \mu_n}{\partial Q} \frac{\partial \alpha^{(1)}_{lm}}{\partial Q} \tag{2c}$$

where N_S is the surface density of the polar-oriented molecules at the surface, $s_i(\omega_i)$ = $E_Z(z=0,\omega_i) / D_Z(z=0,\omega_i)$ for i = z and is equal to unity for i = x or y, $\boldsymbol{\alpha}^{(2)}$ is the second-order nonlinear polarizability, and the angular brackets denote an average over the orientational distribution. In addition, $\partial\boldsymbol{\mu}/\partial Q$ and $\partial\boldsymbol{\alpha}^{(1)}/\partial Q$ (hereafter μ' and α') are the derivatives with respect to the normal mode Q of the infrared transition moment and the polarizability, respectively. Our task is to establish a reasonable $\alpha^{(2)}_{lmn}$. The simplest model is to assume that only $\alpha^{(2)}_{\xi\xi\xi}$ is nonzero where ξ is the coordinate along the OH bond axis. However, this model predicts that $\chi'_{D,yyz} = \chi'_{D,yzy}$ for any orientational distribution, which is clearly excluded by our measurements. Next, we can use Eq. (2c) to obtain the SFG polarizability from literature values for μ' and α', determined from infrared absorption and Raman scattering measurements, respectively. For the next simplest polarizability model, we assume that the transition dipole moment, μ', is strictly along the stretch coordinate and that the Raman polarizability has cylindrical symmetry with two components, $\alpha\mathfrak{d}'_{\parallel}$ and $\alpha'_{\perp}$ where $\parallel$ is the direction along the bond and $\perp$ is perpendicular. The model is now characterized by two SFG polarizibilities, $\alpha^{(2)}_{\perp\perp\xi}$ and $\alpha^{(2)}_{\xi\xi\xi}$, and we denote their ratio by r. For the estimation of orientation, we only need the ratio of the SFG polarizabilities. With the above assumptions, the ratio of the SFG

polarizabilities is given by the ratio of the Raman bond polarizabilities, $\alpha'_{\perp}/\alpha'_{\parallel}$, which we will refer to as r'. This ratio has been determined for both water vapor[20] and for liquid water.[5] It was found that r' varied for liquid water across the broad absorption band with a value of .18 for the strongly hydrogen bonded OH in the low frequency region to .31 for the weakly bound OH groups at the high end, which, compares favorably with the value of .32 determined for water in vapor which is completely free. Here we see why the earlier assumption of only $\alpha^{(2)}_{\xi\xi\xi}$ being nonzero was untenable. Using eq.(2b) we find

$$\chi'_{D,yyz} = N\ .5\ \alpha\ [\ <\sin^2\theta\ \cos\theta>\ (1-r) + 2<\cos\theta>\ r\ ] \tag{3a}$$

$$\chi'_{D,yzy} = N\ .5\ \alpha\ [\ <\sin^2\theta\ \cos\theta>\ (1-r)\ ] \tag{3b}$$

$$\chi'_{D,zzz} = N\ \alpha\ [\ <\cos\theta> - <\sin^2\theta\ \cos\theta>\ (1-r)] \tag{3c}$$

where $\alpha = \alpha^{(2)}_{\xi\xi\xi}$ and we will take r = .32 as indicated from the values of r' for the weakly bound OH groups. If we assume that the ε's are those of bulk water, we find that the above ratios are consistent with $<\cos^2\theta>/<\sin^2\theta\ \cos\theta> \sim 5.5$. For a delta function distribution, this corresponds to $\theta \sim 25°$. If the OH group pointed straight up ($\theta=0°$), then $\chi'_{D,zzz}/\chi'_{D,yyz} = 1/r = 3$, and $\chi'_{D,yzy}/\chi'_{D,yyz} = 0$. As the OH group tilts towards the surface plane, $\chi'_{D,zzz}/\chi'_{D,yyz}$ decreases to .5, $\chi'_{D,yzy}/\chi'_{D,yyz}$ rises monotonically to .7 and all three susceptibilities individually drop to zero. The distribution most certainly has some breadth and is not simply a delta function, but our measurements indicate that the average tilt lies near the surface normal, considerably away from the surface plane.

2) Free Oh Peak - Surface Density

How many of the surface water molecules are oriented with the free OH group pointing out of the liquid? We have shown previously that infrared absorption and Raman scattering data on the vibrational modes of a molecule can be used to obtain quantitative information about the surface molecular layer. Now we will obtain an estimate of the surface density of the free OH species. From Eq. (3a), we can see that in order to determine N, we need to measure χ_{yyz} as well as determine α and the orientational averages in the brackets. By calibrating the SFG signal from the water surface at the peak of the free OH resonance to the signal from a quartz crystal, we obtain $\chi_{D,yyz} = 2.1 \times 10^{-16}$ esu.[21] For the orientational average in the square brackets of Eq. (3a), we obtain a value of .68 for $\theta \sim 25°$.[22] From a matrix isolation study of the water dimer, we obtain for the OH stretch mode of the free OH group of the donor molecule $\mu' = 81.4$ esu.[23] The Raman polarizability for the OH stretch can be obtained from the value for the water molecule in vapor with a correction for the effect of hydrogen bonding, $\alpha'_{||} = 2.0 \times 10^{-4}$ cm^{2}g$^{-1/2}$.[24] From Eq. (2c) we then obtain $\alpha^{(2)}_{\xi\xi\xi} = 2.5 \times 10^{-30}$ esu. From Eqs. (2) and (3) we then find that the surface density $N_s = \varepsilon(\omega_{ir})\, \chi_{D,yyz} / <\alpha> = 1.7 \times 10^{14}$ cm^{-2}. We can compare this with the surface density of a compact water monolayer, N_w, obtained from $N_w = \rho\, \sigma = 8.8 \times 10^{14}$ cm^{-2}, where ρ is the bulk density and σ is the molecular diameter (2.64 Å). Therefore, we have estimated that the surface concentration of free OH groups is about 1/5 of a compact monolayer. This indicates considerably more structure in the surface region than is predicted in the molecular dynamics simulation which obtained a free OH surface density of about 4% N_w.[26]

Are there surface species with two free hydrogens projecting into the vapor? This species should have two vibrational peaks in the region between 3600 and 3750 cm^{-1} as seen in the dimer spectra. The modes would be an antisymmetric stretch

lying above 3700 cm^{-1} and a symmetric stretch falling in the region around 3600 cm^{-1}. With a single peak above 3500 cm^{-1} observed in the ssp spectrum and no resonant features detected in the sps spectrum, there is no evidence for this species at the surface.

3) Hydrogen Bonded Surface Water

What can be deduced from the region of the SFG spectrum between 3100 and 3500 cm^{-1}, clearly assigned to hydrogen bonded OH groups? If we assume that the signal in this region comes from a surface dipole contribution, then we can interpret the peak assignments and the inferred sign of the susceptibility. The spectral region below 3450 cm^{-1} is generally assigned to water that has both of its hydrogens bonded, so called symmetrical water. The region is composed of the OH stretch modes along with intermolecular and Fermi resonance coupling. Again we can ask the question: what is the average orientation of these groups? From the relation $\chi = N \langle\alpha\rangle$, where the brackets denote an average over the molecular orientation distribution, we have shown that the sign of the susceptibility depends on the orientation, up or down, of the molecule. This sign can be determined directly by interference techniques using the susceptibility of a remote nonlinear crystal. Or , more simply, one can use the SFG spectral lineshape to detect the interference between the susceptibility of one peak and the susceptibility of either a nearby overlapping peak or the nonresonant background. The relative phases of the individual peaks and the nonresonant background can come directly from the fit of the spectrum to the lineshape of a resonant nonlinear process. The fit to the SFG spectrum from the pure water surface, Table 1, shows that the susceptibilities of the hydrogen bonded region and the free OH peak have opposite sign. Although it is difficult to be sure about the uniqueness of a nonlinear least squares fit, this

conclusion should be robust by a simple consideration of the asymmetries of the broad and free OH peaks. When a resonant peak is superimposed on a nonresonant suceptibility that is real, the lineshape will become asymmetric, with the asymmetry reflecting the relative sign of χ_{NR} and A_q. The asymmetry of the free OH peak at 3690 cm^{-1} is seen in the sharp rise on the low frequency side versus the more gradual drop on the high frequency side. For the hydrogen bonded region this asymmetry is reversed. This implies that the resonant susceptibilities for these two species have opposite sign. Since the polarizabilities for the bonded and unbonded OH are most likely of the same sign, the relative sign of the susceptibilities indicates that the free and bound OH appearing in the spectrum are, on average, pointing in opposite directions with respect to the surface normal. This implies an interface of considerable complexity with no simple answer to the question which historically has been phrased: Do the hydrogens point up or down? The answer depends on which hydrogens, the free OH group or the hydrogen bonded OH groups. This picture of the interface has also been presented by recent molecular dynamics calculations.[25-27]

4) General Conclusions on Surface Structure

We can relate the structure of water at the liquid/vapor interface to the geometries expected for clusters from quantum mechanical calculations and to calculations and measurements for the surface potential. First we return to the apparent absence of species with two free hydrogens in the SFG spectrum. From the simple relation, $\chi_D = N\langle\alpha\rangle$, the lack of signal could be due to the molecular polarizability α or the population N being small, or due to the orientational distribution denoted by $\langle\rangle$. The polarizability of the singly free OH species and the species with two free hydrogens should have comparable strengths since they both involve free hydrogens. Is N small? Starting from the tetrahedral bonding geometry

of the water molecule, it is clear that molecules at the surface will form three or less hydrogen bonds. Molecular dynamics simulations indicate that in the low density region of the interface the molecules are participating in slightly under 2 hydrogen bonds.[27] Calculations of the lowest energy configurations for water clusters consistently find that the water molecules have a preference to bond to two neighbors with one oxygen lone pair and one hydrogen atom.[6,8,17,18] Cluster geometries which include water molecules bound through both hydrogens or both oxygen lone pairs are found to have a higher energy (Fig. 4(c) and (e)). It is therefore unlikely that a surface molecule would form two bonds with the oxygen lone pairs, leaving two hydrogens free. As for the orientational distribution denoted by <>, the signal from the species with two free hydrogens would be maximized by the orientation with the molecular bisector perpendicular to the surface. This orientation, however, would place the molecular dipole moment normal to the surface, at variance with molecular dynamics simulations which have shown that when a dipole moment is added to a molecule with an asymmetric Lennard Jones potential, it acts to reduce the polar orientation that exists in its absence.[28] We can therefore understand the absence of this species from the SFG spectrum both from considerations of hydrogen bonding and from the surface ordering effects of a molecular dipole moment.

We next discuss how the relative orientation of the free and hydrogen bonded OH groups is consistent with measurements of the surface potential. The surface potential for water is very small, about 100 mv,[29] considering its relatively large dipole moment, 1.8D in the gas phase (~2.6D in the condensed phases).[19] To understand the orientation distribution that might give rise to this surface potential, we can use the simplest model, that of a surface dipole sheet composed of oriented molecules.[30] This gives for the surface potential in units of volts, $\phi = 1200\pi N_s \mu$

$<\cos\theta>$ where N_s is the surface density in units cm^{-2}, μ is the molecular dipole moment(esu) and θ is the tilt angle of the dipole moment from the surface normal. Using ϕ = 100 mv, $N_s = 8.8 \times 10^{14}$ cm^{-2}, μ = 2.2 D, we find that the average tilt angle is around 89°(the molecule bisector lies close to the surface plane). The positive sign presently accepted for the surface potential implies that the dipole moment (i.e. the hydrogens for a fully hydrogen bonded surface species) points into the liquid. The small value for ϕ indicates that any substantial polar orientation by one species would be compensated by the opposing orientation of another. A surface molecule with the free hydrogen tilting less than 35° from the surface normal, as is indicated in our SFG sepctra, would have its dipole moment pointing out of the liquid. This would then have to be compensated by molecules oriented with the dipole moment pointing in, as would be found for water molecules participating in two hydrogen bonds pointing toward the liquid. This is consistent with the relative sign of the free OH peak and the hydrogen bonded broad band.[26]

D. SFG Spectrum of Water Surface with Alcohol Monolayer

1) Peak Assignments

We now return to the SFG spectrum of a monolayer of stearyl alcohol spread on the water. The SFG spectrum is presented in Fig.(2) and the peak parameters are tabulated in Table 2. We have already said that the change in the SFG spectrum from that of the pure water surface demonstrated that the 3690 cm^{-1} peak was due to a surface resonance. In principle, we should rule out the possibility that the monolayer had a resonance of its own that fortuitously canceled the contribution from the pure water. In that case, the change of the spectrum does not prove the surface nature of the pure water signal. The vibrational spectra of alcohols in the OH region has been studied extensively for interest in the association

of alcohols in solution.[31] We have already seen the sensitivity of the OH stretch mode to hydrogen bonding in the case of water. The same is true of the alcohols.[32] In very dilute solution, the alcohol spectra show a single narrow peak at about 3640 cm^{-1}. As the concentration is increased, a peak at 3485 cm-1 grows and is eventually overwhelmed by an intense band centered at around 3350 cm^{-1}. The 3485 cm^{-1} peak is assigned to a dimer while the 3350 cm^{-1} peak is assigned to the internal groups of polymer chains in the liquid. These OH groups are acting as both donor and acceptors (both the H and the O are participating in H-bonds). Unfortunately, deuteration studies of alcohols in aqueous solution are doomed by the fast exchange rate of D and H so that separate assignments for the water and alcohol OH stretches in aqueous solution are not available. We will simply assume that the alcohol hydrogen bonded resonance lies between 3300 and 3500 cm^{-1}.

2) Free OH Group Spectral Region

From the above assignments we can rule out the fortuitous cancelation of resonances. The alcohol possesses no resonances that would overlap with the 3690 cm^{-1} peak. Therefore, as we previously stated, this peak originates from the surface. A more difficult question to answer is: Does the pure water surface signal arise from a surface quadrupole contribution? As discussed in chapter II, this term arises from a gradient in the electric field across the interface due to the discontinuity of the linear dielectric constant at the surface. Ideally we would like to alter the field gradient without changing the structure of the interface. This is very difficult for a free liquid surface. Clearly, the application of the monolayer film will change the surface field gradient and, potentially, the interface structure. At this point, we can answer a more limited question. We can establish with a simple model for the surface quadrupole term that the surface has indeed been modified by the monolayer

film. In other words: Is the decrease in the 3690 cm^{-1} peak, possibly arising from a surface quadrupole term, due to the change in the dielectric constants seen at the water surface or has the hydrogen bonding of the interface changed? The effective surface quadrupole susceptibility can be written as

$$\chi_I = \chi^P [\varepsilon_1^{-1} - \varepsilon_{wat}^{-1}]$$

where ε_1 is the dielectric constant at ω_{ir} seen on one side of the water interface (i.e. the film or air), ε_{wat} is the dielectric constant of the water and χ^P is the quadrupole nonlinear susceptibility of the interface. For the air/water interface, the quantity in the brackets is equal to .28, while at the film/water interface it is -.17 . This means that if the surface signal was due to an interface quadrupole contribution that did not change upon deposition of the alcohol film, then the peak height should drop to $(.17/.28)^2 = .37$ of its original value. Clearly, the peak change is much greater. A fit to the spectrum with the monolayer in place finds the resonance strength (A in eq. (1b)) falls to less than 1/10 of its original value as seen in Tables 1 and 2. This indicates that the free OH groups have become hydrogen bonded. This is likely since the absence of signal at 3640 cm^{-1} implies that the alcohol OH groups are fully hydrogen bonded.

3) Hydrogen Bonded OH Group Region

The changes in the hydrogen bonded region of the spectrum are also dramatic. The loss of intensity on the high frequency side of the broad band demonstrates that we are observing a change in the surface structure of hydrogen bonded OH groups as well. If we again assume that the signal originates from a surface dipole contribution, then the susceptibility of the alcohol OH and the

hydrogen bonded water OH must overlap in the region 3300-3450 cm^{-1}, while the region below 3300 cm^{-1} is due to the hydrogen bonded water alone. It would be interesting to know if the hydrogen bonded water has reoriented due to the monolayer. This might be indicated in the relative sign of the resonance peaks and the nonresonant background. In the case of pure water, the lower frequency features had the opposite sign from χ_{NR} whereas for the air/alcohol monolayer/water interface, the resonances and χ_{NR} have the same sign. If the signs of χ_{NR} for the two interfaces have the same sign, then the water molecules have changed their orientation. However, a more conclusive determination requires a phase measurement using a remote reference. Finally, we note the similarity between the change of the SFG spectra for the water surface upon deposition of the alcohol monolayer (Fig. 4(e), (f)) and the change seen in the infrared absorption spectra of liquid and solid water (Fig. 4(g), (h)). Though the interpretation of an SFG spectrum requires consideration of the possible cancelation effects of different species in the total suceptibility (i.e. between the alcohol and water OH groups), the alcohol monolayer SFG spectrum suggests a possible increase in the ordering of the underlying water.

E. Conclusion

In conclusion, we have obtained the vibrational spectrum from the liquid/vapor interface of pure water. The spectrum unambiguously identifies the presence of a surface species with one free hydrogen projecting into the vapor. The surface density for this species has been estimated to be 20% of a compact monolayer. In addition, the spectrum of the hydrogen bonded water suggests that it is oriented opposite to the free OH and therefore projects its hydrogens into the liquid. This complexity for the water surface has been predicted by molecular

dynamics simulations and is consistent with the relatively small surface potential of water. In addition, we have shown how the water surface structure is consistent with the bonding geometries found in water clusters. These results constitute the most direct experimental evidence for the surface ordering of water presently available and indicate the promise of SFG as a study of the vastly important aqueous interfaces.

References

1 see, for example, *Water, A Comprehensive Treatise: The Physics and Physical Chemistry of Water*, F. Franks, ed. (Plenum, New York, 1972).

2 see W. A. Weyl, J. Coll. Sci. **6**, 389 (1951) and J. Frenkel, *Kinetic Theory of Liquids* (Dover, New York, 1955) for early discussions.

3 W. Drost-Hansen, Ind. Eng. Chem. **57-4**, 18 (1965): W. Drost-Hansen, in *Chemistry and Physics of Interfaces*, S. Ross, ed. (Amer. Chem. Soc. Publications, Washington, 1964) for a review of early work.

4 M. C. Phillips, in ref. 1, Vol. 5, Ch. 3.

5 *Advances in Infrared and Raman Spectroscopy*, R. J. H. Clark, R. E. Hester, eds.(Heyden, London, 1978) Vol. 5, Ch. 3.

6 M. F. Vernon, et al., J. Chem. Phys. **77**, 47 (1982).

7 R. H. Page, J. G. Frey, Y. R. Shen and Y. T. Lee, Chem. Phys. Lett. **106**, 373 (1984).

8 D. F. Coker, R. E. Miller and R. O. Watts, J. Chem. Phys. **82**, 3554 (1985).

9 R. H. Page, M. F. Vernon, Y. R. Shen and Y. T. Lee, Chem. Phys. Lett. **141**,1 (1987).

10 *Water- A Comprehensive Treatise*, F. Franks ed., (Plenum, New York, 1972) Vol. 1, Ch. 5; *Structure of Water and Aqueous Solutions*, W. A. P. Luck ed. (Verlag Chemie Gmbh, WQeinheim, 1974).

11 W. F. Murphy and H. J. Bernstein, J. Phys. Chem. **76**, 1147 (1972).

12 J. R. Scherer, M. K. Go, and S. Kint, J. Phys. Chem. 78, 1304 (1974).

13 C. I. Ratcliffe and D. E. Irish, J. Phys. Chem. **86**, 4897 (1982).

[14] M. S. Bergren, D. Schuh, M. G. Sceats, and S. A. Rice, J. Chem. Phys. **69**, 3477 (1978).

[15] G. E. Walrafen, M. R. Fisher, M. S. Hokmabadi, and W. H. Yang, J. Chem. Phys. **85**,6970 (1986); G. E. Walrafen, M. S. Hokmabadi and W. H. Yang, J. Chem. Phys. **85**, 6964 (1986).

[16] J. R. Reimers and R. O. Watts, Chem. Phys. **85**, 83 (1984).

[17] J. E. Del Bene and J. A. Pople, J. Chem. Phys. **52**,4858 (1970); J. E. Del Bene and J. A. Pople, J. Chem. Phys. **58**,3605 (1973).

[18] P. Barnes, J. L. Finney, J. D. Nicholas, and J. E. Quinn, Nature **282**, 459 (1979).

[19] D. Eisenberg and W. Kauzmann, The Structure and Properties of Water (Oxford University Press, New York, 1969)

[20] W. F. Murphy, Mol. Phys. **36**, 727 (1978).

[21] If the peak is resolution limited then this is a lower bound on the peak susceptibility.

[22] For comparison, the upper bound for the orientational average is .71, corresponding to the OH groups all pointing with $\theta \sim 40°$, and a distribution that is constant for all tilt angles gives .48 . Therefore, the value we are using should give a lower bound on N.

[23] W. Hagen, A. G. G. M. Tielens and J. M. Greenberg, Chem. Phys. **56**, 367 (1981); W. B. Person, NATO ASI Matrix Isolation Spectroscopy. Montpelier (1980); M. Gussoni, J. Mol. St. **141**, 63 (1986); S. A. Clough, Y. Beers, G. P. Klein, and L. S. Rothman, J. Chem. Phys. **59**, 2554 (1973).

[24] we have used the value for the bond polarizability from W. F. Murphy, Mol. Phys. **36**,727 (1978); S. Montero and G. del Rio, Mol. Phys. **31**,357 (1976); A. R. Hoy, I. M. Mills and G. Strey, Mol. Phys. **24**, 1265 (1972) but have included the higher absolute differential raman cross section and hydrogen bonded correction obtained by N. Abe and M. Ito, J. Raman Spect. **7**, 161 (1978).This again serves to ensure that our estimate is a lower bound.

[25] R. M. Townsend and S. A. Rice, J. Chem. Phys. **94**, 2207 (1991).

[26] M. Matsumoto and Y. Kataoka, J. Chem. Phys. **88**, 3233 (1988).

[27] M. A. Wilson, A. Pohorille and L. R. Pratt, J. Phys. Chem. **91**, 4873 (1987).

[28] K. E. Gubbins in *Fluid Interfacial Phenomena*, C. A. Croxton, ed. (J. Wiley, Chichester, 1986), Ch. 10.,

[29] J. E. B. Randles, Phys. Chem. Liq. **7**, 107 (1977).

[30] J. D. Jackson, *Classical Electrodynamics*, (Wiley, New York, 1975) p. 38.

[31] A. Ens and F. E. Murray, Can. J. Chem. **35**, 170 (1957).

[32] U. Liddel and E. D. Becker, Spectrochim. Acta **10**, 70 (1957).

Table 1

Parameters for fit of eqs. (1) and (2) to SFG spectrum of the pure water liquid/vapor interface, Fig.(1).

q	A_q (a.u.)	ω_q (cm^{-1})	Γ_q (cm^{-1})
1	30	3690	28
2	-86	3425	85
3	-13	3316	46
4	-14	3213	47

$\chi_{NR} = .5$.

Table 2

Parameters for fit of eqs.(1) and (2) to SFG spectrum of stearyl alcohol monolayer spread on the water surface, fig(2). Note that while the relative signs of A and χ_{NR} are fixed by the fit, the overall signs are not.

q	A_q (a.u.)	ω_q (cm^{-1})	Γ_q (cm^{-1})
1	-1.0	3690	28
2	-28.2	3424	84
3	25	3214	50
4	45	3140	47

$\chi_{NR} = .46$.

Figure Captions

Fig. 1. SFG spectrum of pure water liquid/vapor interface with beam polarization combination sum frequency - s, visible - s, infrared - p polarized. The fit to Eq. 1 (see table 1) is shown as a solid line.

Fig. 2. SFG spectrum taken of water surface with the ssp beam polarization combination after deposition of stearyl alcohol monolayer compressed to 10 mN/m surface pressure. The fit from table 2 is shown as the solid line. The fit from the pure water surface SFG spectrum is shown in the dashed line.

Fig. 3. Collection of spectra for various forms of water (adapted from Ref. 6). (a) - (d) Infrared predissociation spectra of water clusters for sizes indicated. Spectrum of $(H_2O)_{19}$ is from Ref. 9. (e),(f) SFG spectrum of pure water liquid/vapor interface, before (e) and after (f) deposition of alcohol monolayer, this work. (g) infrared absorption spectrum of liquid water (from G. Walrafen, J. Chem. Phys. **47**,114 (1967)). (h) infrared absorption spectrum of solid water (from E. Whalley and J. E. Bertie, J. Chem. Phys. **46**, 1264 (1967).

Fig. 4. Water cluster geometries. The lowest energy configurations calculated for the dimer (a), the trimer (b) and the tetramer (d). Other configurations shown are representative of those with a water molecule acting as a double acceptor,(c) top, or as a double donor, (c) bottom, for the trimer. In the case of the tetramer, (e) shows configurations which include both of these types of water molecule in a single cluster. (e) and (c) are consistently calculated to have a higher energy than configurations (a), (b) and (d). Fig. (a) is from Ref. 8; figs. (b) - (e) from Ref. 16.

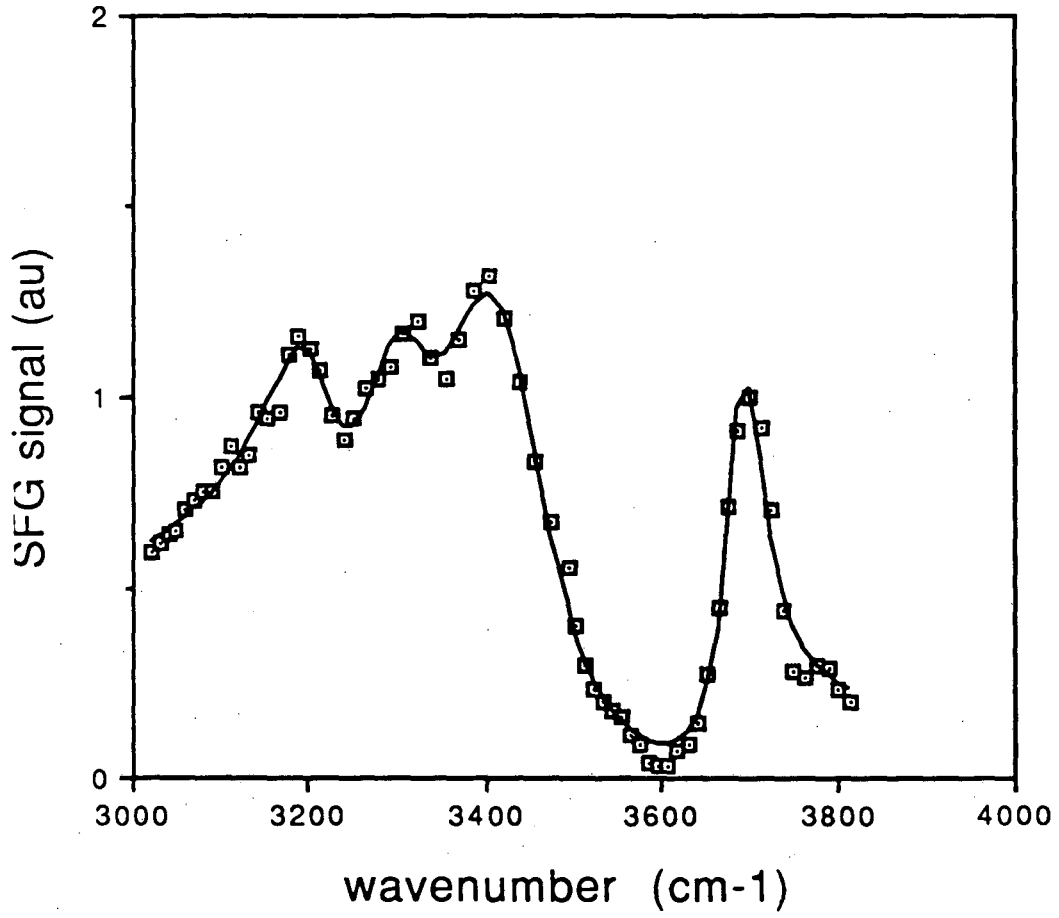

XBL 917-1510

Fig.1

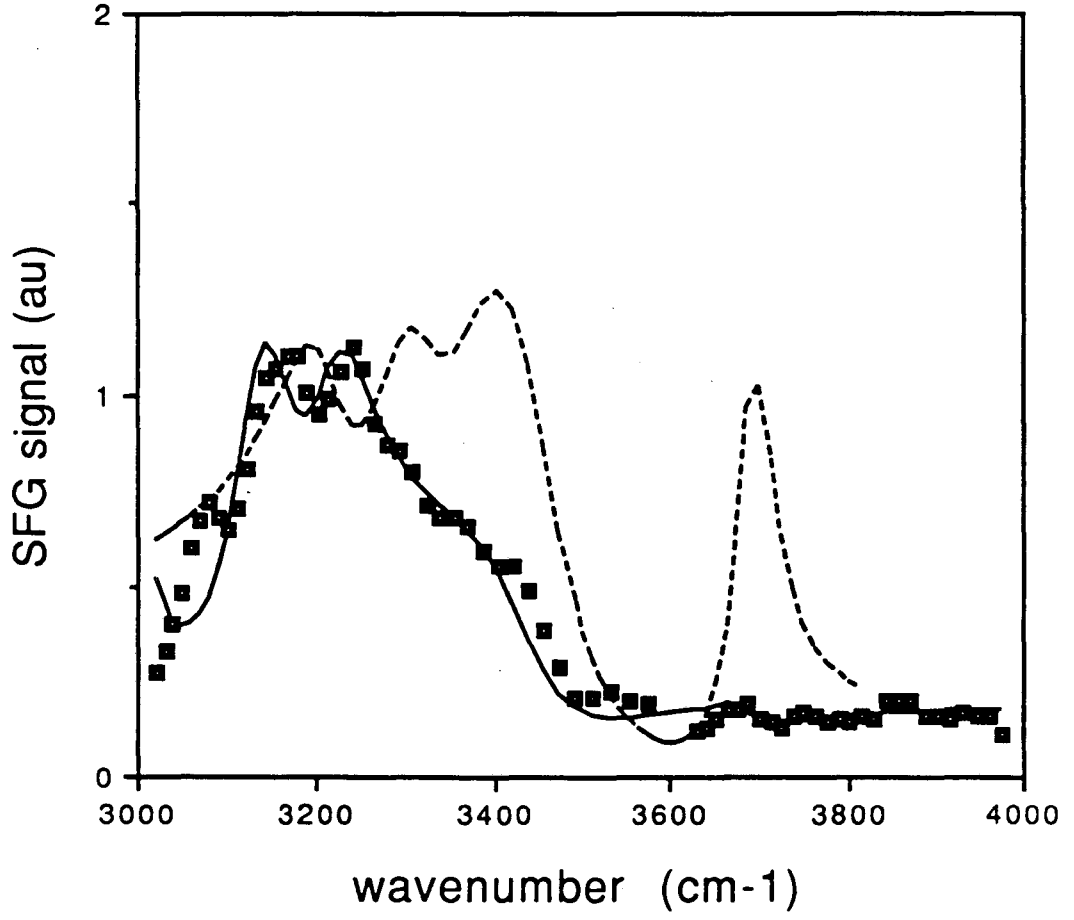

XBL 917-1511

Fig.2

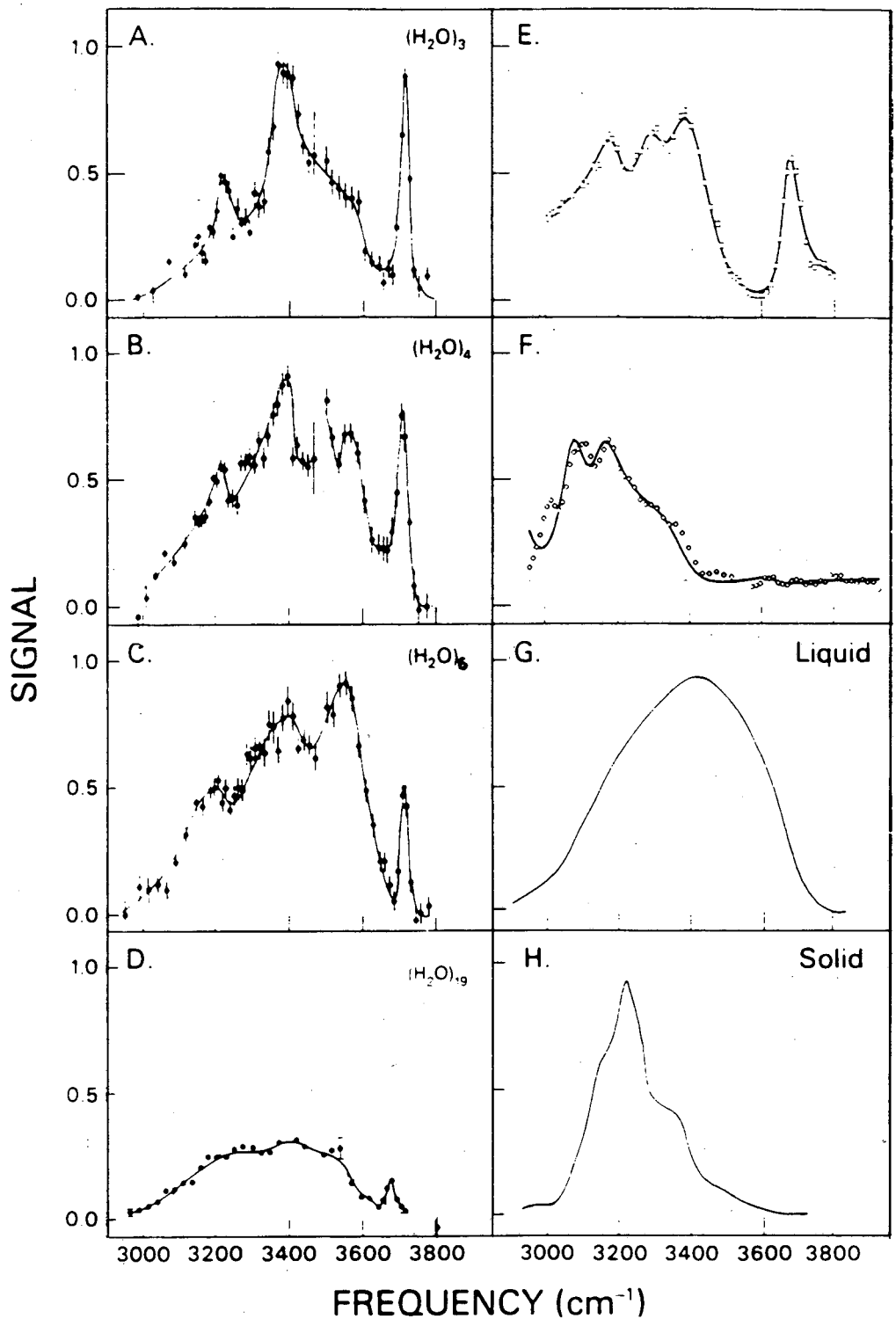

XBL 917-1512

Fig.3

Water Cluster Geometries

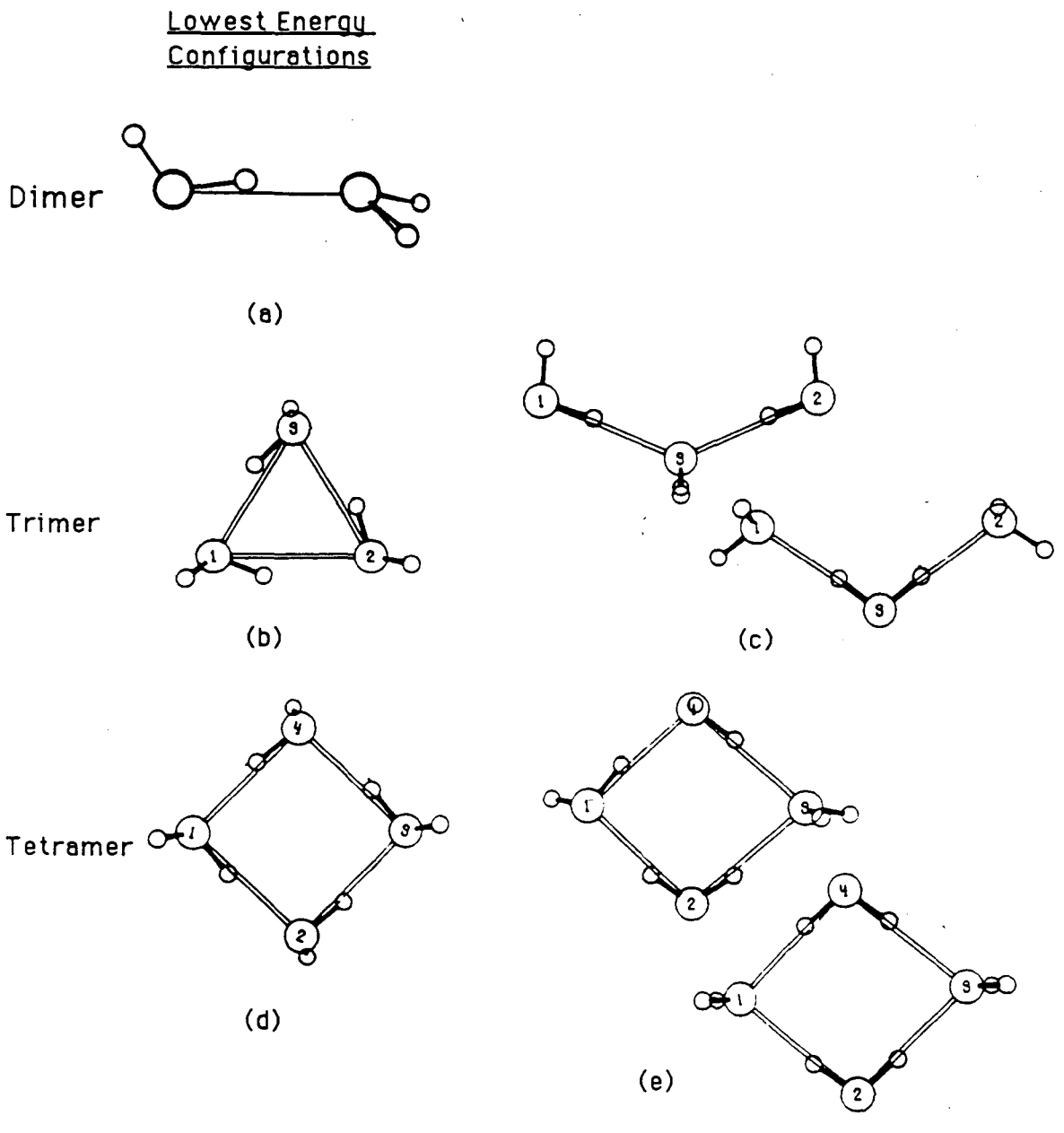

Fig.4

LAWRENCE BERKELEY LABORATORY
UNIVERSITY OF CALIFORNIA
INFORMATION RESOURCES DEPARTMENT
BERKELEY, CALIFORNIA 94720